NATIONAL ADVISORY COMMITTEE FOR AERONAUTICS

WARTIME REPORT

ORIGINALLY ISSUED

September 1944 as
Memorandum Report

LONGITUDINAL CHARACTERISTICS AND AILERON EFFECTIVENESS

OF A MIDWING AIRPLANE FROM HIGH-SPEED

WIND-TUNNEL TESTS

By Charles F. Hall and Robert L. Mannes

Ames Aeronautical Laboratory
Moffett Field, California

NACA

WASHINGTON

NATIONAL ADVISORY COMMITTEE FOR AERONAUTICS

MEMORANDUM REPORT

for the

Air Materiel Command, U.S. Army Air Forces

LONGITUDINAL CHARACTERISTICS AND AILERON EFFECTIVENESS

OF A MIDWING AIRPLANE FROM HIGH-SPEED

WIND-TUNNEL TESTS

By Charles F. Hall and Robert L. Mannes

SUMMARY

Wind-tunnel tests of a 0.175-scale model of a midwing airplane were made in order to determine its high-speed longitudinal characteristics, to test devices for improving the longitudinal control at high Mach numbers, and to determine the aileron effectiveness at high Mach numbers.

The force and moment coefficients computed from the test data are presented in this report. The control forces, elevator angle, and aileron angle for several flight conditions are predicted. The maximum speed and Mach number attained at several gliding angles are estimated.

The data indicate that, with respect to elevator-angle variation with speed, the airplane will become unstable at approximately 0.7 Mach number. Two devices for improving the longitudinal control – a wing-profile modification and auxiliary control flaps – increase the Mach number at which this instability occurs. The former device increases it by as much as 0.075 and the latter by 0.05. However, because the effectiveness of the flaps decreases between 0.75 and 0.8 Mach number, their over-all characteristics are less favorable than those of the wing-profile modification.

INTRODUCTION

At the request of the Air Materiel Command, U.S. Army Air Forces, tests of a 0.175-scale model of a midwing airplane were conducted in the Ames 16-foot high-speed wind tunnel.

The purpose of these tests was to determine the effect of Mach number on the aerodynamic characteristics of the airplane and to find methods of increasing the longitudinal control at high Mach numbers. The aerodynamic characteristics investigated were the lift, drag, and pitching-moment coefficients; the effectiveness of the elevator, the elevator tab, and the aileron; and the hinge-moment coefficients for the elevator and the aileron. Two methods to increase the longitudinal control at high Mach numbers were tested. They were auxiliary control flaps, and a wing-profile modification designed to lower the critical Mach number of the inboard lower surface of the wing to that of the upper surface at 0.1 lift coefficient.

DESCRIPTION OF MODEL

The 0.175-scale model was supplied by the manufacturer. The steel wing, fuselage, and empennage structures were covered with mahogany. The elevator and aileron were solid dural. A dummy tail fairing was supplied for tail-off tests.

The elevator hinge moment was measured by an electric resistance strain gage mounted on a cantilever arm. A small electric motor and a slide-wire resistor coupled to the elevator mechanism provided remote control and indication of the elevator angle. Measurement of the aileron hinge moment was by means of a torsional strain gage. It was necessary to set the aileron at the desired angle before each test. Both gages were calibrated, before testing, by applying known moments to the control surfaces.

Photographs of the model mounted in the 16-foot wind tunnel are shown in figures 1 to 5, and a drawing of the model is shown in figure 6.

The chord and span of the auxiliary control flaps (fig. 5) were 1 inch and 12 inches (model scale), respectively. The hinge line was at 62.5 percent of the wing chord between wing stations 20 inches and 32 inches from the center line. The flaps were tested at angles of 30° and 45°.

The wing-profile modification (subsequently called the wing bump) is shown in figure 7. As the bump was only 0.0658 inch thick, it was made of balsawood, glued to the wing surface, and contoured from templates furnished by the manufacturer.

Model and airplane dimensions used in this report are as follows:

Wing	Model	Airplane
Area, square feet	16.99	554.6
Aspect ratio	8.96	8.96
Mean aerodynamic chord, feet	1.498	8.56

Horizontal tail plane

Area, square feet	4.27	139.3
Distance between aerodynamic center of tail plane and normal airplane center of gravity	3.48	19.9

Elevator

Chord aft of hinge line, percent of total tail-plane chord	35.0	35.0
Geometric overhang, percent	40.5	45.0
Span, one elevator, feet	1.78	10.17
Root-mean-square chord behind hinge line, feet	0.325	1.86
Ratio of stick force to elevator hinge moment, pounds per pound-foot	-----	0.60

Aileron

Chord aft of hinge line, percent of total wing chord	22.0	22.0
Geometric overhang, percent	40	43
Span, one aileron, feet	2.025	11.56
Root-mean-square chord behind hinge line, feet	0.207	1.18
Ratio of wheel moment to aileron hinge moment	-----	0.119
Wheel diameter, inches	-----	13

General

Normal gross weight, pounds	-----	25,000
Normal wing loading, pounds per square foot	-----	45

	Model	Airplane
Normal center-of-gravity position		
Horizontal, percent mean aerodynamic chord	------	25
Vertical, inches above fuselage reference line	------	7.00

SYMBOLS

The definitions of the symbols used in this report are as follows:

S — wing area, square feet

b — wing span, feet

b_x — span of control surface x, feet

$\bar{c}_x$ — root-mean-square chord behind hinge line of control surface x, feet

α — angle of attack of model, degrees
The angle is measured relative to fuselage reference line.

δ_x — angle of control surface x, degrees
The angle is considered positive when trailing edge of surface is down.

g — indicated normal acceleration, in units of gravitational acceleration

V_{mph} — velocity of airplane, miles per hour

V — velocity of airplane, feet per second

a — velocity of sound in undisturbed air, feet per second

M — Mach number (V/a)

M_{cr} — critical Mach number
The Mach number at which speed of sound is reached locally on the airplane.

ρ mass density of air, slugs per cubic foot

q dynamic pressure $\left(\frac{1}{2}\rho V^2\right)$, pounds per square foot

C_L lift coefficient (lift/qS)

C_D drag coefficient (drag/qS)

$C_{m_{c/4}}$ pitching-moment coefficient about 25 percent mean aerodynamic chord $\left[\dfrac{\text{pitching moment}}{qS \ (\text{M.A.C.})}\right]$

C_l rolling-moment coefficient $\left(\dfrac{\text{rolling moment}}{qSb}\right)$

C_{h_x} hinge-moment coefficient of control surface x $\left(\dfrac{\text{hinge moment}}{q \ \overline{c}_x{}^2 b_x}\right)$

p_o static pressure in undisturbed stream, pounds per square foot

p local static pressure, pounds per square foot

P pressure coefficient $\left(\dfrac{p - p_o}{q}\right)$

P_{cr} critical pressure coefficient
Pressure coefficient which corresponds to the local speed of sound

p_U pressure on upper surface of balance seal, pounds per square foot

p_L pressure on lower surface of balance seal, pounds per square foot

ΔP balance-pressure coefficient $\left(\dfrac{p_L - p_U}{q}\right)$

p rolling velocity, radians per second

$pb/2V$ helix angle of the path of the wing tip in roll

Subscripts

e   elevator

t   tab

a   aileron

REDUCTION OF DATA

Corrections

The forces, moments, and pressures were converted to coefficient form by use of the equations given in the list of symbols. To these coefficients were added the following corrections for tunnel-wall effects (reference 1):

$$\Delta\alpha = 0.668\ C_L$$

$$\Delta C_D = 0.01167\ C_L$$

$$\Delta C_m = 0.00546\ C_L$$

The tare corrections to the coefficients and the angle of attack were evaluated by mounting the model on wing-tip supports and calculating the differences between the aerodynamic characteristics obtained from tests with the three vertical struts in place and with them removed. These differences were measured at a constant lift coefficient. Two streamline tie rods (fig. 4) were attached to the model to reduce its deflection when wing tip supported. The data indicate, however, that these tie rods produced an interference drag, causing the tare-drag increase — normally associated with the critical Mach number of the struts — to occur at a considerably lower Mach number. The drag tares were therefore determined by adding to the drag of the struts alone a component caused by the upflow angle of the air. This method does not include the interference drag between the struts and the model.

Dynamic-Pressure and Mach Number Calibration

The calibration used during the tests was obtained by a pitot-tube survey in a plane perpendicular to the longitudinal axis of the tunnel at a longitudinal position which coincided with the 25-percent point of the mean aerodynamic chord of the model when in the tunnel. As the vertical struts were in the tunnel, this method of calibration corrects for the constricting effect of the supporting system. A calibration obtained with the supporting struts removed from the tunnel was used during those tare tests in which the model was supported only at the wing tips.

Elevator Control Forces

The elevator stick forces for rectilinear flight were computed in the following manner: At a lift coefficient calculated from the selected wing loading, altitude, and Mach number, the elevator angle for balance was determined from the data. Due to the effects of the tunnel wall and the supporting struts, the angle of air flow at the tail of the model is different from that at the tail of the airplane. In order to rectify this, a correction was made to the lift coefficient in such a manner that the angle of air flow at the tail of the model, at the corrected lift coefficient, would be the same as that at the tail of the airplane. The change in downwash with lift coefficient, needed to make this correction, was approximated from results in reference 2. The stick force was computed using the hinge-moment coefficient corresponding to the elevator angle and corrected lift coefficient. In computing the stick force for curved flight, a correction to the elevator angle because of the damping moment of the tail (reference 3) and a correction to the lift coefficient because of the change in the angle of flow at the tail were made.

The stick force for elevator balance areas other than that area tested on the model was computed. The balance-pressure data were used to calculate the increment of hinge-moment coefficient caused by the increase in the balance area and moment arm.

Stick forces for configurations other than the normal were calculated by adding to the previously determined elevator angle an increment to balance the pitching-moment changes due to the configuration change. The hinge-moment coefficient corresponding to this corrected elevator angle was used.

Gliding Velocity

The velocity, Mach number, and time to descend in relation to the angle of glide were computed by a step-by-step process using the drag data.

Aileron Wheel Forces

The wheel force for aileron control was calculated in the following manner: A relation between the wing-tip helix angle $pb/2V$ and the rolling-moment coefficient was found from equation (5) and figure 8 of reference 4. The helix angle computed in this manner was reduced 20 percent as recommended in reference 5. With this relation, the change in the angle of attack of the wing as a function of rolling-moment coefficient was determined. Corrections were applied to the angle of attack, at the selected flight condition, and the corresponding rolling-moment coefficient because of this angle-of-attack change. The hinge-moment coefficient was determined from the data for the corrected angle of attack.

RESULTS AND DISCUSSION

The airplane has an estimated center-of-gravity travel from 20 to 36 percent of the mean aerodynamic chord, and a weight variation from 21,500 to 35,000 pounds. The data in this report, in general, are shown for the center of gravity at 25 percent of the mean aerodynamic chord and for a weight of 25,000 pounds.

The geometric overhang on the model elevator was 40.5 percent of the elevator chord aft of the hinge line, while that required by the airplane elevator is estimated by the manufacturer to be 45 percent. Unless otherwise stated, the stick forces presented in this report are for a geometric overhang of 40.5 percent.

The geometric overhang for the aileron is 40 and 43 percent of the aileron chord aft of the hinge line on the model and airplane, respectively. Wheel forces are shown for a 40-percent overhang only.

Except when noted otherwise or when the control angle is one of the variables, the data for the figures have been obtained from tests of the model with all controls set at $0°$.

Pitching-Moment Characteristics

Significance of M^2C_L.- A relationship between M^2C_L and wing loading, normal acceleration, and altitude is shown both graphically and algebraically in figure 8. The equation for M^2C_L shows it to be independent of speed and to remain constant for any selected wing loading, normal acceleration, and altitude, assuming the air temperature does not change. (The velocity of sound a is a function of temperature only.) Because of these facts, the quantity M^2C_L has been used as a parameter in presenting the pitching-moment coefficient as a function of Mach number.

In figure 9, the lift coefficient and Mach number are shown for constant M^2C_L values. In addition, the maximum lift coefficient obtained from tests of the model with the empennage off is shown, thus indicating the maximum M^2C_L value possible for the airplane. Tests to determine the maximum lift coefficient were made with the empennage on and off. However, because the pitching-moment coefficients at the maximum lift coefficients with the empennage off were nearly zero (fig. 10), thereby closely approximating balance conditions, these data were used.

Pitching-moment coefficient for empennage on and off.- The pitching-moment coefficients for the model with the empennage removed are shown in figure 10, and with the empennage on, in figure 11. The effect of Mach number on the stick-fixed static longitudinal stability is presented in figure 12. Figure 12(a) was obtained by cross-plotting the data in figure 11. The slopes of the curves in figure 11, at the lift coefficient corresponding to the selected M^2C_L values, were plotted in figure 12(b).

Figure 12(b) gives the usual derivative associated with static stability. It is seen that below an M^2C_L of 0.30, this derivative is almost twice as large at 0.8 Mach number as at the lower Mach numbers. This indicates a doubling of the stability. It must be remembered, however, that this derivative was obtained by considering the Mach number constant.

A stability derivative in which the Mach number is held
constant does not completely represent flight conditions, for
in flight a change of lift coefficient usually causes a
change of speed and Mach number. Therefore, in presenting
static stability characteristics, the effect of Mach number
as well as of lift, on the pitching-moment coefficient should
be included. This is especially true at high Mach numbers,
for the pitching-moment coefficient is more affected by Mach
number than by lift variations. The combined effects of Mach
number and lift variations on the pitching-moment coefficient
are indicated in figure 12(a). A positive slope of the curves
indicates that a climbing moment results for an increase of
Mach number and corresponding decrease of lift coefficient.
The climbing moment tends to increase the lift coefficient,
decrease the Mach number, and return the airplane to its
original flight condition, thus providing stick-fixed static
longitudinal stability. Conversely, a negative slope indi-
cates an unstable condition.

The slopes of the curves in figure 12(a) are related to
the constant Mach number stability derivative (fig. 12(b)) by
the following equation, the derivation of which appears in
the appendix:

$$\left(\frac{dC_m}{dM}\right)_{M^2 C_L, \delta_e} = \left(\frac{\partial C_m}{\partial M}\right)_{C_L, \delta_e} + \frac{\text{wing loading}}{\rho a^2 M^3}\left(\frac{-\partial C_m}{\partial C_L}\right)_{M, \delta_e}$$

Subsequent discussions of stability in this report will refer
to the left-hand member of the equation.

It will be noticed that the derivative $(-\partial C_m/\partial C_L)_{M, \delta_e}$
is the predominant factor influencing static stability at low
Mach numbers because of the factor $1/M^3$ in the last term.
With increasing Mach number its influence diminishes. This
fact is shown by a comparison of figures 12(a) and 12(b). At
high Mach numbers when $(-\partial C_m/\partial C_L)_{M, \delta_e}$ has its greatest
value, figure 12(a) indicates stick-fixed longitudinal insta-
bility. The equation also shows that an increase of wing
loading or altitude increases the stability, assuming other
factors to remain constant. In addition, assuming the ele-
vator effectiveness remains constant, $(\partial C_m/\partial M)_{M^2 C_L, \delta_e}$ is
closely related to the variation of elevator angle with speed.
This variation is commonly used in the analysis of flight-test

results as an indication of stick-fixed static stability.

The data of figure 12(a) indicate instability above 0.7 Mach number between 0.025 and 0.10 M^2C_L. These data are for the center of gravity at 25 percent of the mean aerodynamic chord. A rearward movement of the center of gravity, by reducing $(-\partial C_m/\partial C_L)_{M,\delta_e}$, would increase the static instability and reduce the Mach number at which the airplane becomes unstable.

Figure 12(b) shows that below 0.74 Mach number $(-\partial C_m/\partial C_L)_{M,\delta_e}$ is positive for all center-of-gravity positions back to 40 percent of the mean aerodynamic chord. Also, figure 11 indicates that below 0.7 Mach number $(\partial C_m/\partial M)_{C_L,\delta_e}$ is either positive or just slightly negative for lift coefficients below the stall. Static stability is therefore assured at the lower Mach numbers even with the center of gravity at the estimated farthest aft location.

The pitching-moment coefficient contributed by the horizontal tail with the elevator fixed (fig. 13) undergoes a large decrease for constant lift coefficient at high Mach numbers. This characteristic is the factor contributing most to static instability. It is caused by the increase in the angle of attack of the airplane necessary to maintain a constant lift coefficient at supercritical Mach numbers. This angle-of-attack increase reduces the download on the tail, and therefore the pitching-moment coefficient. (See reference 6 for a further analysis of high-speed longitudinal instability.)

The pitching-moment coefficient of the wing-fuselage combination increases with Mach number above lift coefficients from 0.7 to 0.05 at 0.65 and 0.75 Mach number, respectively (fig. 10). This reduces the destabilizing effect of the horizontal tail. The pressure-distribution results indicate that the compression shock on the upper surface of the wing moves forward with increasing Mach number and angle of attack, which may account for the increase of pitching moment. Also, the peak-pressure coefficient on the lower surface decreases greatly and moves from the 40-percent-chord position at low Mach numbers to at least the 60-percent-chord position at 0.8 Mach number. (Pressure-distribution measurements were taken over only the forward 60 percent of the chord.)

<u>Pitching-moment coefficient from elevator.</u>- The elevator effectiveness for the model (fig. 14) increases slightly with Mach number up to 0.775 at an M^2C_L of zero, and up to 0.7 at an M^2C_L of 0.30. Below 0.7 Mach number, the effectiveness also increases slightly with M^2C_L. The decrease in the effectiveness at high Mach numbers aggravates the undesirable control characteristics caused by the decrease in the elevator-fixed pitching-moment coefficient (fig. 12(a)).

The effect of the tab on the pitching-moment coefficient is also shown in figure 14. Being of such small magnitude, the variation with M^2C_L is indiscernible. It must be remembered that normally the tab will produce a pitching-moment coefficient in opposition to that of the elevator, thus reducing the elevator effectiveness shown.

<u>Pitching-moment coefficient due to the wing bump.</u>- The purpose of the wing bump is to increase the Mach number at which the airplane becomes longitudinally unstable (fig. 12(a)). A further purpose is to alleviate the decrease in the elevator-fixed pitching-moment coefficient at high Mach numbers. This will reduce the upward elevator angle and the pull on the stick required to maintain balance with increasing Mach number.

The bump was designed to reduce the critical Mach number on the inboard lower surface of the wing to that of the upper surface at a lift coefficient of 0.10. It was reasoned (reference 7) that the bump would decrease the effect of compressibility on the lift of the center portion of the wing span and increase the downwash at the tail. This would reduce the angle of attack of the tail and increase the pitching-moment coefficient at supercritical Mach numbers. The maximum thickness of the bump was at the 50-percent-chord station. Reference 7 shows that a bump placed at this location had the greatest effect in relieving longitudinal-stability difficulties at high Mach numbers for a twin-boom low-wing model.

A comparison of the pitching-moment coefficients obtained from tests of the model with and without the bump is shown in figure 15. The effect of the bump at and below 0.7 Mach number was negligible. Above 0.7 Mach number, however, the bump increased the pitching-moment coefficient. The bump, therefore, increased $(\partial C_m/\partial M)_{C_L, \delta_e}$ in the stability equation, and thus the stick-fixed static stability. Figure 15 shows

that the bump makes the model stable for a Mach number as much as 0.075 higher. The effect of the bump on the lift and pitching-moment coefficients with the tail off was negligible.

For the bump tests, it will be noticed that the data are compared at an elevator angle of $-1°$. During the latter part of the tests, considerable difficulty was encountered with the elevator control mechanism. At the conclusion of the wing-bump test the elevator angle was measured and found to be $-1°$. The possibility of the angle having changed during the test seems remote in light of the fact that at the lower Mach numbers, the data compare so well with those obtained for the normal configuration at an elevator angle of $-1°$.

The pressure distribution at wing station 12 with and without the bump is shown in figure 16. With the bump, the critical Mach number of the lower surface is approximately 0.65, while that of the upper surface is approximately 0.68. Reducing the size of the bump to meet the original specifications would probably reduce the beneficial effects. The broken lines in the pressure-distribution diagrams indicate the approximate position of the compression shock. The exact position is not known, due to the small number of pressure orifices. The critical Mach numbers of the wing at these stations are shown in figure 17.

Pitching-moment coefficient due to auxiliary control flaps.- Because of the large decreases in the pitching-moment coefficient at high Mach numbers with the elevator fixed, the upward elevator angle required to balance the airplane may become very large and the pull on the stick excessive. The use of auxiliary control flaps is a proven method of reducing the elevator angle and the stick force on several high-speed airplanes. (See reference 7 for performance of auxiliary control flaps on another airplane model.) Auxiliary control flaps, therefore, were tested on the model.

The increments of pitching-moment coefficient due to the net effect of the auxiliary control flaps, and to their separate effects on the tail plane and on the wing, are shown in figure 18. The greater part of the increase of pitching-moment coefficient is due to the decrease in angle of attack to maintain a constant lift coefficient after deflecting the

flaps. A small part is due to the increase in the downwash from the inboard wing section caused by the flaps. The effect of the flaps on the wing is to decrease the pitching moment in practically all cases shown. This effect is probably due to the rearward location of the flaps on the wing, this position on the airplane being dictated only by structural reasons. A comparison of figures 12 and 19 indicates that deflecting the auxiliary control flaps will keep the airplane statically stable for 0.05 Mach number higher between 0 and 0.15 M^2C_L. In addition, the net effect of the flaps is to increase the pitching-moment coefficient throughout the Mach number range (fig. 18). This characteristic reduces the upward elevator angle required for balance. The data, however, show that in most cases this desirable effect of the flaps is diminishing between 0.75 and 0.8 Mach number. It is possible that this trend may continue and the flaps may be useless or detrimental at somewhat higher Mach numbers. Because of their decreasing effectiveness at high Mach numbers, the flaps are perhaps a less desirable means of relieving the longitudinal-control difficulties of the airplane than is the wing bump.

Elevator Hinge-Moment Coefficient

Elevator hinge-moment coefficient with 0° tab angle.- The elevator hinge-moment coefficient as a function of elevator angle, Mach number, and M^2C_L is shown in figure 20. The presentation of these data is in "carpet" form. The axes of the curves showing the data at a constant Mach number are staggered proportional to their respective Mach numbers. Dashed lines are drawn to connect the hinge-moment coefficients for constant elevator angles.

Equation (2) of the appendix shows that the quantity $(d\delta_e/dM)_{M^2C_L, C_{h_e}=0}$ must be negative in order for the stick-free stability to be greater than the stick-fixed. This quantity is negative at the high Mach numbers, as indicated by the negative slopes of the curves for constant elevator angle (fig. 20). This negative quantity also indicates that stick-free stability will be maintained to a higher Mach number than stick-fixed stability.

Tab effectiveness.- The effectiveness of the tab in changing the elevator hinge moment is shown in figure 21. The effectiveness increases slightly with elevator angle from

-5° to 5° and, in general, decreases slightly with Mach number. These variations in the effectiveness, however, are so small as to be unimportant. The predicted control forces, discussed in a later section, indicate that the tab is sufficiently effective to trim the airplane up to at least 0.8 Mach number, the limit of the tests.

Elevator balance pressure.- The coefficients of the pressures acting on the balance seal are shown in figure 22. A leak at the inboard end of the seal on the left half of the elevator, discovered at the conclusion of the tests, caused the absolute magnitude of the pressure coefficient at negative elevator angles to be less at the inboard station. This leak will tend to cause the calculated stick forces to be larger than experienced by the airplane. However, it should have no effect on the pitching-moment coefficient, and little effect on the speed at which the stick-force variation becomes unstable.

Elevator Angle and Stick Force

Elevator angle and stick force as a function of velocity.- The elevator angle and computed stick force are shown as a function of velocity for several wing loadings and center-of-gravity positions in figure 23. The effect of the bump on the control force and angle is shown in figure 24, and the effect of the auxiliary control flaps is shown in figure 25. The data are shown for sea-level and 20,000 feet altitudes. Conclusions with respect to stability characteristics similar to those made in discussing the pitching-moment coefficients can be derived from these data. (The increases in the elevator angle and in the push required on the stick with increasing speed indicate stick-fixed and stick-free stability, respectively.) Figure 23 shows that an increase in wing loading or a forward movement of the center of gravity increases both the stick-fixed and stick-free stability. The results indicate that the airplane will become unstable, stick fixed, above approximately 530 miles per hour at sea level and 480 miles per hour at 20,000 feet altitude (approx. 0.7 Mach number in both cases). The predicted effect of the bump (fig. 24) is to maintain stick-fixed stability throughout the speed range of the tests at sea level and up to 530 miles per hour at 20,000 feet altitude. A deflection of the

flaps gives a large increase in the elevator angle and in the push required on the stick at all speeds (fig. 25). The data indicate that the airplane will remain stable, stick fixed, to a higher speed with the flaps deflected than with the flaps up.

Figures 26 and 27 show the effect of tab angle on the stick force for the normal and the wing-bump configurations. These data indicate that the tab is capable of trimming the airplane up to speeds corresponding to 0.8 Mach number, the limit of the tests (approx. 610 mph at sea level and 570 mph at 20,000 ft altitude). The data also indicate that stick-free instability will occur at approximately 570 miles per hour at sea level and 530 miles per hour at 20,000 feet altitude.

Stick-force gradient.- The stick-force gradient as a function of geometric overhang is shown for the normal center-of-gravity location in figure 28. The gradient is higher than that recommended in reference 8 for a limit load factor of 4 (33 lb per g) even with a geometric overhang of 45 percent. However, with the center of gravity at its farthest aft position and for a geometric overhang of 40.5 percent, the gradient is very small except at the highest speed (fig. 29). It is possible that if the elevator seal had not leaked, the predicted stick-force gradient, although perhaps satisfactory for the normal location of the center of gravity, might have indicated overbalance at the furthest aft position.

Lift and Drag Characteristics

Lift coefficient.- The lift-coefficient data are presented as a carpet plot in figure 30. The data show that the lift coefficient at constant angle of attack decreases above about 0.69 Mach number for level-flight conditions (lift coefficients up to approximately 0.3 at 0.69 Mach number). This Mach number is 0.05 higher than the critical Mach number of the wing (fig. 17). The large decrease in $\partial C_L/\partial \alpha$ at supercritical Mach numbers is one factor causing the increase in angle of attack with Mach number necessary to maintain a constant lift coefficient. Another factor is the increase in the angle of zero lift indicated in the figure. These factors are largely responsible for the decrease in pitching-moment coefficient.

Drag coefficient.- The drag coefficient for the complete model is presented as a function of lift coefficient in figure 31, and as a function of Mach number in figure 32. The increase of drag coefficient with Mach number for the lower lift coefficients begins at 0.6 Mach number. The drag coefficient at the lower lift coefficients is approximately 55 percent greater at 0.72 (the airplane is placarded at 0.72 Mach number) than at the lower Mach numbers.

The drag coefficient for the wing alone (fig. 33) was obtained from tests of the wing with a thin sting replacing the fuselage. A comparison of figures 32 and 33 shows the drag coefficient of the wing (including the sting) to be about 55 percent of the total drag at the low Mach numbers and approximately 70 percent at 0.72 Mach number.

The increments of drag coefficient for the component parts of the model are shown in figure 34. The data indicate that the fuselage drag decreases at the high Mach numbers. This is probably due to the fact that the drag of that part of the wing covered by the fuselage was eliminated when the fuselage was in place. No consistent drag coefficient was obtained for the wing bump below 0.65 Mach number. The drag coefficient obtained was of such a small magnitude that it was assumed to be zero.

The increment of drag coefficient due to the auxiliary control flaps is shown in figure 35. The increment from the 30° flaps is approximately the same as for the fuselage and about one-half the increment from the 45° flaps. The general tendency is for the increment of drag coefficient from the flaps to decrease at high Mach numbers. This may be due to the following factors:

1. A reduction in the over-all drag caused by the angle-of-attack decrease necessary in maintaining a constant lift coefficient after deflecting the flaps.

2. An increase in the critical Mach number of the lower surface of the wing because of the increase in the peak pressure caused by the flaps.

3. The separation of the flow over the wing (partly responsible for the drag increment of the flaps at low Mach numbers) at supercritical Mach numbers even in the absence of the flaps.

Gliding velocity.- The velocity, time to descend, and the Mach number for the airplane at several glide angles (fig. 36) have been computed for zero propeller thrust. However, the difference due to the propeller at the larger glide angles should be small because the propeller efficiency becomes smaller at high Mach numbers, and the thrust is small compared with the weight component in the thrust direction. For example, for an airplane weight of 25,000 pounds, the thrust at normal rated power would be only 14 percent of the weight component in a 20° glide (assuming a propulsive efficiency of 80 percent at 0.7 Mach number and 10,000 ft altitude).

The maximum velocity and Mach number predicted for the several gliding angles in figure 36, together with those from similar data for other configurations, are shown in figures 37 and 38. The altitudes at which the maximum velocity and Mach number are reached are also shown. These figures show that the flaps could be used as dive brakes in addition to their function of increasing the lift coefficient at balance. The 30° and 45° flaps reduce the maximum predicted velocity by 20 and 40 miles per hour, respectively. The maximum Mach number is reduced by 0.025 and 0.045. Comparing airplane weights of 25,000 and 35,000 pounds, the maximum velocity for the heavier load is between 20 and 30 miles per hour higher, and the maximum Mach number between 0.025 and 0.030 larger (depending on the gliding angle). The data indicate that the bump has no effect on the maximum velocity or Mach number except at the higher gliding angles.

Aileron Characteristics

Rolling-moment and hinge-moment coefficients.- The aileron rolling-moment and hinge-moment coefficients are shown in figure 39. The data show that the aileron effectiveness ($\delta C_l / \delta \delta_a$) decreases at the larger aileron angles. The negative rolling-moment coefficient is slightly smaller than that shown by other data for approximately the same size aileron (reference 9). This may be due to the low-drag wing section used on the airplane.

Angle and wheel force.- The aileron angle and wheel forces as functions of pb/2V, the helix angle of the path of the wing tip, are shown in figure 40. The data show that the increase in pb/2V with aileron angle is smaller at the higher angles. The data also indicate that the aileron was not powerful enough at the maximum angle tested, as the Army

Air Forces specifications (reference 8) require a pb/2V
of at least 0.07. It is possible, however, that decreasing
pb/2V by 20 percent (see Reduction of Data) was too
conservative, and that the aileron is slightly more powerful
than indicated.

The predicted wheel force is excessive at sea level.
(Reference 8 specifies 80 lb as the maximum wheel force for
a pb/2V equal to 0.07.) Although the force should be
smaller on the airplane due to the larger balance area, it
may still be greater than the desired limit. This large
wheel force, together with the decreasing effectiveness of
the aileron at large angles, restricts the use of larger
control-surface deflections necessary to obtain the required
pb/2V.

CONCLUDING REMARKS

The more important predictions and conclusions made from
the analysis of the data from the tests of a midwing airplane
model are as follows:

1. The airplane will be unstable stick fixed above 0.7
Mach number (530 mph at sea level to 480 mph at 20,000 ft
altitude).

2. A wing-profile modification (called a wing bump) on
the lower surface maintains stick-fixed stability to a Mach
number as much as 0.075 higher. Below 0.7 Mach number the
wing bump had no noticeable effect on the aerodynamic char-
acteristics of the model.

3. Auxiliary control flaps increase the Mach number at
which stick-fixed instability occurs by approximately 0.05.
However, the effectiveness of the flaps decreases between 0.75
and 0.80 Mach number. They are therefore a less desirable
means of improving the longitudinal control at high Mach
numbers than the wing bump.

4. The data indicate that the tab will trim the airplane
up to speeds corresponding to 0.8 Mach number, the limit of the
tests (approx. 610 mph at sea level and 570 mph at 20,000 ft
altitude).

5. Stick-free stability is maintained to a higher speed than stick-fixed stability.

6. The data indicate that the aileron is not as effective as desirable, and that the wheel force is higher than recommended by U.S. Army specifications.

Ames Aeronautical Laboratory,
      National Advisory Committee for Aeronautics,
            Moffett Field, Calif.,

APPENDIX

Stick-Fixed Stability Considering Mach Number in Addition to Lift Coefficient

The general relation for the pitching-moment coefficient is

$$C_m = f(C_L) + f(\delta_e) + f(M)$$

or

$$dC_m = \left(\frac{\partial C_m}{\partial C_L}\right)_{\delta_e, M} dC_L + \left(\frac{\partial C_m}{\partial \delta_e}\right)_{C_L, M} d\delta_e + \left(\frac{\partial C_m}{\partial M}\right)_{C_L, \delta_e} dM$$

The subscripts to each derivative indicate the variables which are held constant.

For stick-fixed stability

$$d\delta_e = 0$$

For an airplane in steady flight at a constant altitude and wing loading, and with the temperature remaining constant,

$$M^2 C_L = \frac{\text{wing loading}}{\frac{1}{2}\rho \, a^2} = \text{constant}$$

therefore

$$dC_L = -\frac{4(\text{wing loading})}{\rho \, a^2 M^3} dM$$

and

$$dC_m = \left(\frac{\partial C_m}{\partial M}\right)_{C_L, \delta_e} dM + \frac{4(\text{wing loading})}{\rho \, a^2 M^3}\left(-\frac{\partial C_m}{\partial C_L}\right)_{\delta_e, M} dM$$

$$\left(\frac{dC_m}{dM}\right)_{M^2C_L,\delta_e} = \left(\frac{\partial C_m}{\partial M}\right)_{C_L,\delta_e} + \frac{4(\text{wing loading})}{\rho \, a^2 \, M^3}\left(-\frac{\partial C_m}{\partial C_L}\right)_{\delta_e,M} \tag{1}$$

Stick-Free Stability Considering Mach Number in Addition to Lift Coefficient

From the original relationship

$$dC_m = \left(\frac{\partial C_m}{\partial C_L}\right)_{\delta_e,M} dC_L + \left(\frac{\partial C_m}{\partial \delta e}\right)_{C_L,M} d\delta_e + \left(\frac{\partial C_m}{\partial M}\right)_{C_L,\delta_e} dM$$

The same relation between Mach number and lift coefficient will hold as before, but for stick-free stability $d\delta_e$ will not equal zero. However, dC_{h_e} will equal zero. Therefore

$$\left(\frac{dC_m}{dM}\right)_{M^2C_L,C_{h_e}=0} = \left[\frac{\text{wing loading}}{\rho \, a^2 \, M^3}\left(-\frac{\partial C_m}{\partial C_L}\right)_{\delta_e,M} + \left(\frac{\partial C_m}{\partial M}\right)_{C_L,\delta_e}\right]$$

$$+ \left[\left(\frac{\partial C_m}{\partial \delta_e}\right)_{C_L,M}\right]\left[\left(\frac{d\delta_e}{dM}\right)_{M^2C_L,C_{h_e}=0}\right]$$

or

$$\left(\frac{dC_m}{dM}\right)_{M^2C_L,C_{h_e}=0} = \left[\left(\frac{dC_m}{dM}\right)_{M^2C_L,\delta_e}\right] + \left[\left(\frac{\partial C_m}{\partial \delta e}\right)_{C_L,M}\right]$$

$$\left[\left(\frac{d\delta_e}{dM}\right)_{M^2C_L,C_{h_e}=0}\right] \tag{2}$$

REFERENCES

1. Silverstein, Abe, and White, James A.: Wind-Tunnel Interference with Particular Reference to Off-Center Positions of the Wing and to the Downwash at the Tail. NACA Rep. No. 547, 1935.

2. Silverstein, Abe, and Katzoff, S.: Design Charts for Predicting Downwash Angles and Wake Characteristics Behind Plain and Flapped Wings. NACA Rep. No. 648, 1939.

3. Jones, B. Melvill: Dynamics of the Airplane, vol. V, div. N, chap. II, sec. 29 - 33 of Aerodynamic Theory, W.F. Durand ed., Julius Springer (Berlin), 1935.

4. Pearson, Henry A., and Jones, Robert T.: Theoretical Stability and Control Characteristics of Wings with Various Amounts of Taper and Twist. NACA Rep. No. 635, 1938.

5. Swanson, Robert S., and Toll, Thomas A.: Estimation of Stick Forces from Wind-Tunnel Aileron Data. NACA ARR No. 3J29, 1943.

6. Hood, Manley J., and Allen, H. Julian: The Problem of Longitudinal Stability and Control at High Speeds. NACA CB No. 3K18, 1943.

7. Erickson, Albert L.: Wind-Tunnel Investigation of Devices for Improving the Diving Characteristics of P-38 Airplanes. NACA CiR No. 3F12, 1943.

8. Anon.: Stability and Control Requirements for Airplanes. Spec. No. C-1815, U.S. Army Air Forces, Aug. 31, 1943.

9. Wenzinger, Carl J.: Wind-Tunnel Investigation of Tapered Wings with Ordinary Ailerons and Partial-Span Split Flaps. NACA Rep. No. 611, 1937.
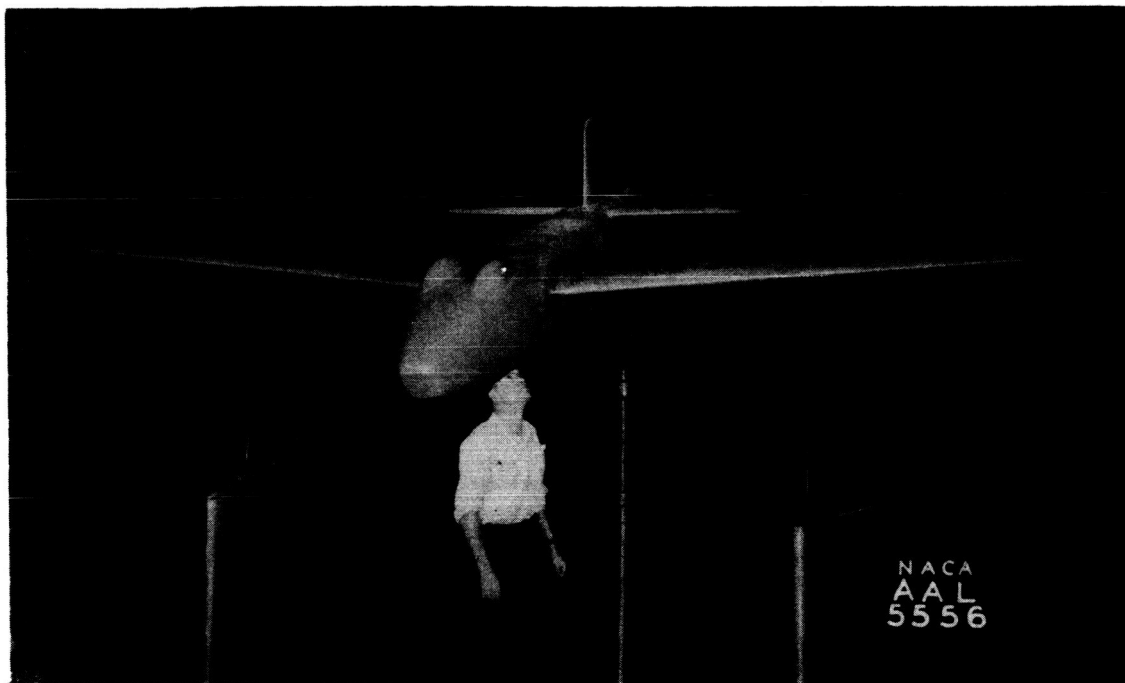
Figure 1.- The complete 0.175-scale model of the airplane in the 16-foot wind tunnel.
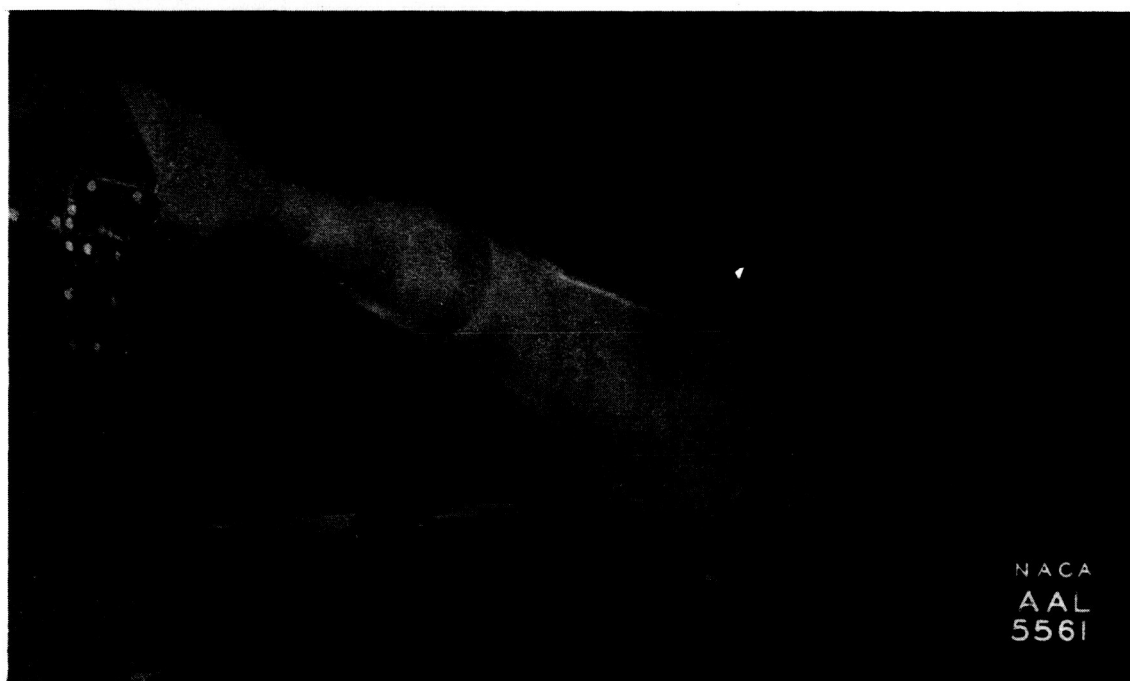
Figure 2.- The 0.175-scale model of the airplane with the empennage removed.

Figure 3.- The empennage of the 0.175-scale model of the airplane.
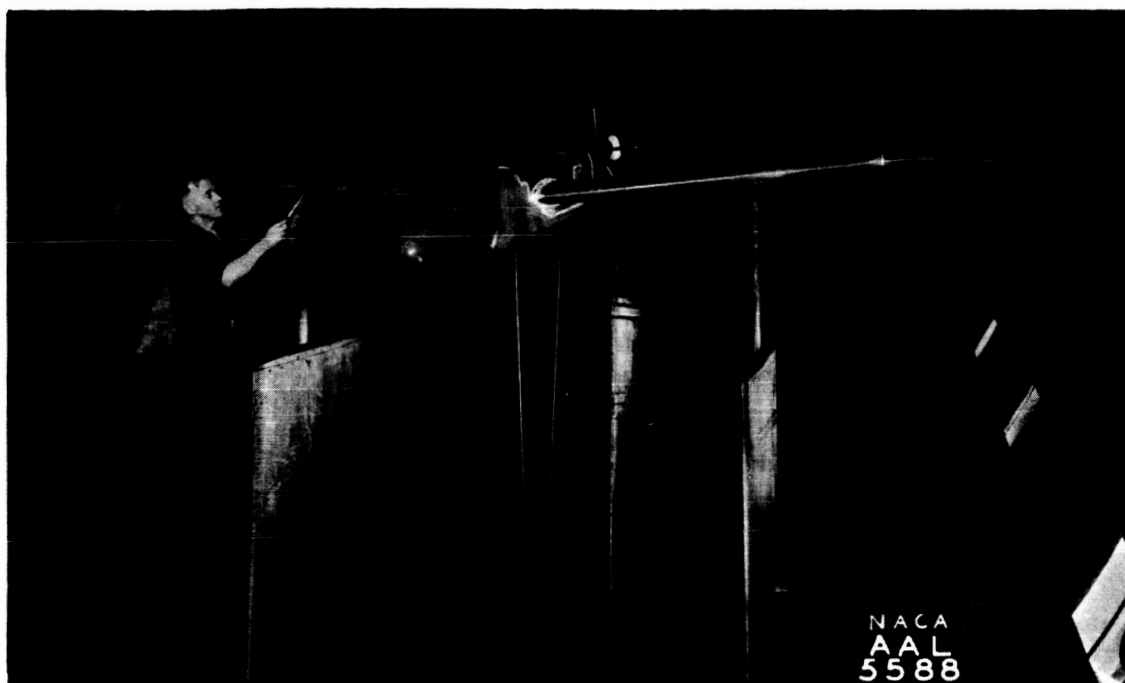
Figure 4.- The 0.175-scale model of the airplane mounted on the tip supports and three struts.
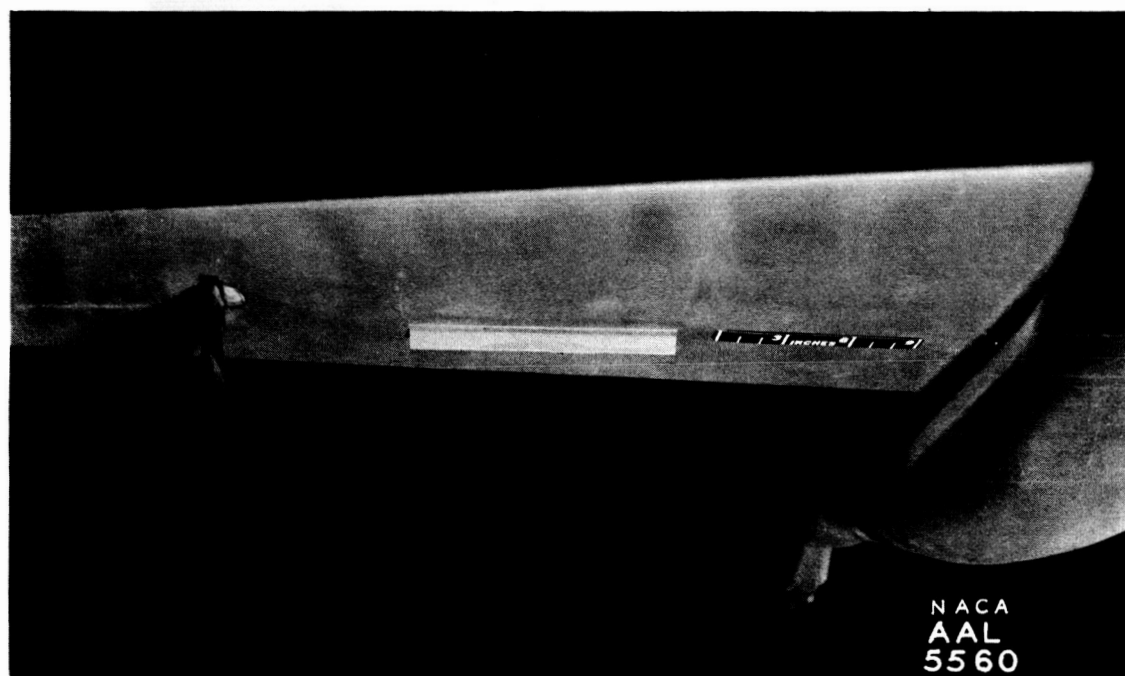
Figure 5.- The 45° auxiliary control flaps on the 0.175-scale model of the airplane.

FUSELAGE
REF. LINE

WING REF.
PLANE AT ROOT

TAIL REF. PLANE

110.5"

21.2"

36.5"

.50"

0.437"

52.5"

HINGE LINE
65% CHORD

26% M.A.C_H
MAC_H = 12.14"

41.8"

85% CHORD

HINGE LINE
78% CHORD

25% M.A.C.
M.A.C. = 17.98"

24.6"

148"

45.0"

DIHEDRAL OF WING
REF. PLANE = 4°

₵ SYM.
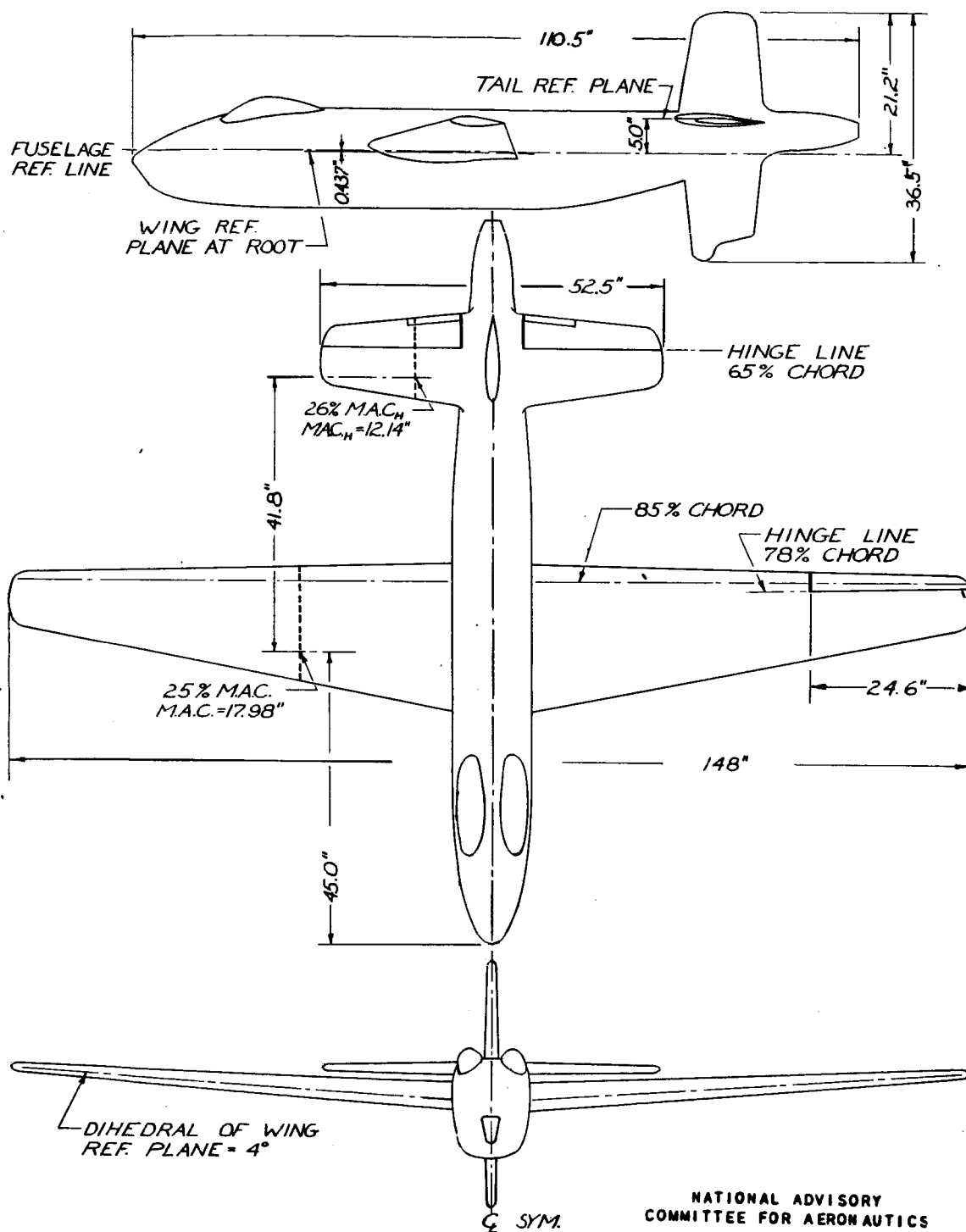
FIGURE 6 - THE 0.175-SCALE MODEL.

WING TRAILING EDGE

85% CHORD

BUMP OUTLINE

57% CHORD

A

42% CHORD

A

STA 26.25

PRESSURE
ORIFICES
STA. 12

℄
SYM

FUSELAGE
OUTLINE
STA 6.25

57%
CHORD

SEC. AA
FULL MODEL SCALE

42%
CHORD

% CHORD LOWER SURFACE	WING - BUMP COORDINATES INCHES	
	STA. 6.25	STA. 26.25
42	0	0
43	0.0048	0.0039
44	0.0066	0.0053
45	0.0094	0.0076
46	0.0122	0.0099
47	0.0188	0.0152
48	0.0366	0.0296
49	0.0638	0.0516
49.5	0.0658	0.0531
50	0.0658	0.0531
51	0.0384	0.0310
52	0.0160	0.0129
53	0.0094	0.0076
54	0.0076	0.0062
55	0.0048	0.0039
56	0.0048	0.0039
57	0	0
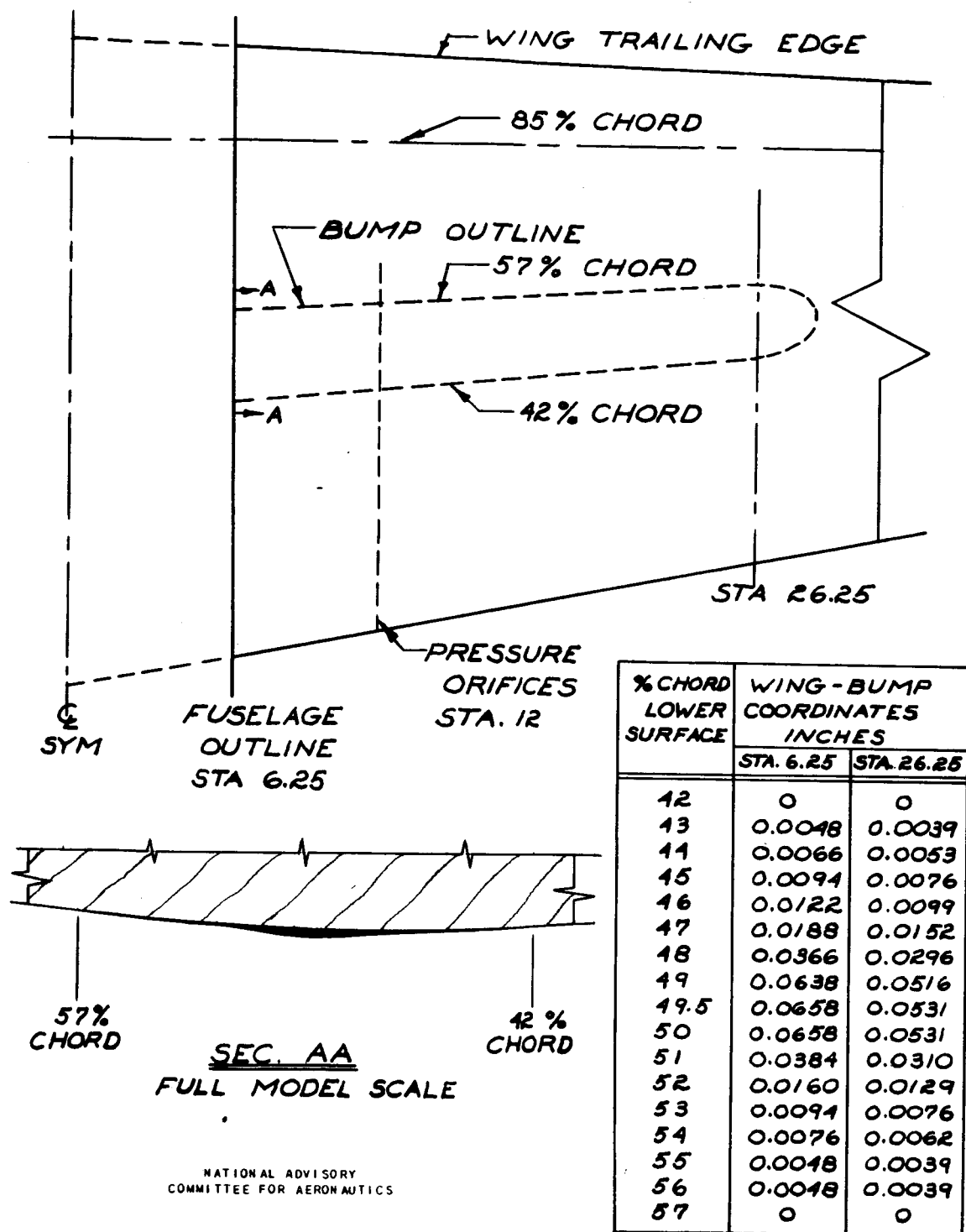
FIGURE 7.—THE LOCATION AND COORDINATES OF
THE BUMP ON THE WING OF THE 0.175-SCALE,
MODEL.

$$M^2 C_L = \frac{WING\ LOADING \times g}{\tfrac{1}{2} e\, a^2}$$

EXAMPLE
  GIVEN:
    WING LOADING = 45
    ACCELERATION = 2 g
    ALTITUDE = 20,000 FT.
  RESULT:
    $M^2 C_L$ = 0.130

MAXIMUM $M^2 C_L$ FROM WIND-TUNNEL DATA

$M^2 C_L$

.5
.4
.3
.2
.1
0

ALTITUDE 40,000 FT.
35,000 FT.
30,000 FT.
25,000 FT.
20,000 FT.
15,000 FT.
10,000 FT.
5,000 FT.
SEA LEVEL

NATIONAL ADVISORY
COMMITTEE FOR AERONAUTICS

WING LOADING LB. PER SQ. FT.
30
40
50
60

ACCELERATION
1 g
2 g
3 g
4 g

LIMIT LOAD FACTOR
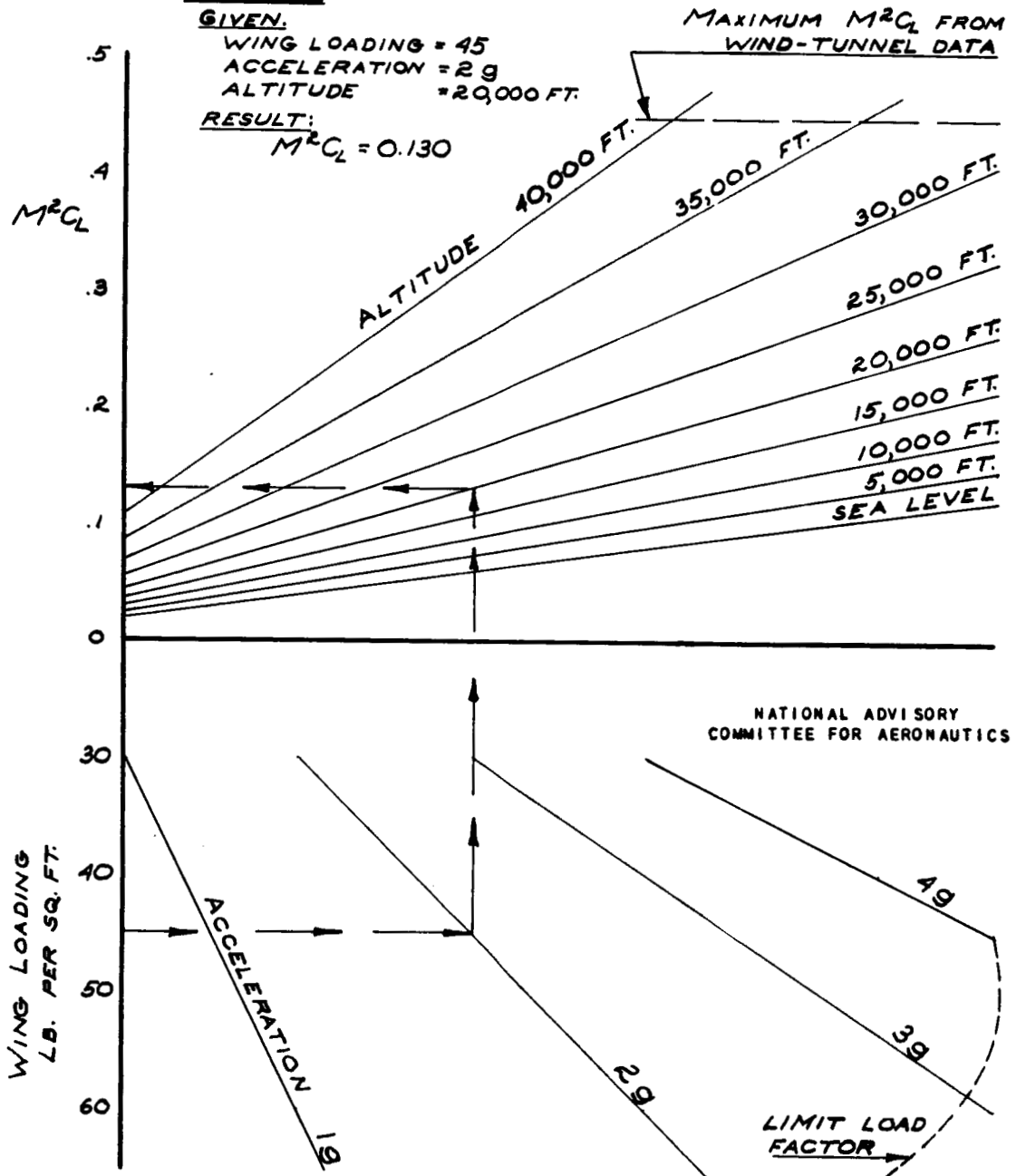
FIGURE 8.- THE RELATION BETWEEN $M^c C_L$ AND WING LOADING, NORMAL ACCELERATION, AND ALTITUDE FOR THE AIRPLANE.

$C_{L\,MAX}$ FOR MODEL WITH TAIL OFF
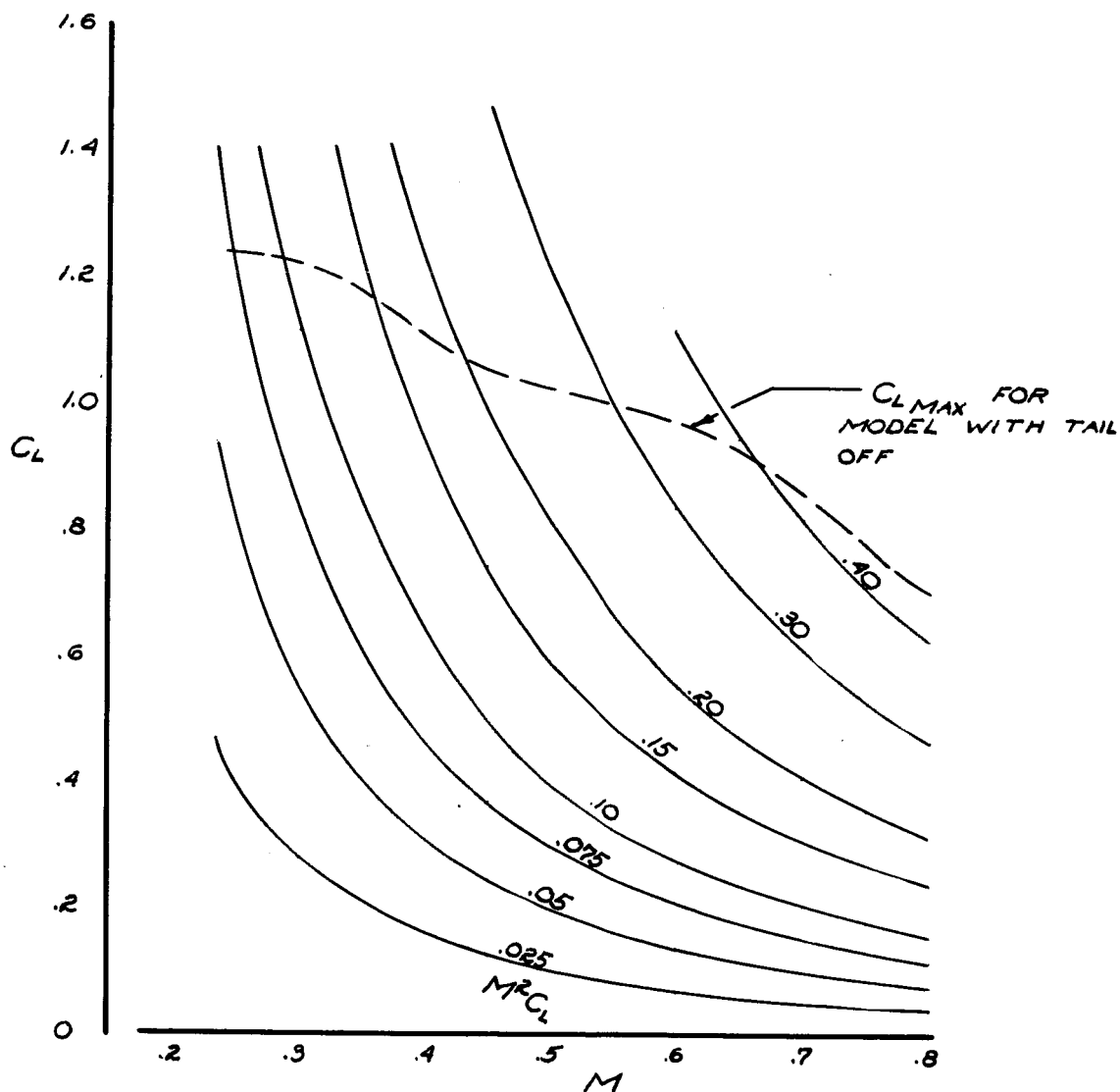
$M^2 C_L$

FIGURE 9.- THE RELATION BETWEEN THE LIFT COEFFICIENT, MACH NUMBER, AND $M^2 C_L$.
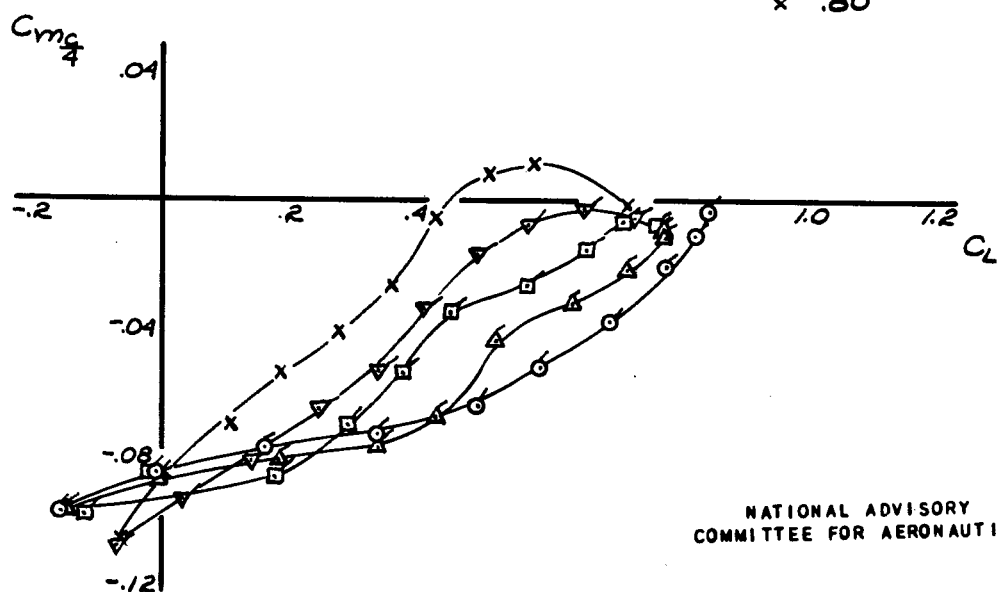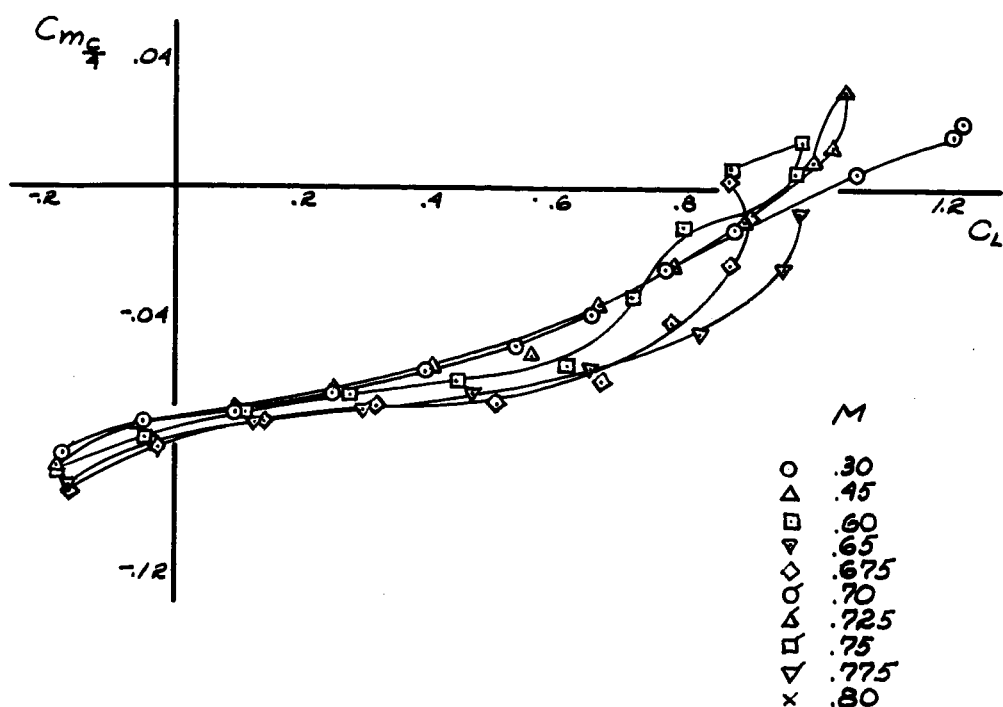
FIGURE 10.—THE VARIATION OF THE PITCHING-
MOMENT COEFFICIENT WITH LIFT COEFFICIENT
FOR THE MODEL WITHOUT THE TAIL PLANE.
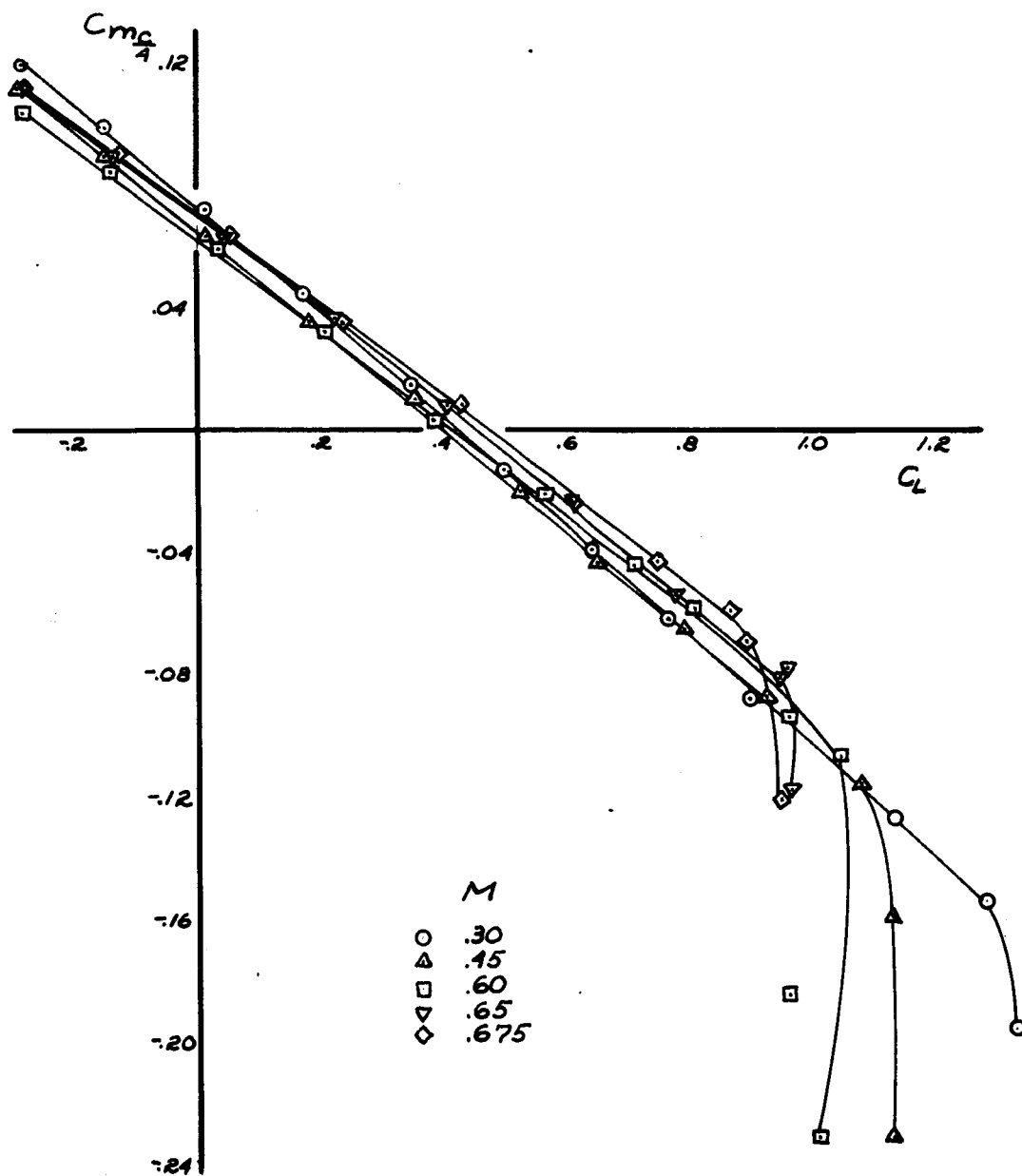
(a) M=0.30 TO 0.65

FIGURE 11.- THE VARIATION OF THE PITCHING-
MOMENT COEFFICIENT WITH LIFT COEFFICIENT
FOR THE MODEL.
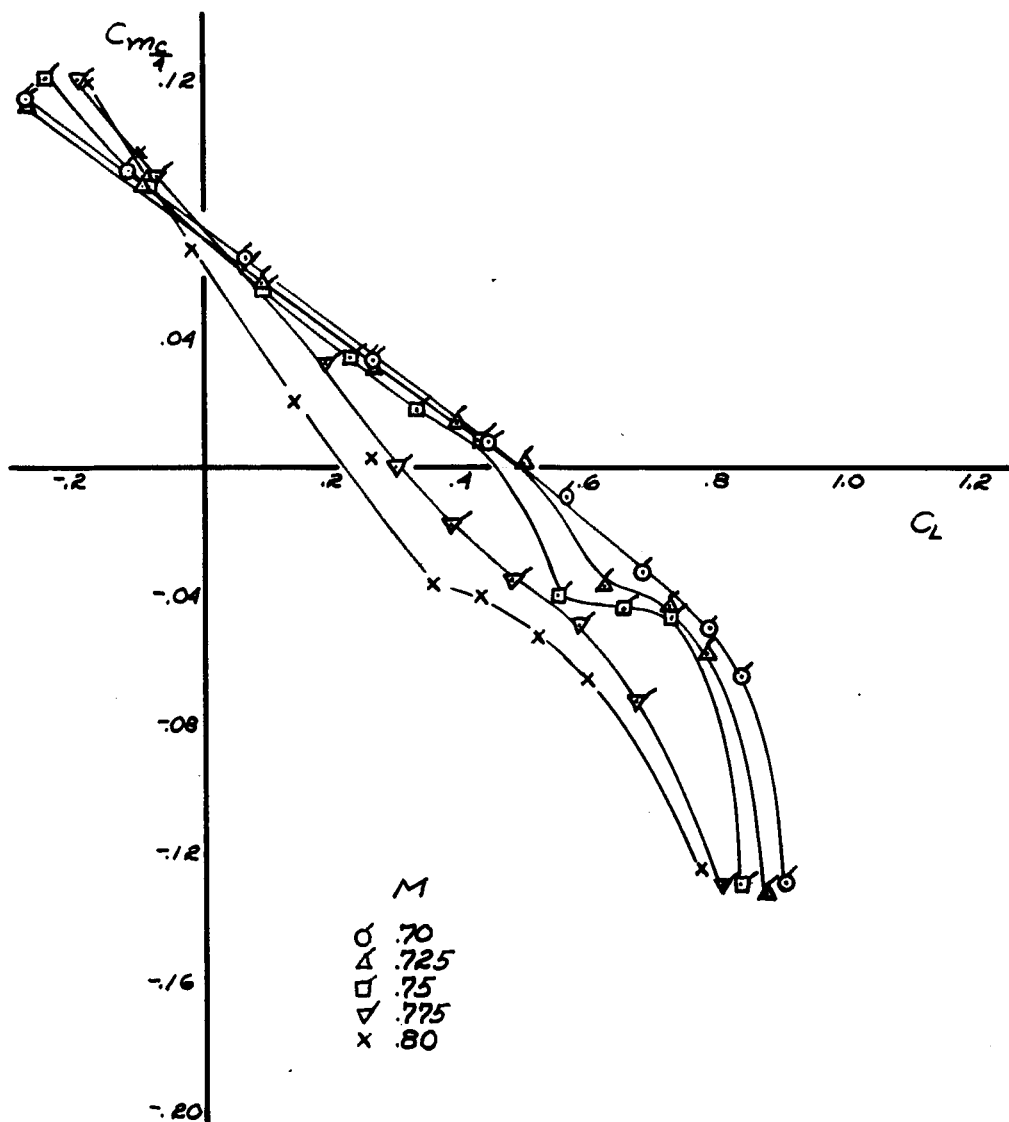
(b) M=0.70 TO 0.80
FIGURE 11.-(CONCLUDED) THE VARIATION OF THE
PITCHING-MOMENT COEFFICIENT WITH LIFT
COEFFICIENT FOR THE MODEL.
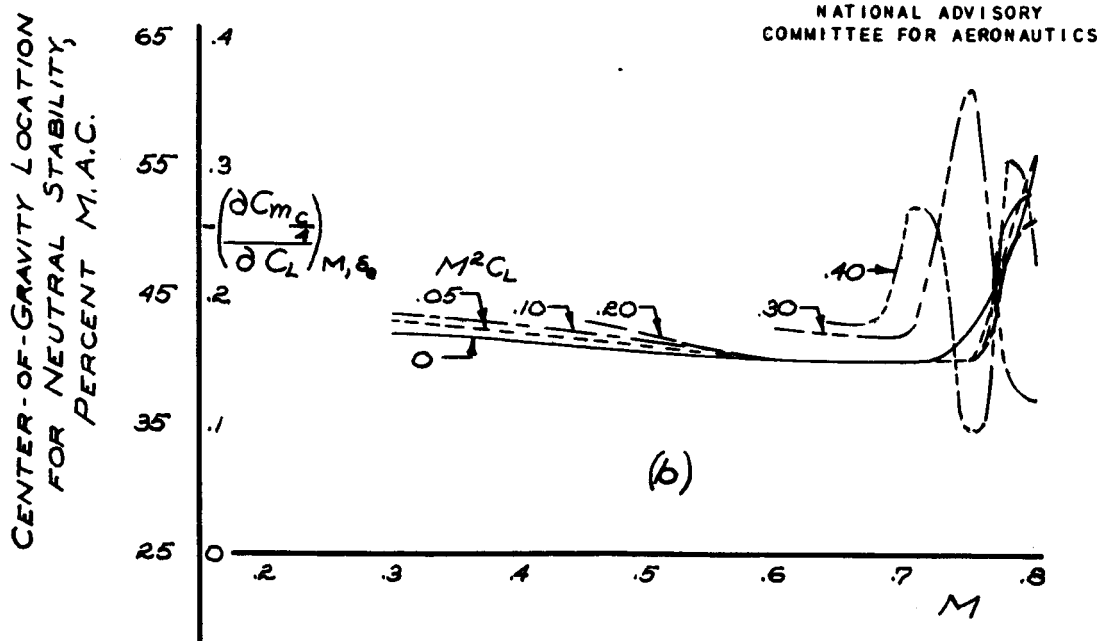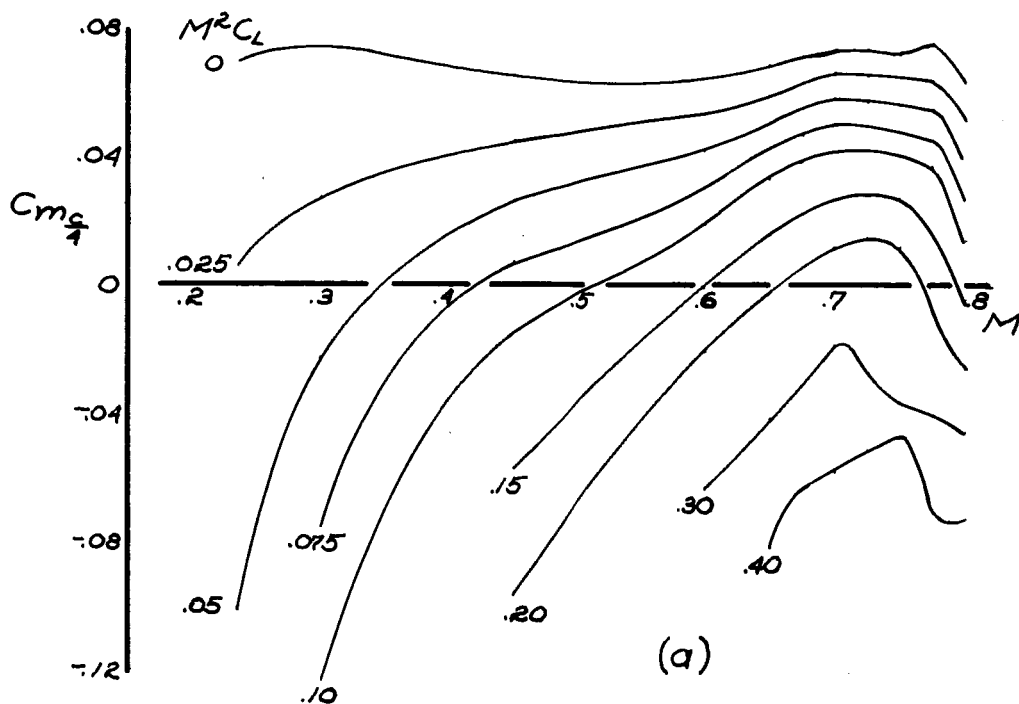
FIGURE 12.- THE EFFECT OF MACH NUMBER ON THE STICK-FIXED STABILITY CHARACTERISTICS OF THE MODEL.
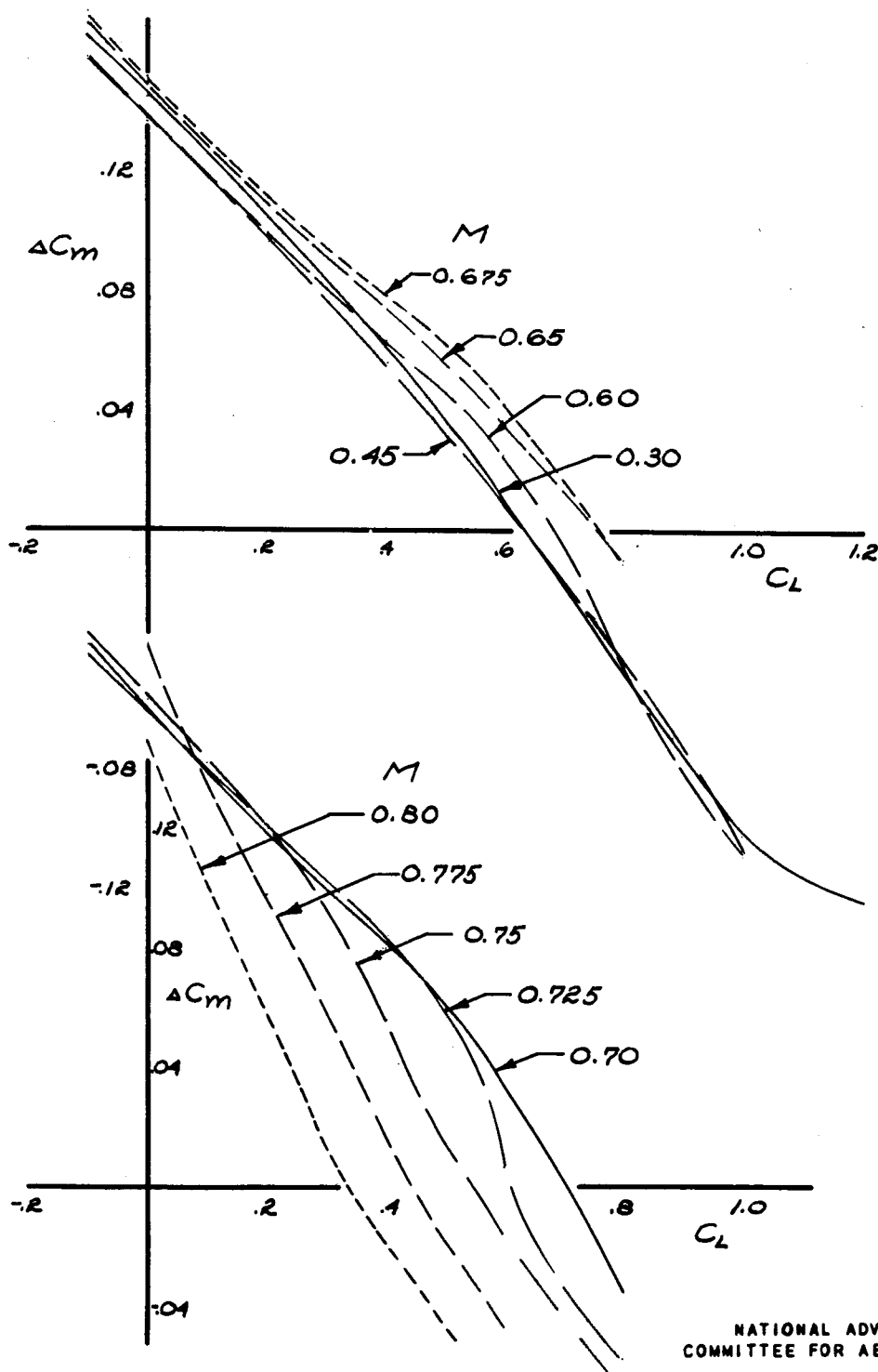
FIGURE 13.—THE PITCHING-MOMENT COEFFI-
CIENT CONTRIBUTED BY THE HORIZONTAL TAIL
PLANE OF THE MODEL.

FIGURE 14.— THE ELEVATOR EFFECTIVENESS AND THE EFFECT OF THE TAB ON THE PITCHING-MOMENT COEFFICIENT FOR THE MODEL.
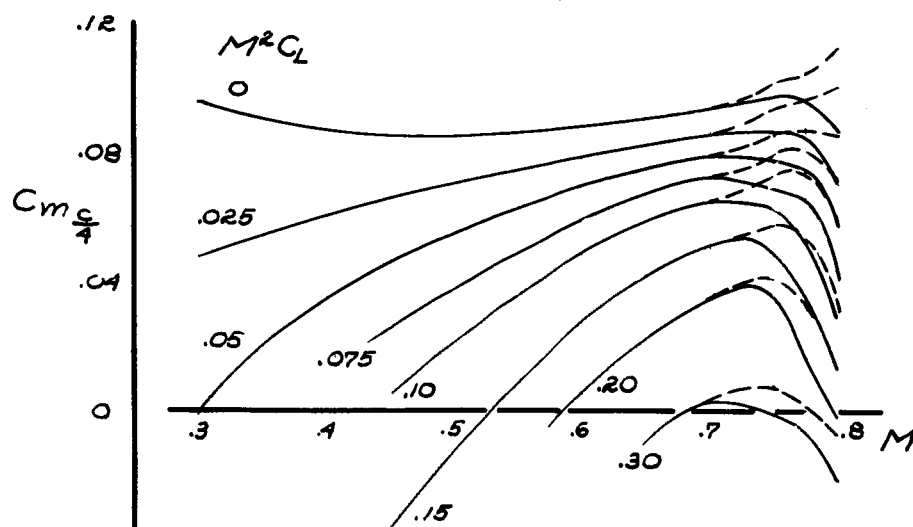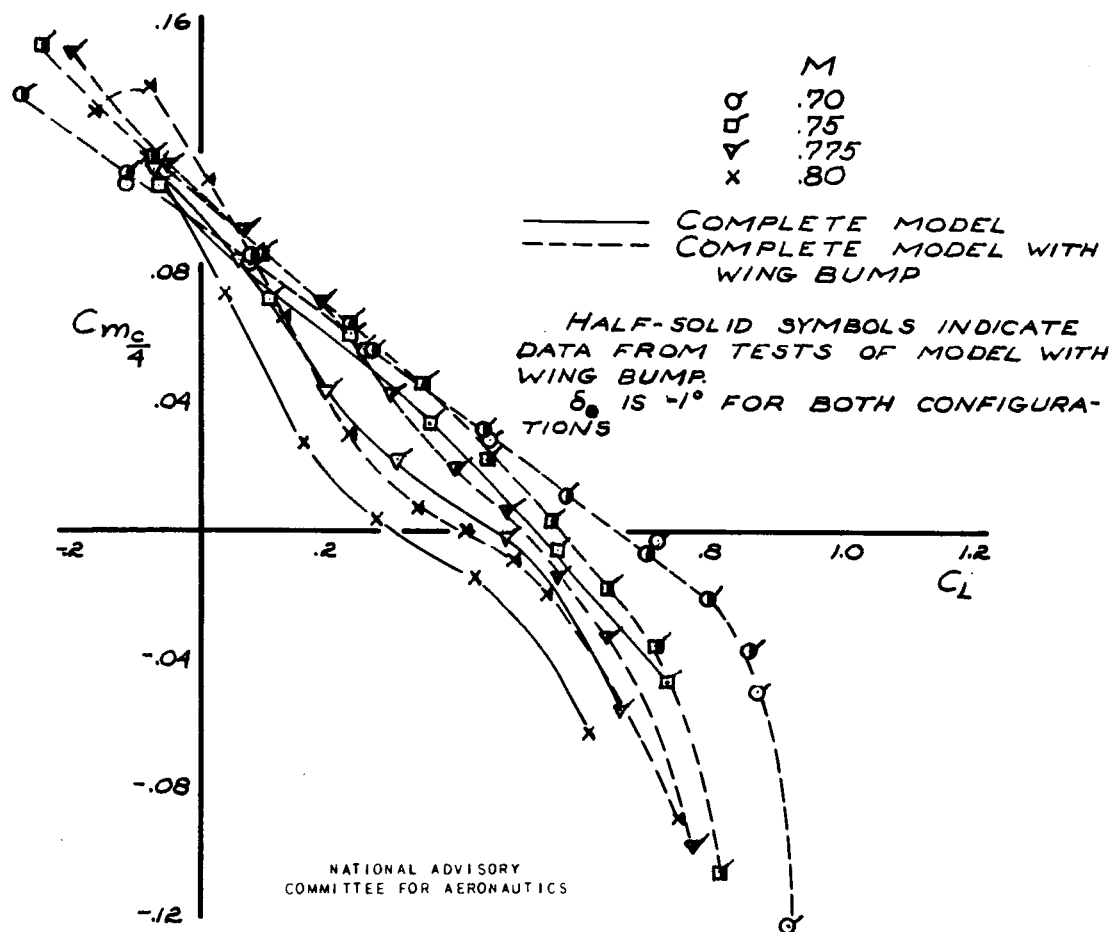
FIGURE 15.- THE EFFECT OF THE WING BUMP
ON THE PITCHING-MOMENT COEFFICIENT AT HIGH
MACH NUMBERS FOR THE MODEL.

M = 0.30
P_{cr} = -6.95
α = -2.9°

M = 0.45
P_{cr} = -2.76
α = -3.0°

M = 0.60
P_{cr} = -1.29
α = -3.1°

M = 0.65
α = -3.1°

——— WITHOUT WING BUMP
----- WITH WING BUMP

NATIONAL ADVISORY
COMMITTEE FOR AERONAUTICS
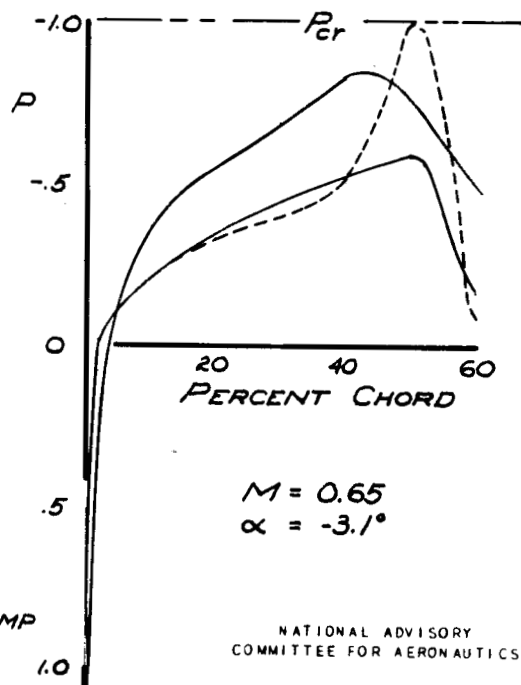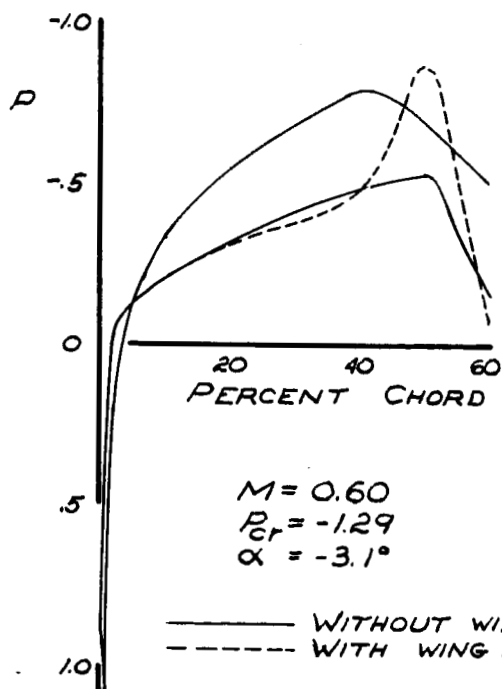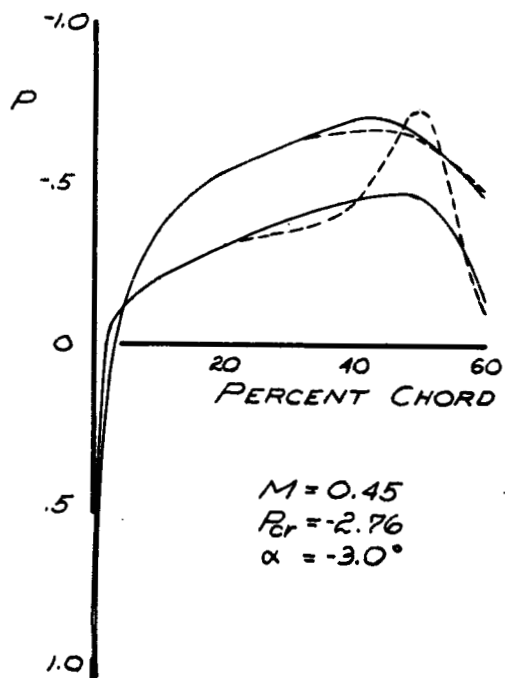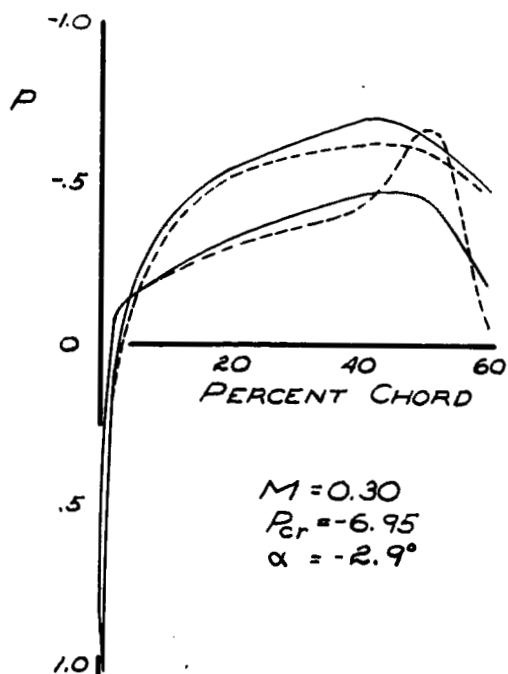
(a) M = 0.30, 0.45, 0.60, 0.65
FIGURE 16.- THE PRESSURE DISTRIBUTION AT WING STATION 12 OF THE MODEL WITH AND WITHOUT WING BUMP, AT A LIFT COEFFICIENT OF 0.1 FOR THE COMPLETE MODEL.

P_{cr}

PERCENT CHORD

$M = 0.70$
$\alpha = -3.2°$

P_{cr}

PERCENT CHORD

$M = 0.75$
$\alpha = -3.0°$

P_{cr}

PERCENT CHORD

$M = 0.775$
$\alpha = -2.4°$

P_{cr}

PERCENT CHORD

$M = 0.80$
$\alpha = -1.5°$

——— WITHOUT WING BUMP
------- WITH WING BUMP

NATIONAL ADVISORY
COMMITTEE FOR AERONAUTICS
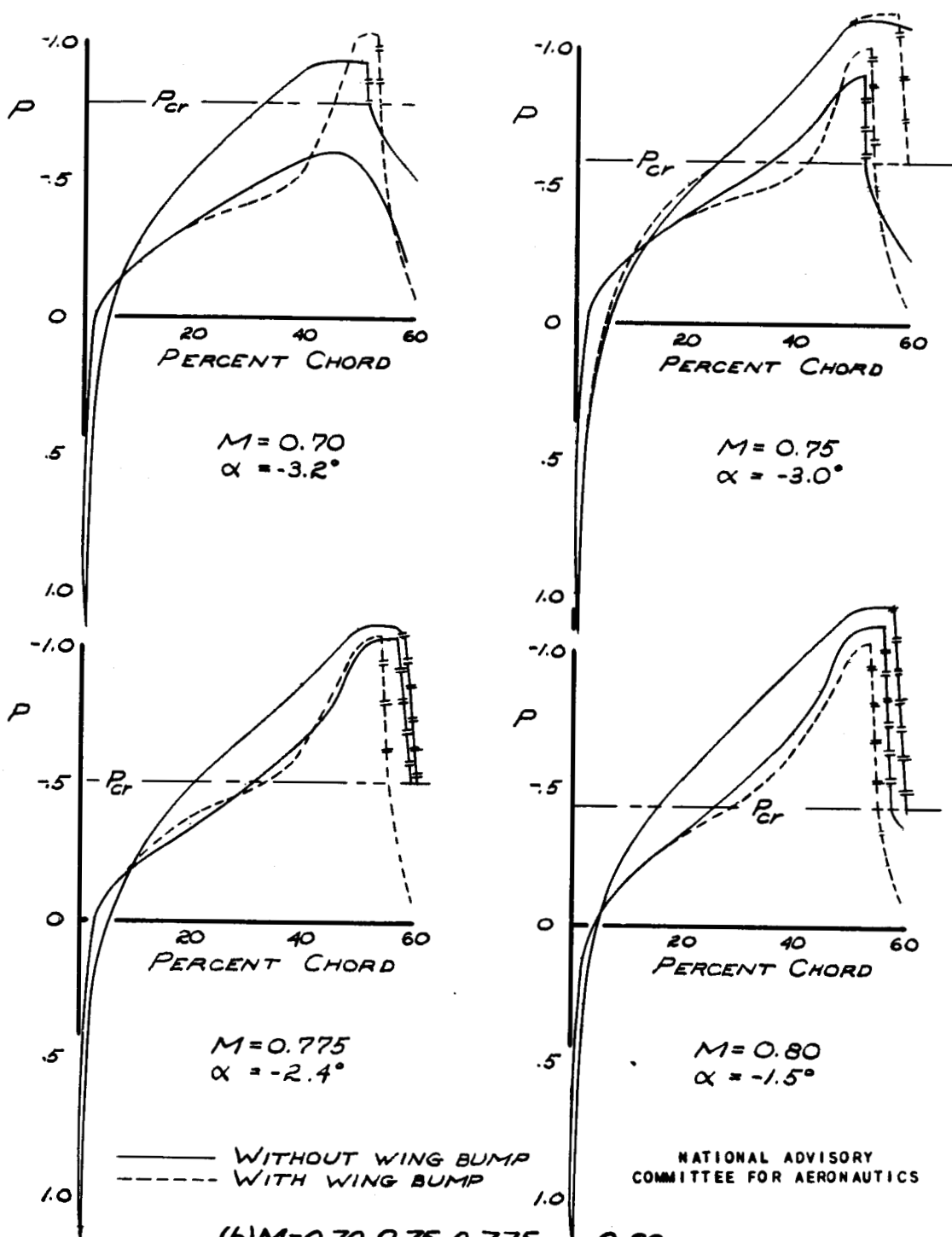
(b) M=0.70, 0.75, 0.775, 0.80

FIGURE 16.-(CONCLUDED) THE PRESSURE DISTRIBU-
TION AT WING STATION 12 OF THE MODEL WITH AND
WITHOUT WING BUMP AT A LIFT COEFFICIENT OF 0.1
FOR THE COMPLETE MODEL.

FIGURE 17.- THE CRITICAL MACH NUMBER AT SEVERAL WING STATIONS FOR THE MODEL.
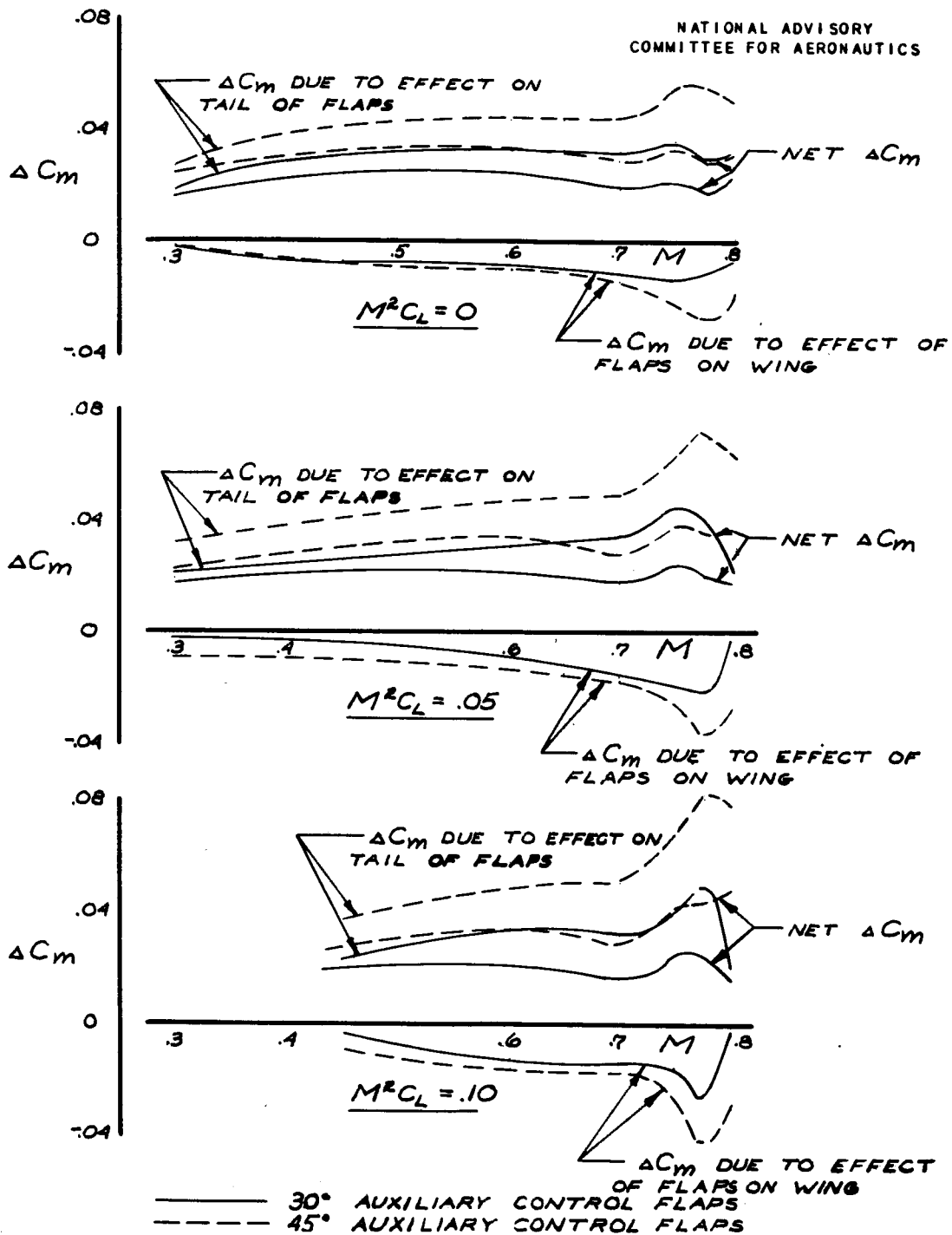
(a) $M^2C_L = 0, .05, .10$

FIGURE 18.- THE INCREMENT OF THE PITCHING-MOMENT COEFFICIENT DUE TO AUXILIARY CONTROL FLAPS ON THE MODEL.

.08

.04

ΔC_m

ΔC_m DUE TO EFFECT
ON TAIL OF FLAPS

NET ΔC_m

0

.3   .4   .5   .6   .7 M .8

ΔC_m DUE
TO EFFECT OF
FLAPS ON WING

-.04

$M^2 C_L = .15$

.08

.04

ΔC_m

ΔC_m DUE TO EFFECT
ON TAIL OF FLAPS

NET ΔC_m

0

.3   .4   .5   .6   .7 M .8

ΔC_m DUE TO
EFFECT OF
FLAPS ON WING

-.04

$M^2 C_L = .20$

.08

.04

ΔC_m

ΔC_m DUE TO EFFECT
ON TAIL OF FLAPS

NET ΔC_m

0

.3   .4 M .5   .6   .7   .8

ΔC_m DUE TO
EFFECT OF
FLAPS ON WING

-.04

$M^2 C_L = .30$
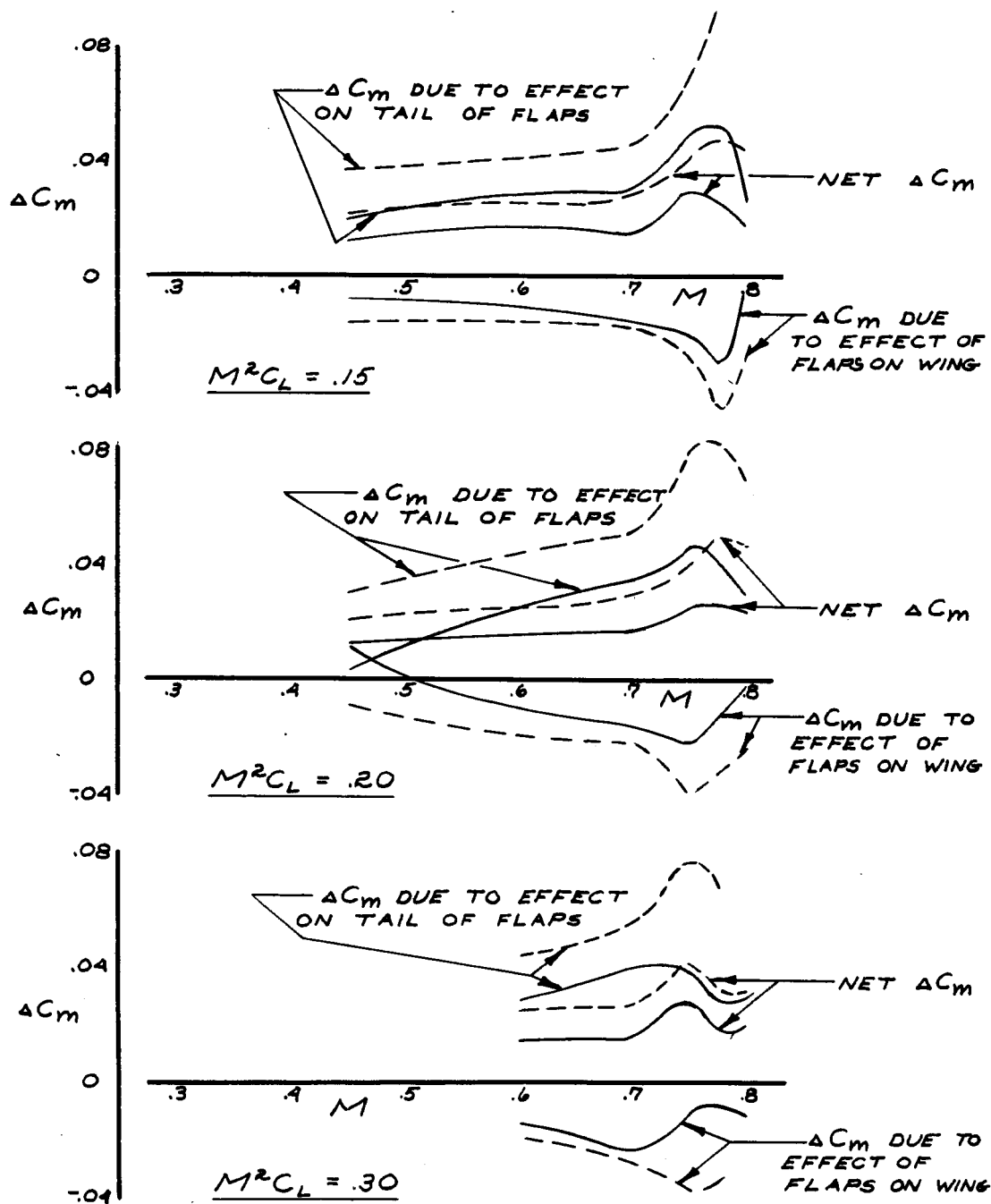
NATIONAL ADVISORY
COMMITTEE FOR AERONAUTICS

————————   30° AUXILIARY CONTROL FLAPS
- - - - - - -   45° AUXILIARY CONTROL FLAPS

(b) $M^2 C_L = .15, .20, .30$

FIGURE 18.-(CONCLUDED) THE INCREMENT OF
PITCHING-MOMENT COEFFICIENT DUE TO AUXILIARY
CONTROL FLAPS ON THE MODEL.

30° AUXILIARY CONTROL FLAPS

45° AUXILIARY CONTROL FLAPS
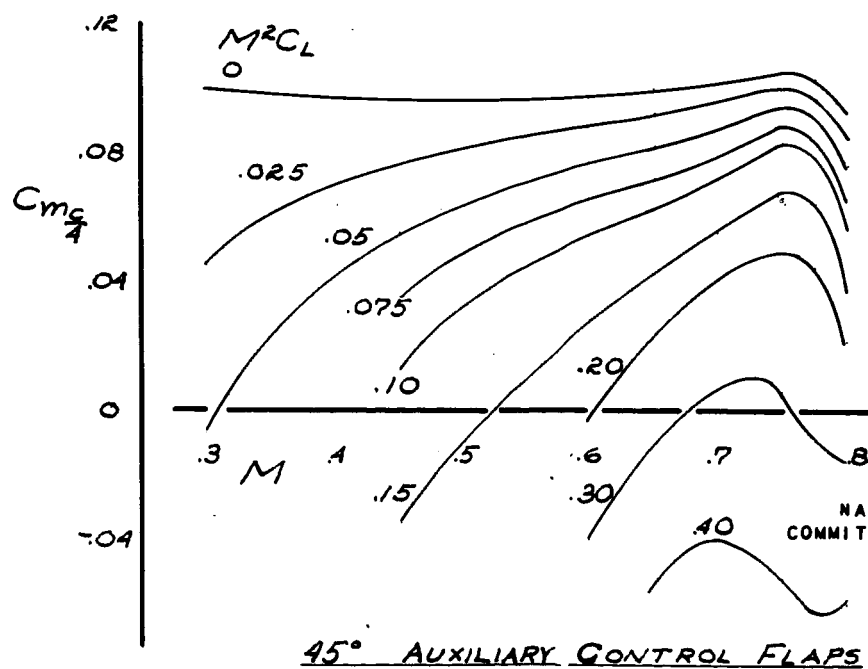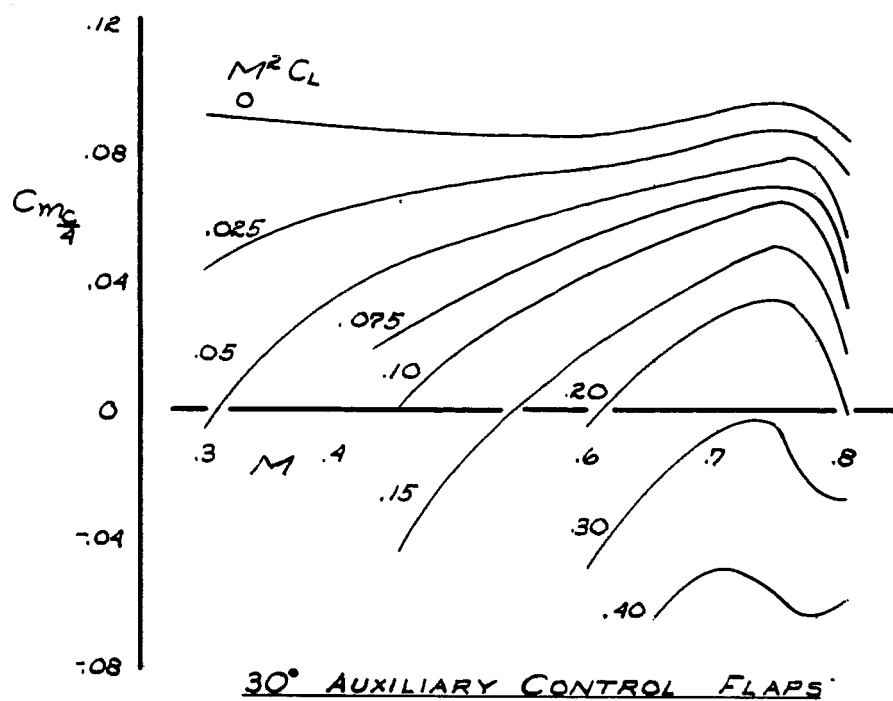
NATIONAL ADVISORY
COMMITTEE FOR AERONAUTICS

FIGURE 19.—THE STICK-FIXED STABILITY CHAR-
ACTERISTICS OF THE MODEL WITH AUXILIARY
CONTROL FLAPS.
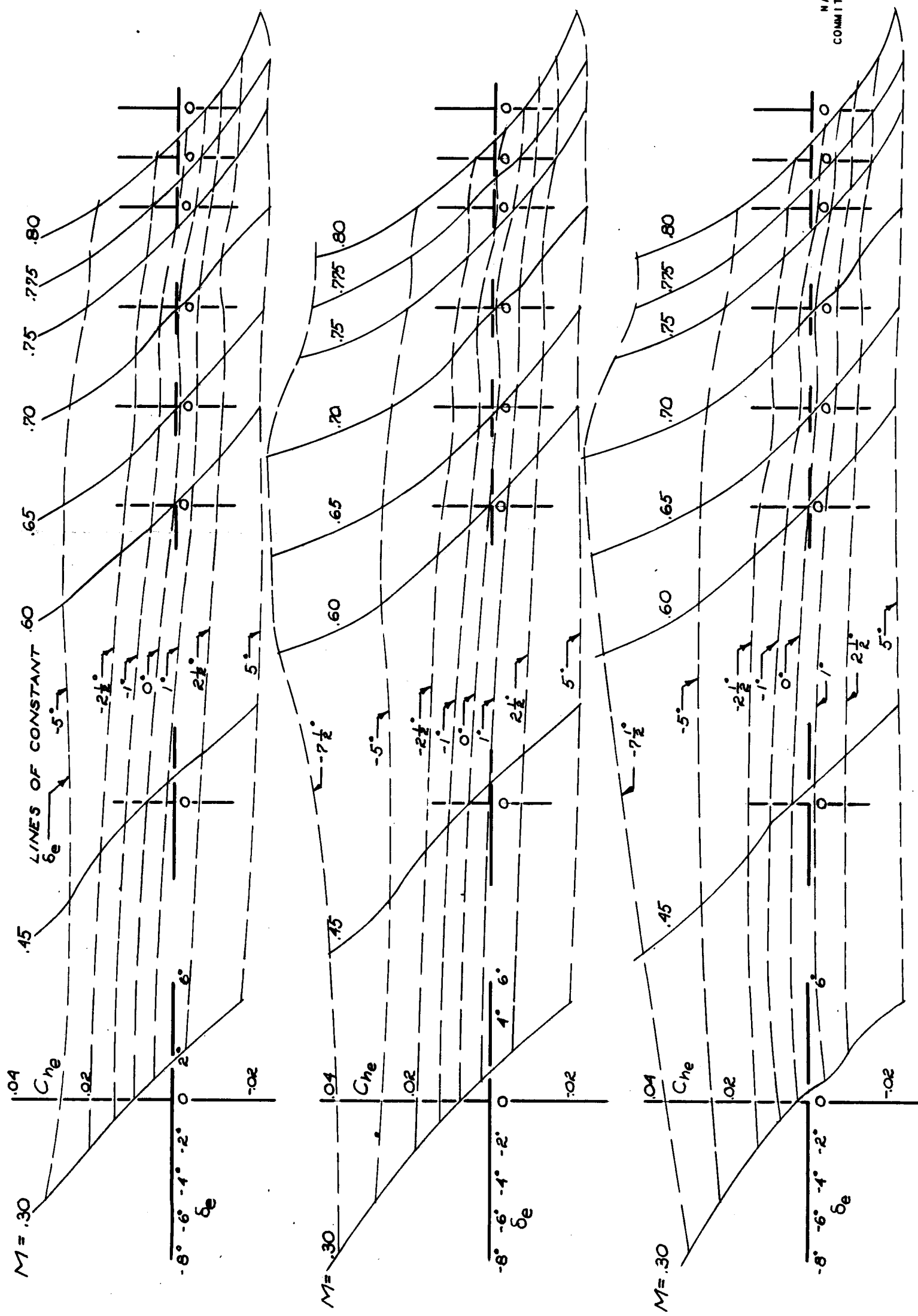
(a) $M^2C_L = 0, .025, .05$

FIGURE 20.—THE ELEVATOR HINGE-MOMENT COEFFICIENT AT CONSTANT M^2C_L FOR THE MODEL.
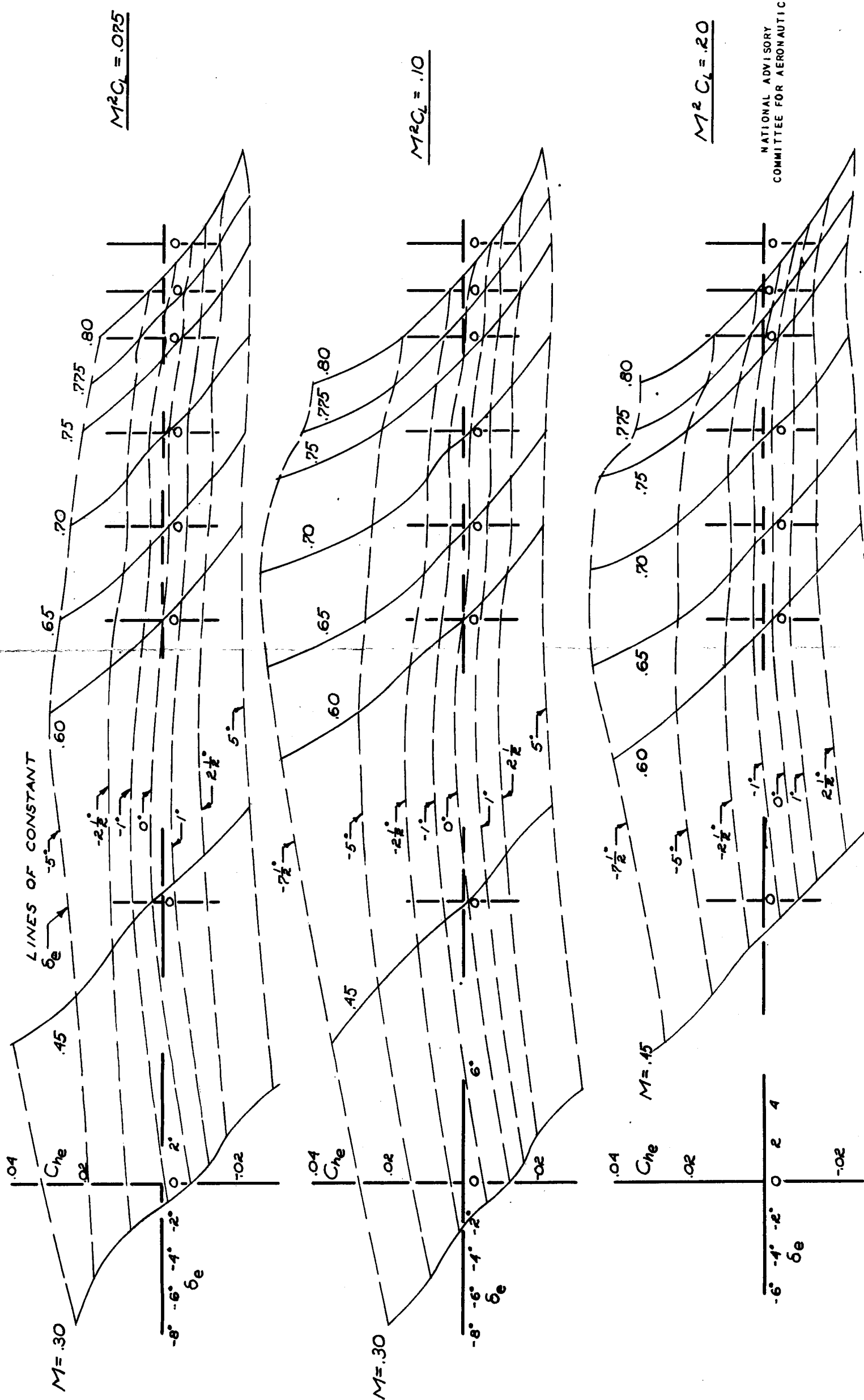
FIGURE 20.-(CONCLUDED) THE ELEVATOR
HINGE-MOMENT COEFFICIENT AT CONSTANT
$M^2 C_L$ FOR THE MODEL.

(b) $M^2 C_L = .075, .10, .20$
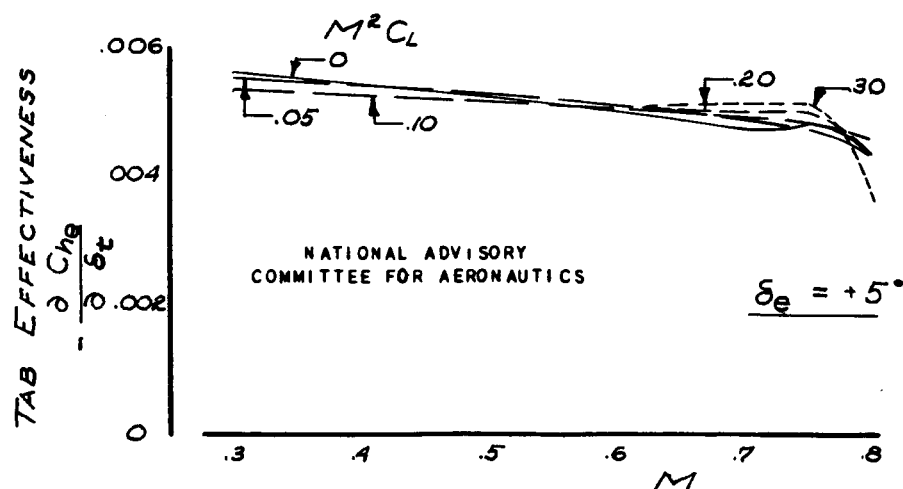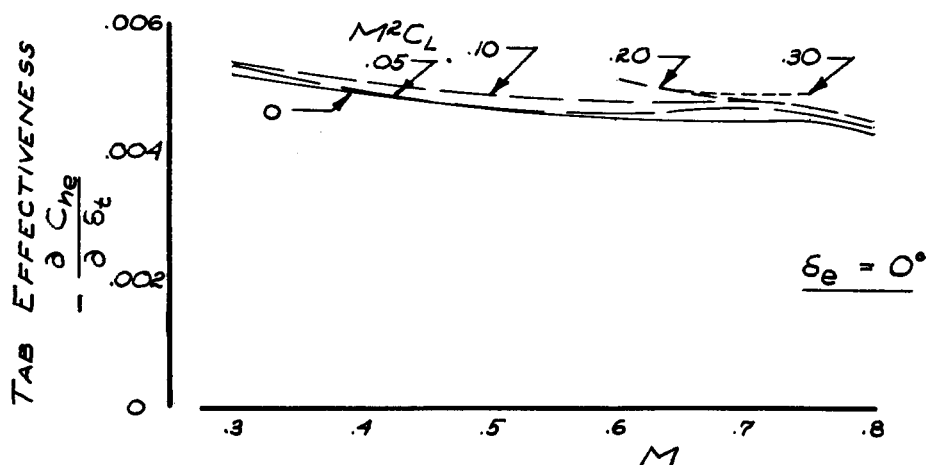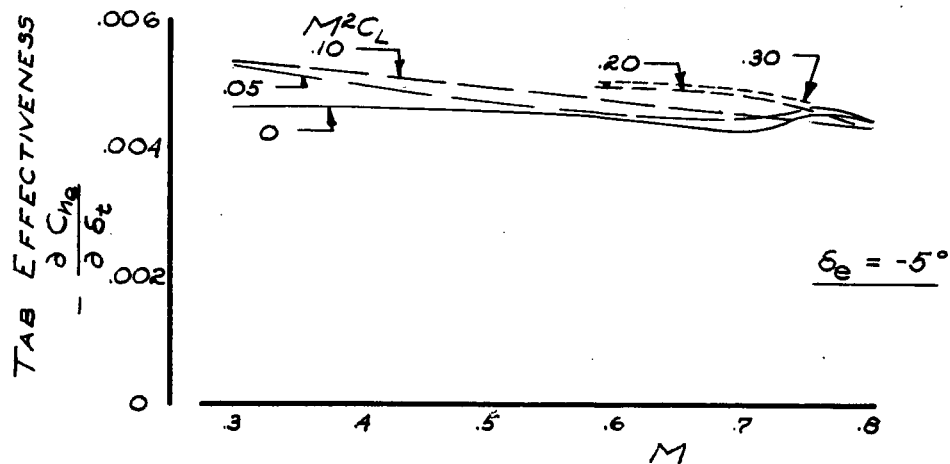
FIGURE 21.-THE ELEVATOR-TAB EFFEC-
TIVENESS FOR THE MODEL.

A84

(a) M = 0.30, 0.45, 0.60, 0.65
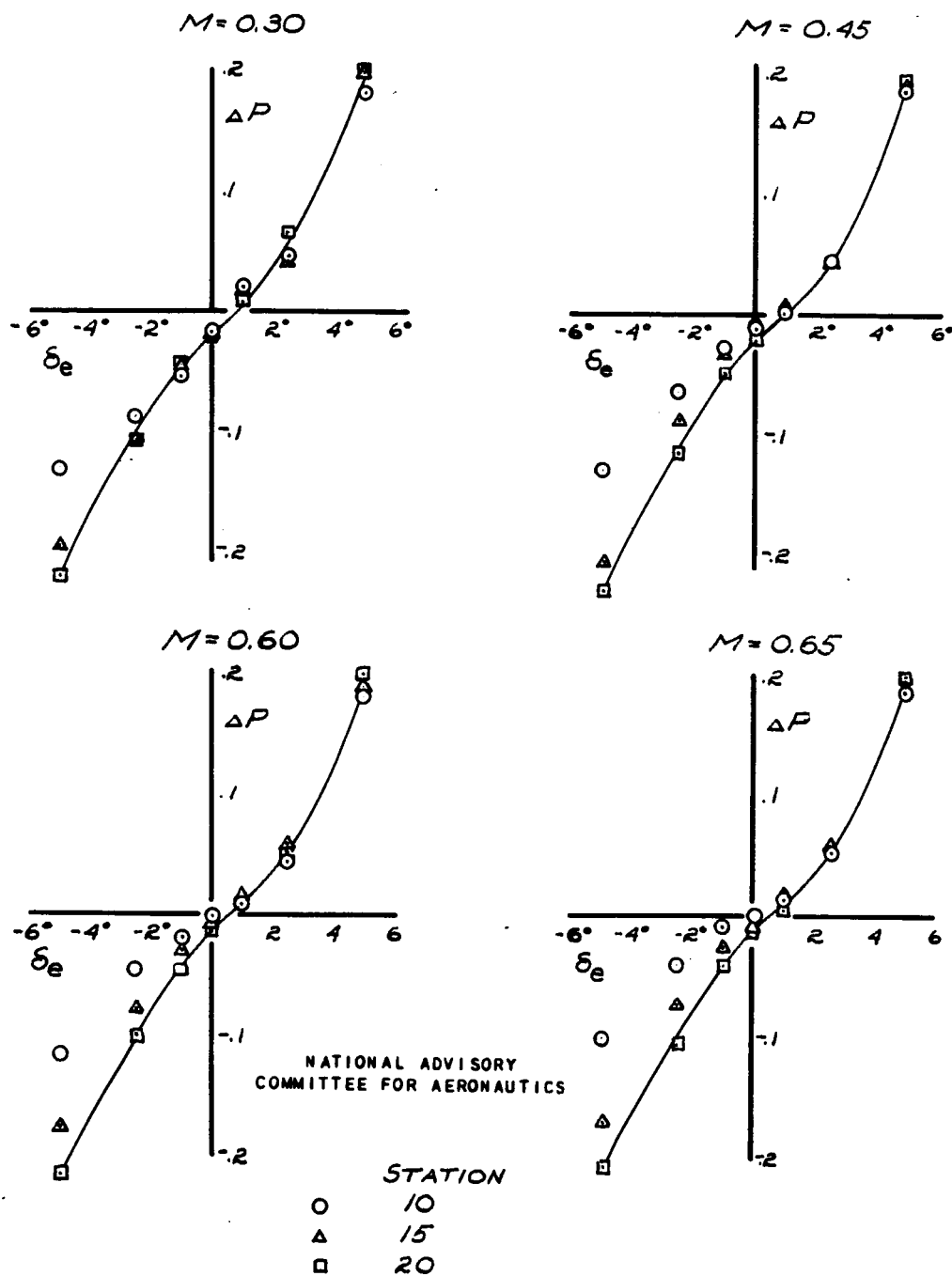
FIGURE 22.—THE ELEVATOR BALANCE PRESSURES AT THREE SPANWISE STATIONS ON THE MODEL.

M= 0.70
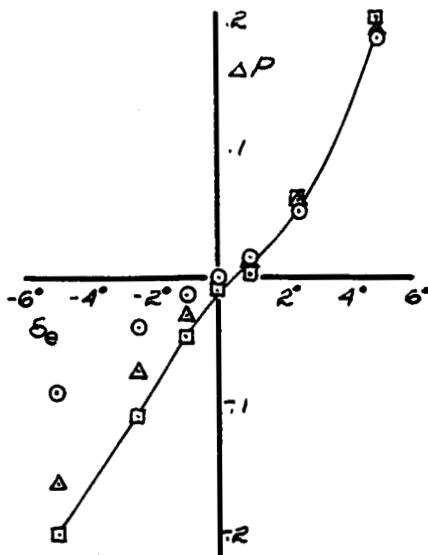
M= 0.75
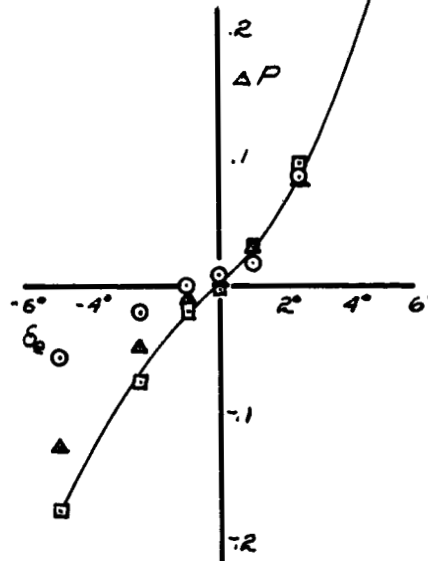
M= 0.775
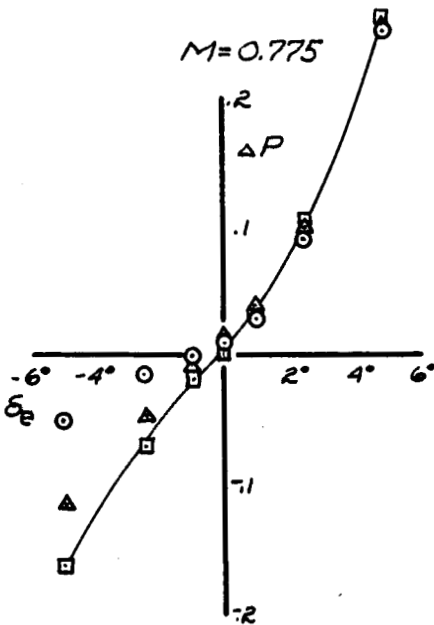
M=0.80
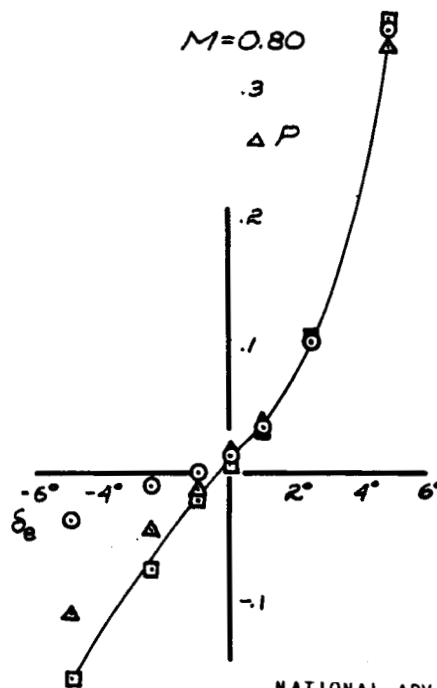
STATION
○   10
△   15
□   20

NATIONAL ADVISORY
COMMITTEE FOR AERONAUTICS

(b) M= 0.70, 0.75, 0.775, 0.80

FIGURE 22.- (CONCLUDED) THE ELEVATOR BALANCE PRESSURES AT THREE SPANWISE STATIONS ON THE MODEL.

TRIMMED AT HIGH-SPEED
LEVEL FLIGHT, NORMAL RATED POWER
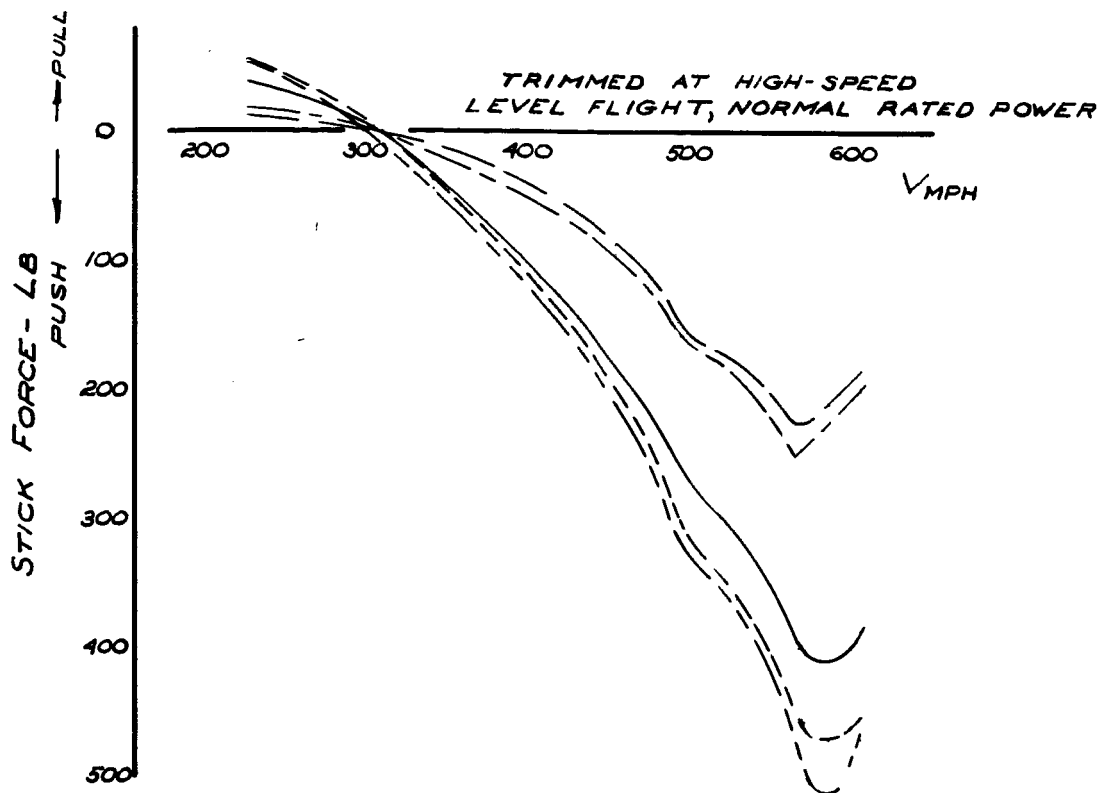
WEIGHT LB.	C.G. POSITION % M.A.C.
25,000	25
25,000	20
25,000	35
21,500	36
35,000	25
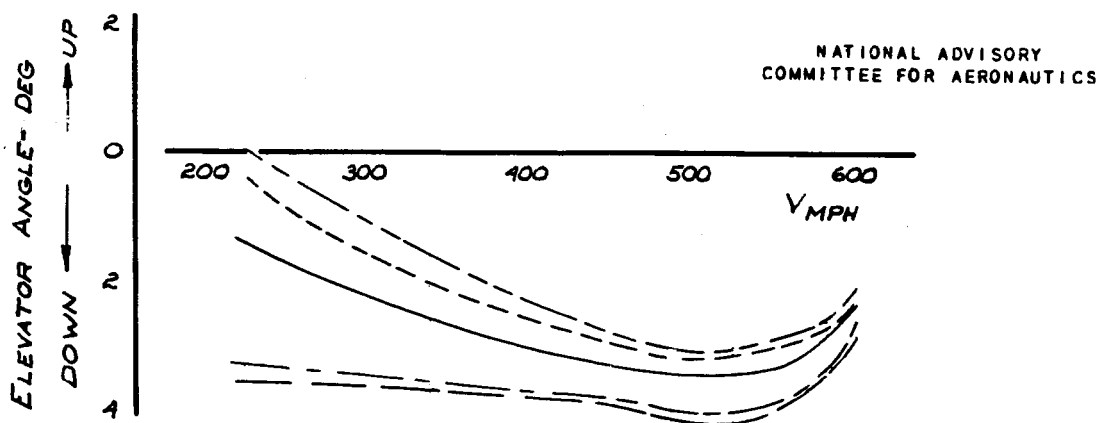
(a) SEA LEVEL

FIGURE 23.— THE STICK FORCE AND ELEVATOR
ANGLE IN RELATION TO THE VELOCITY FOR THE
AIRPLANE.
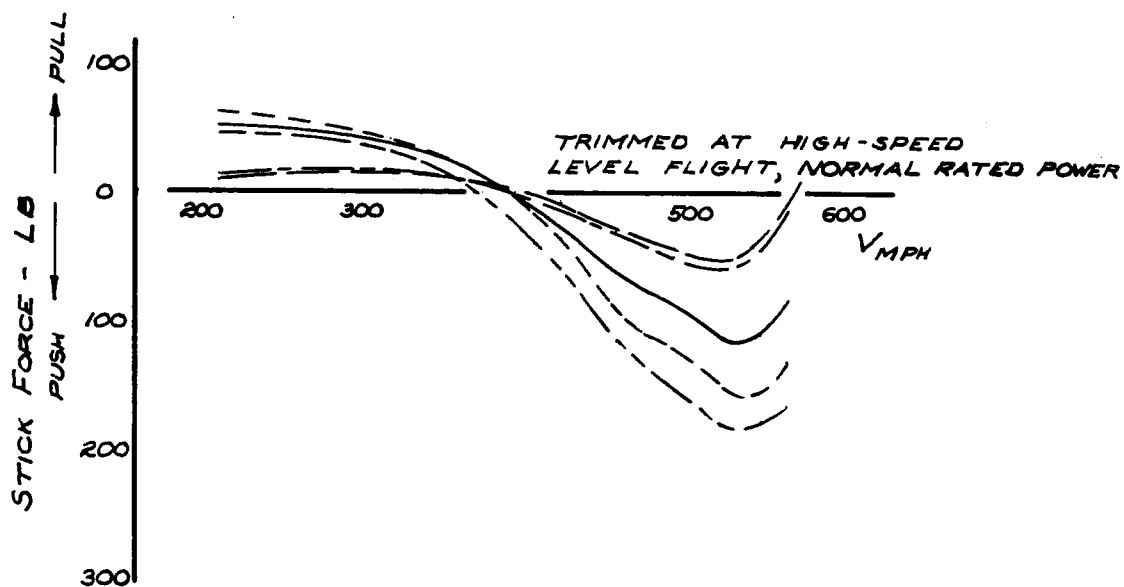
STICK FORCE - LB

PULL

PUSH

100

0

100

200

300

200   300   500   600

V_{MPH}

TRIMMED AT HIGH-SPEED
LEVEL FLIGHT, NORMAL RATED POWER

	WEIGHT LB.	C.G. POSITION % M.A.C.
———————	25,000	25
-------	25,000	20
—·——·—	25,000	35
— — —	21,500	36
—— ——	35,000	25

ELEVATOR ANGLE - DEG

UP

DOWN

6

4

2

0

2

4

200   300   400   500   600

V_{MPH}
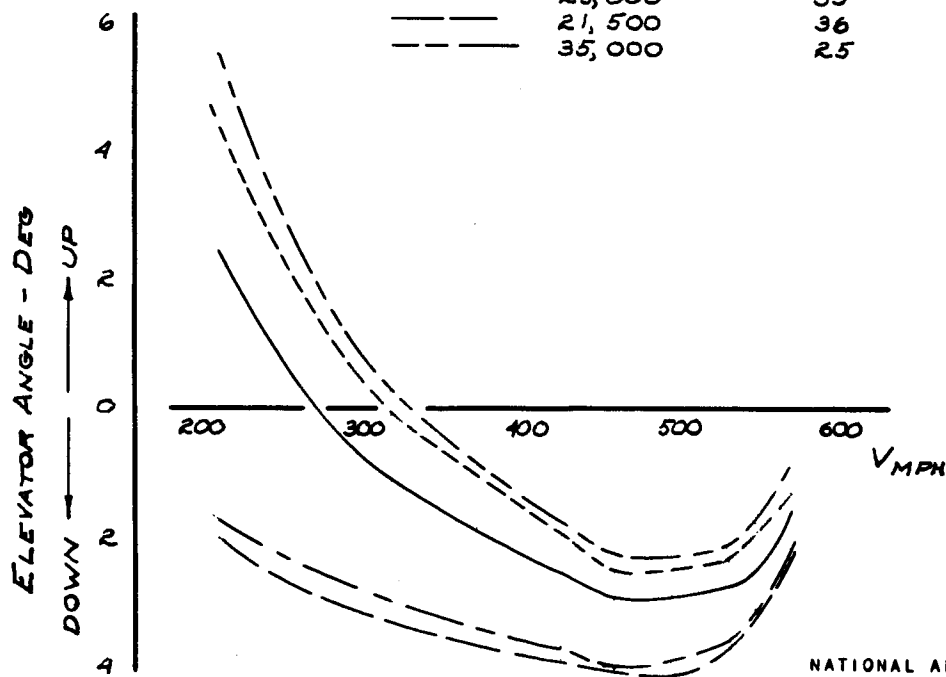
(b) 20,000-FT. ALTITUDE

FIGURE 23.-(CONCLUDED) THE STICK FORCE AND
ELEVATOR ANGLE IN RELATION TO THE VELOCITY
FOR THE AIRPLANE.

TRIMMED AT HIGH-SPEED
LEVEL FLIGHT, NORMAL RATED POWER

────────── NORMAL WING
─ ─ ─ ─ ─ WING WITH BUMP ON LOWER SURFACE

(a) SEA LEVEL
FIGURE 24.—THE EFFECT OF THE WING BUMP ON THE STICK FORCE AND ELEVATOR ANGLE FOR THE AIRPLANE.

STICK FORCE - LB

PULL

PUSH

100

0

100

200

TRIMMED AT HIGH-SPEED
LEVEL FLIGHT, NORMAL RATED POWER

200   300   500   600 V_{MPH}

——————— NORMAL WING
— — — — WING WITH BUMP ON LOWER SURFACE

ELEVATOR ANGLE - DEG

UP

DOWN

2

0

2

4

200   300   400   500   600 V_{MPH}
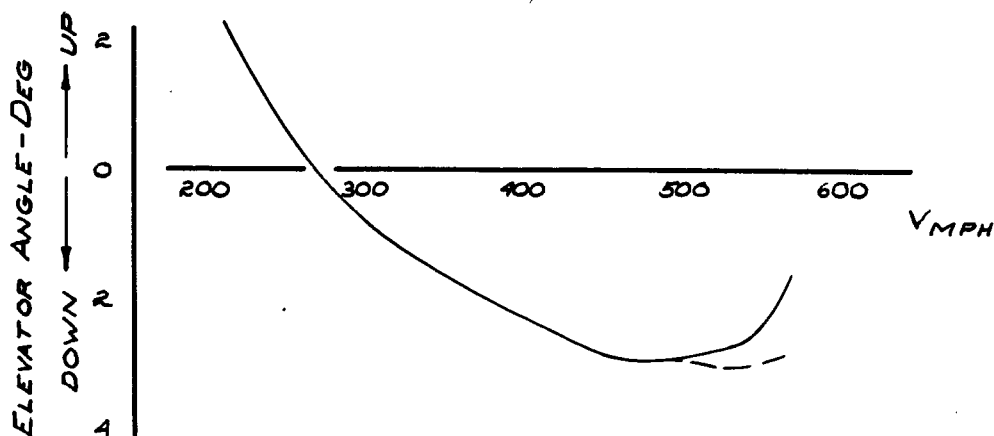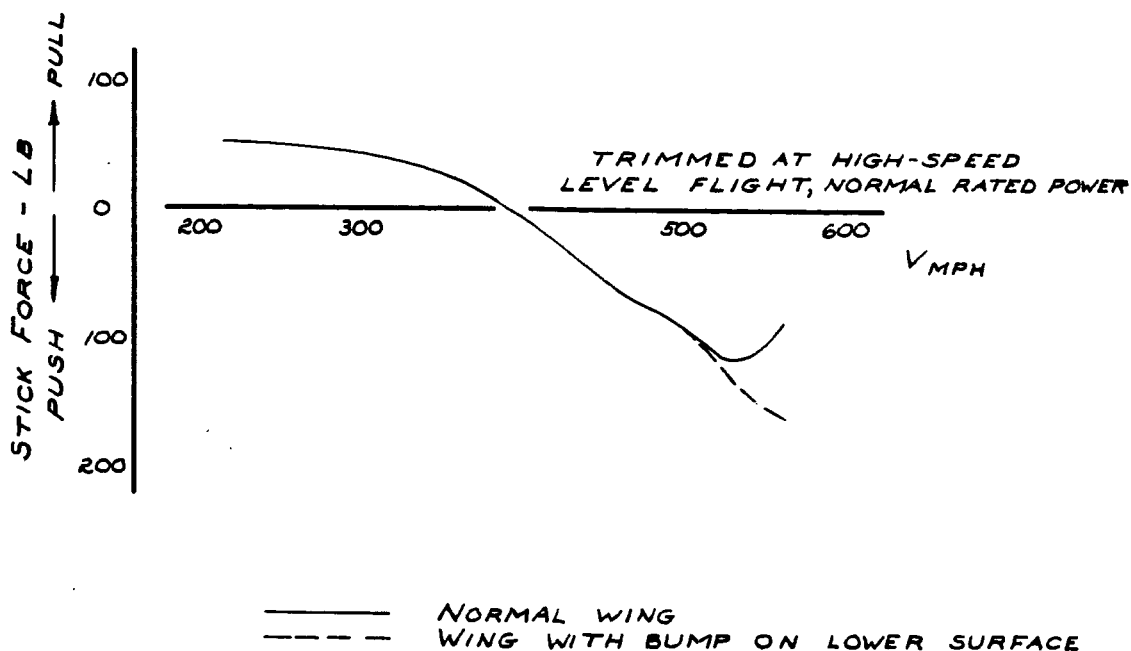
(b) 20,000-FT ALTITUDE
FIGURE 24.- (CONCLUDED) THE EFFECT OF THE
WING BUMP ON THE STICK FORCE AND ELEVATOR
ANGLE FOR THE AIRPLANE.

TRIMMED AT HIGH-SPEED LEVEL
FLIGHT, CONTROL FLAPS UP

————————— AUXILIARY CONTROL FLAPS UP
— — — — 30° AUXILIARY CONTROL FLAPS
— — — 45° AUXILIARY CONTROL FLAPS
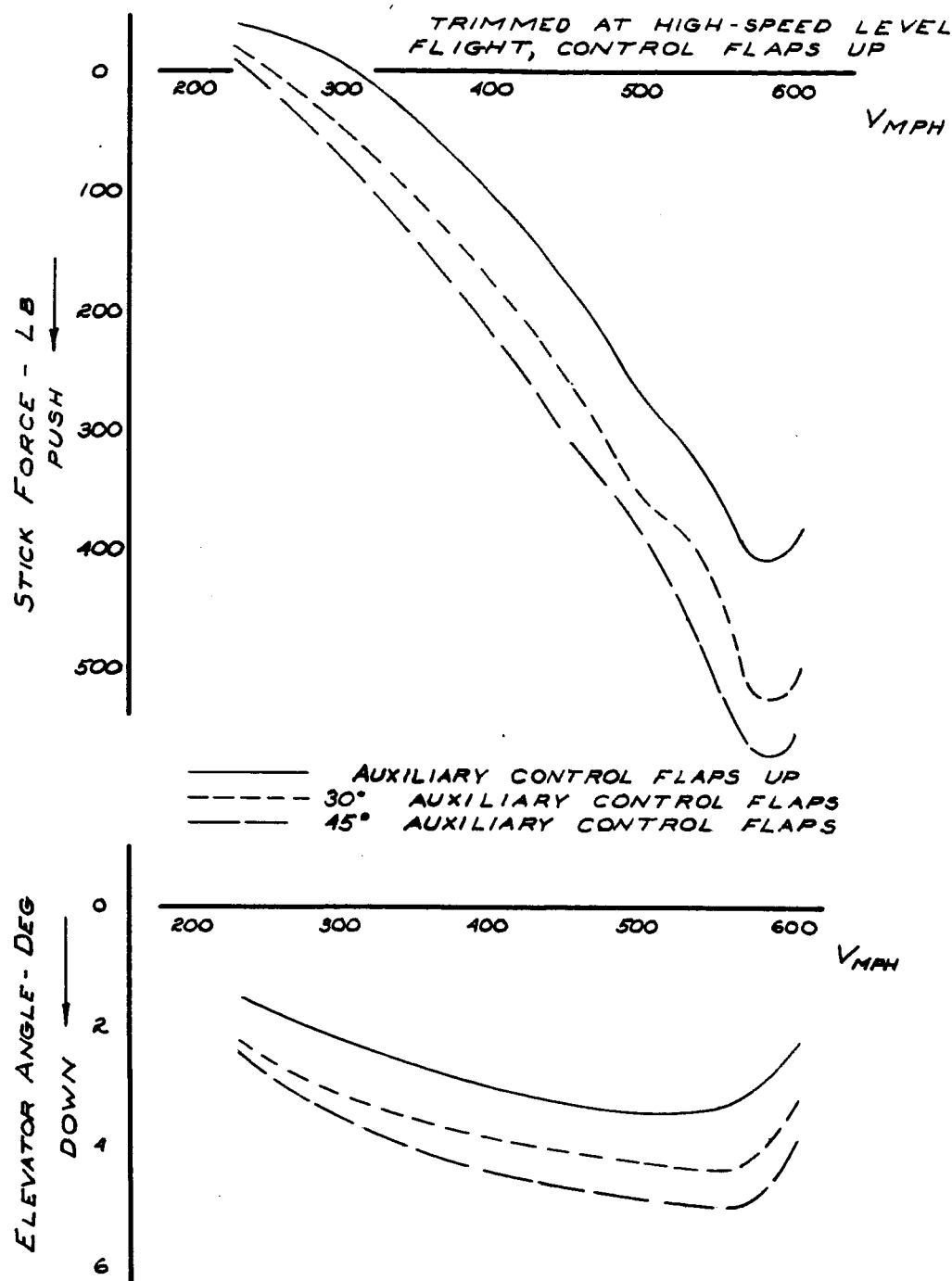
NATIONAL ADVISORY
COMMITTEE FOR AERONAUTICS

(a) SEA LEVEL
FIGURE 25.- THE EFFECT OF AUXILIARY CONTROL
FLAPS ON THE STICK FORCE AND ELEVATOR ANGLE
FOR THE AIRPLANE.
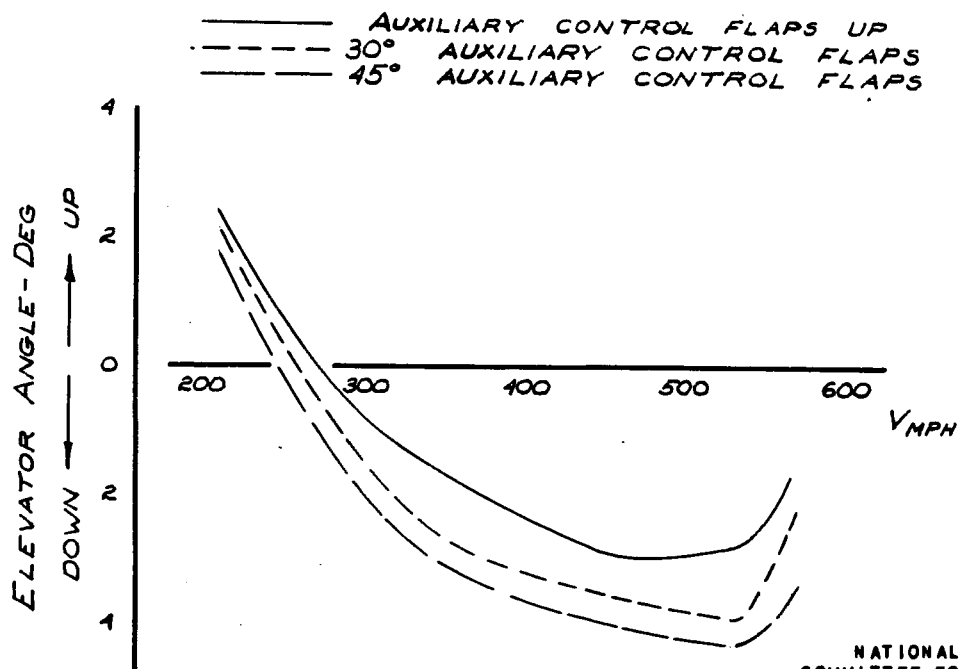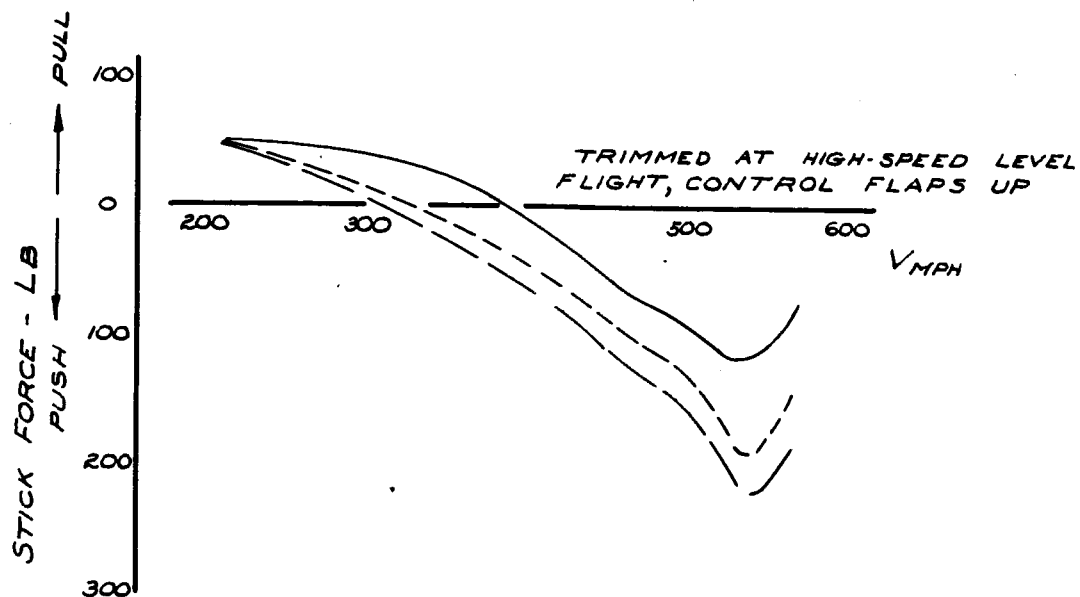
(b) 20,000 FT. ALTITUDE
FIGURE 25.-(CONCLUDED) THE EFFECT OF
AUXILIARY CONTROL FLAPS ON THE STICK
FORCE AND ELEVATOR ANGLE FOR THE AIRPLANE.
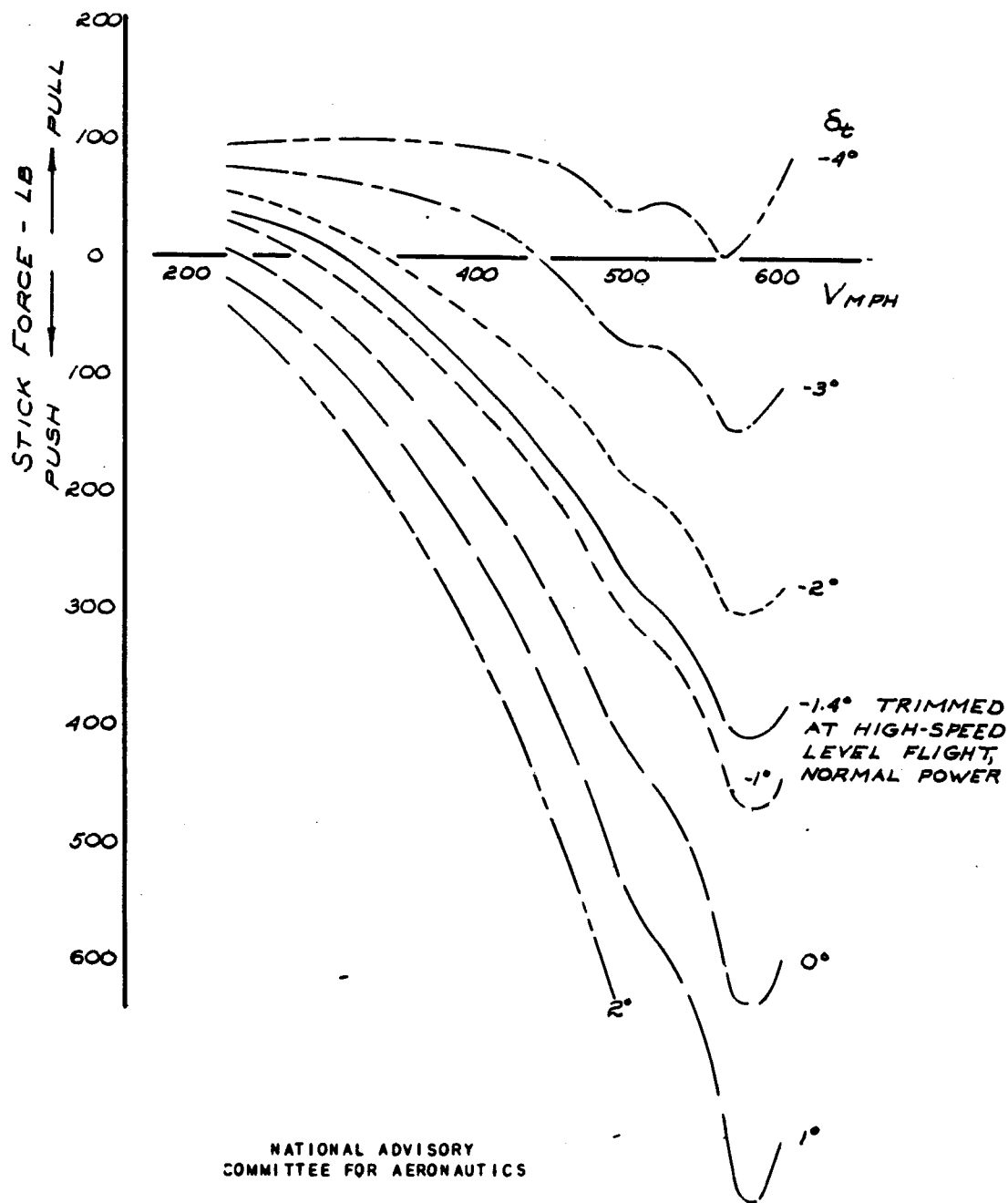
(a) SEA LEVEL

FIGURE 26.- THE STICK FORCE FOR SEVERAL TAB ANGLES IN RELATION TO THE VELOCITY FOR THE AIRPLANE.
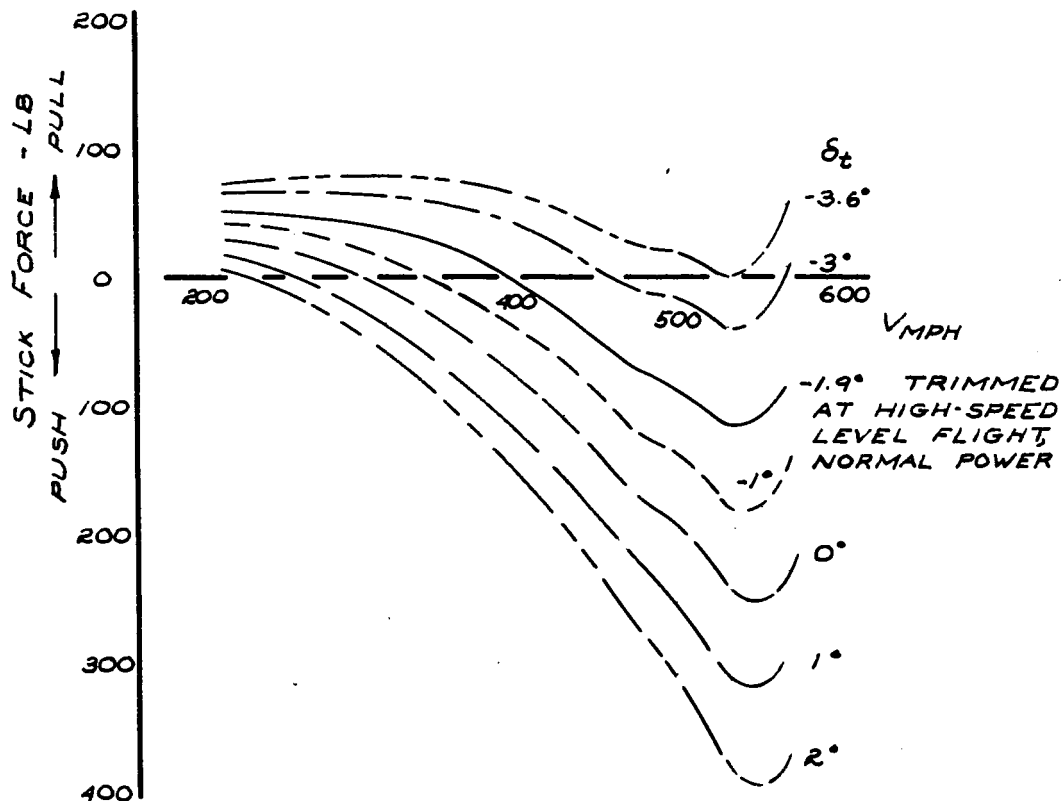
(b) 20,000-FT ALTITUDE

FIGURE 26.— (CONCLUDED) THE STICK FORCE FOR SEVERAL TAB ANGLES IN RELATION TO THE VELOCITY FOR THE AIRPLANE.
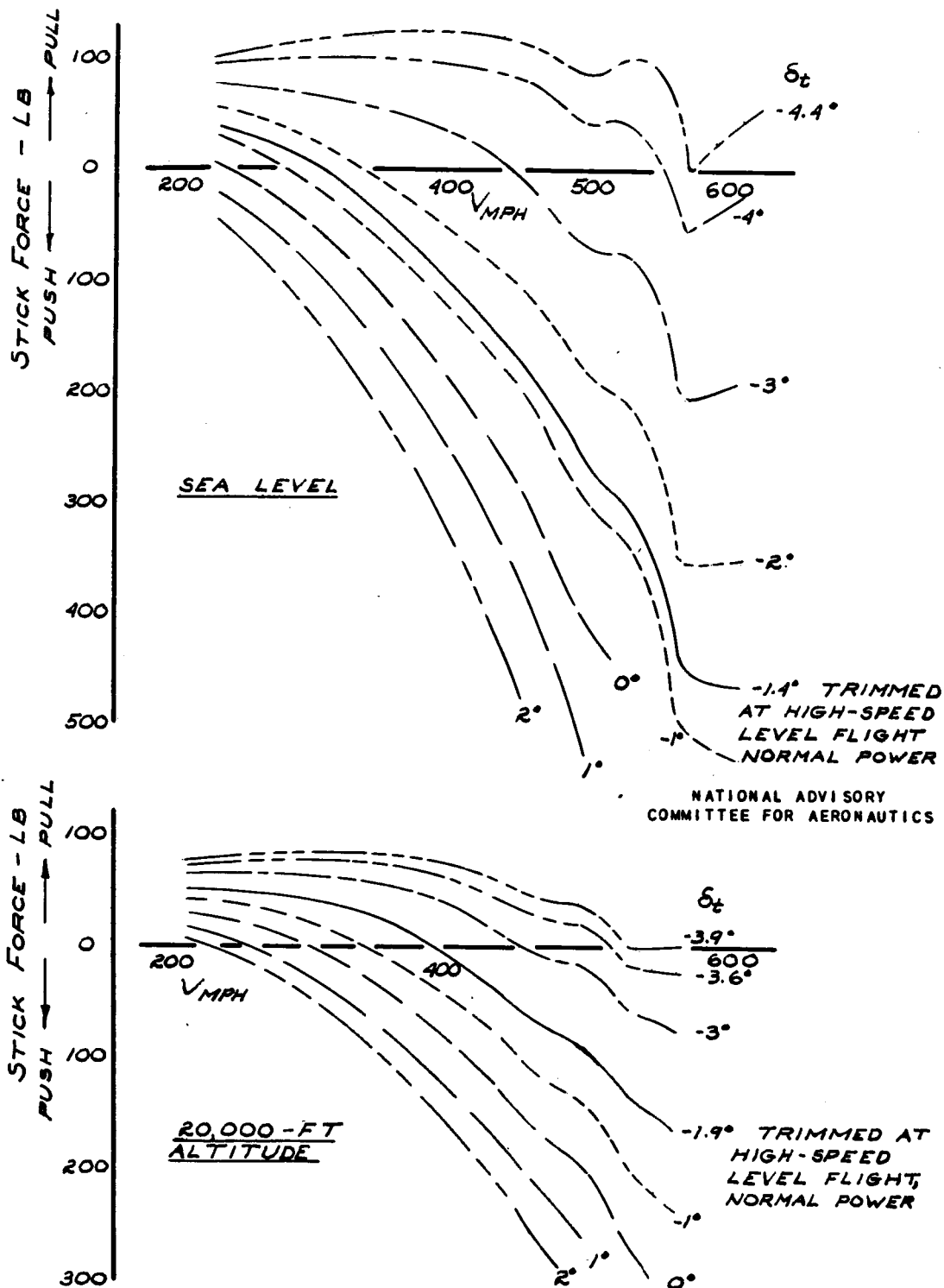
FIGURE 27.- THE STICK FORCE FOR SEVERAL TAB ANGLES FOR THE AIRPLANE WITH THE WING BUMP.
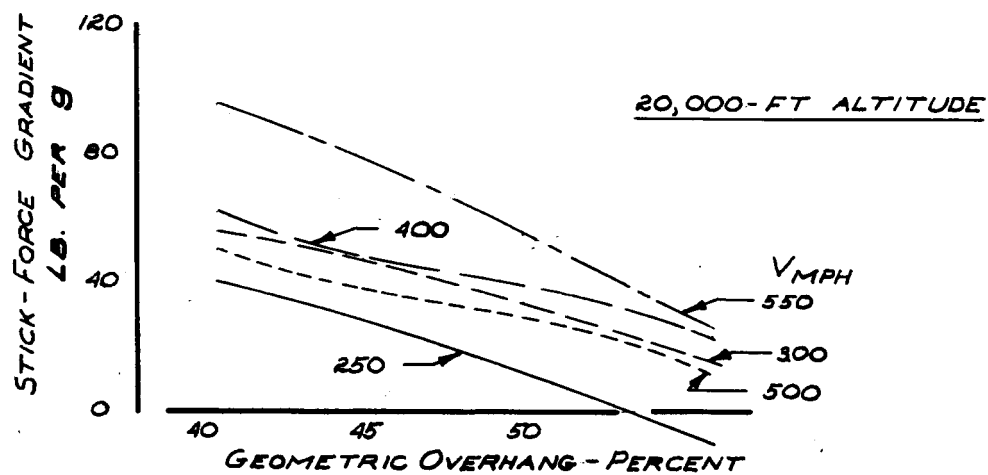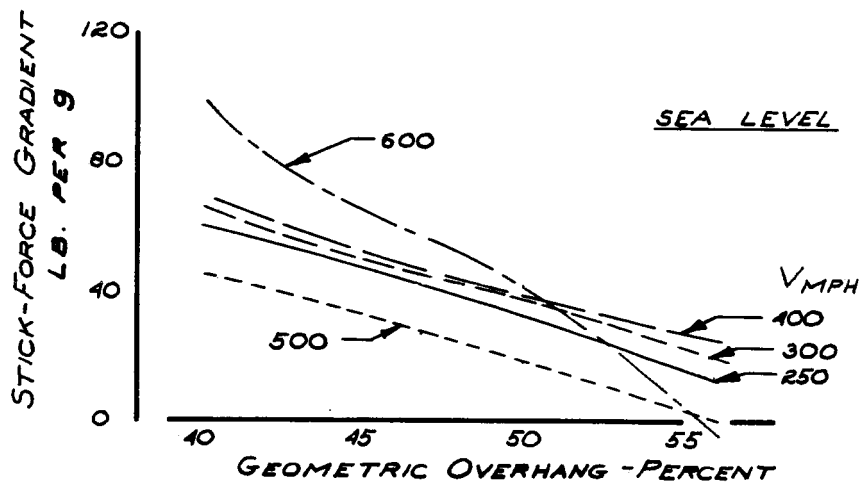
FIGURE 28.- THE EFFECT OF THE ELEVATOR GEOMETRIC OVERHANG ON THE STICK-FORCE GRADIENT FOR THE AIRPLANE.

STICK-FORCE GRADIENT LB. PER g

120

80

40

0

SEA LEVEL

300

V_{MPH}

600

250

500

400

20   25   30   35

CENTER-OF-GRAVITY LOCATION
PERCENT M.A.C.

STICK-FORCE GRADIENT LB PER g

120

80

40

0

V_{MPH}
550

20,000-FT. ALTITUDE

400

500

300

200

20   25   30   35
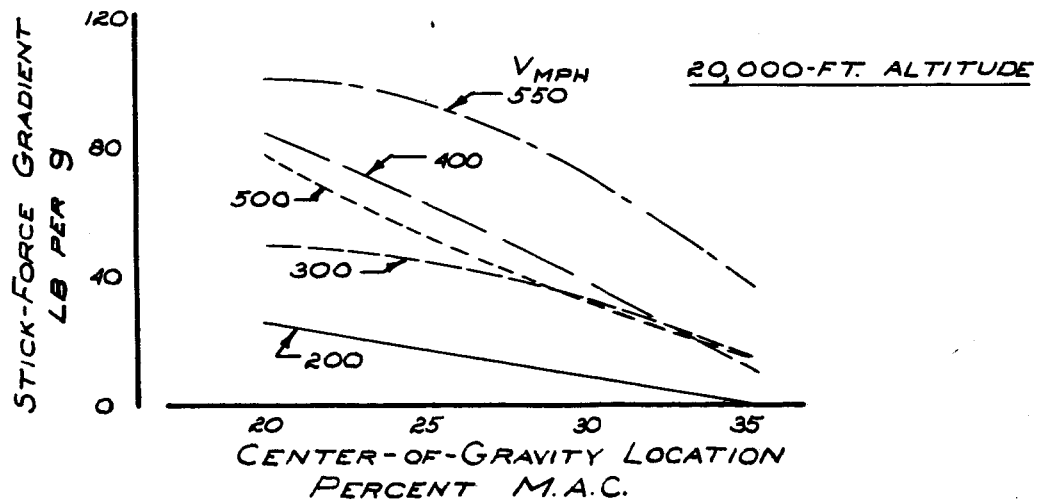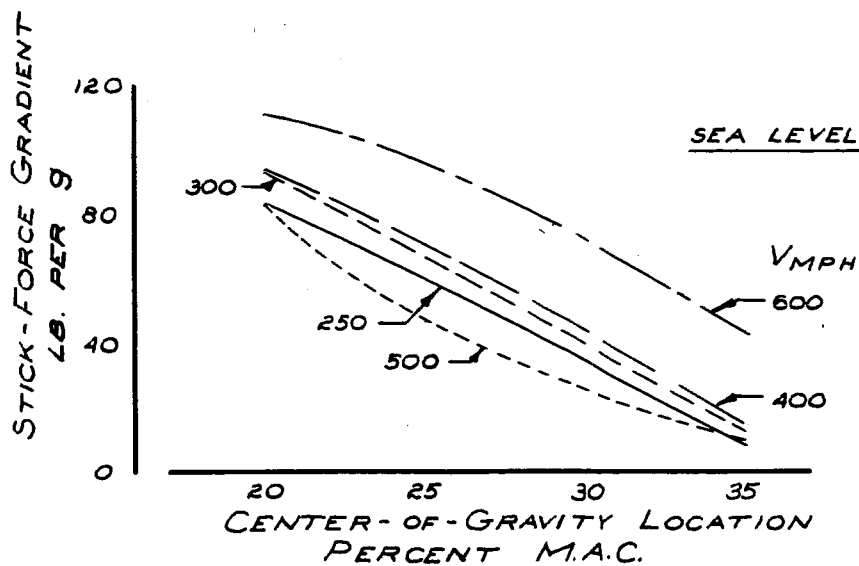
CENTER-OF-GRAVITY LOCATION
PERCENT M.A.C.

FIGURE 29.- THE EFFECT OF THE CENTER-OF-GRAVITY LOCATION ON THE STICK-FORCE GRADIENT FOR THE AIRPLANE.
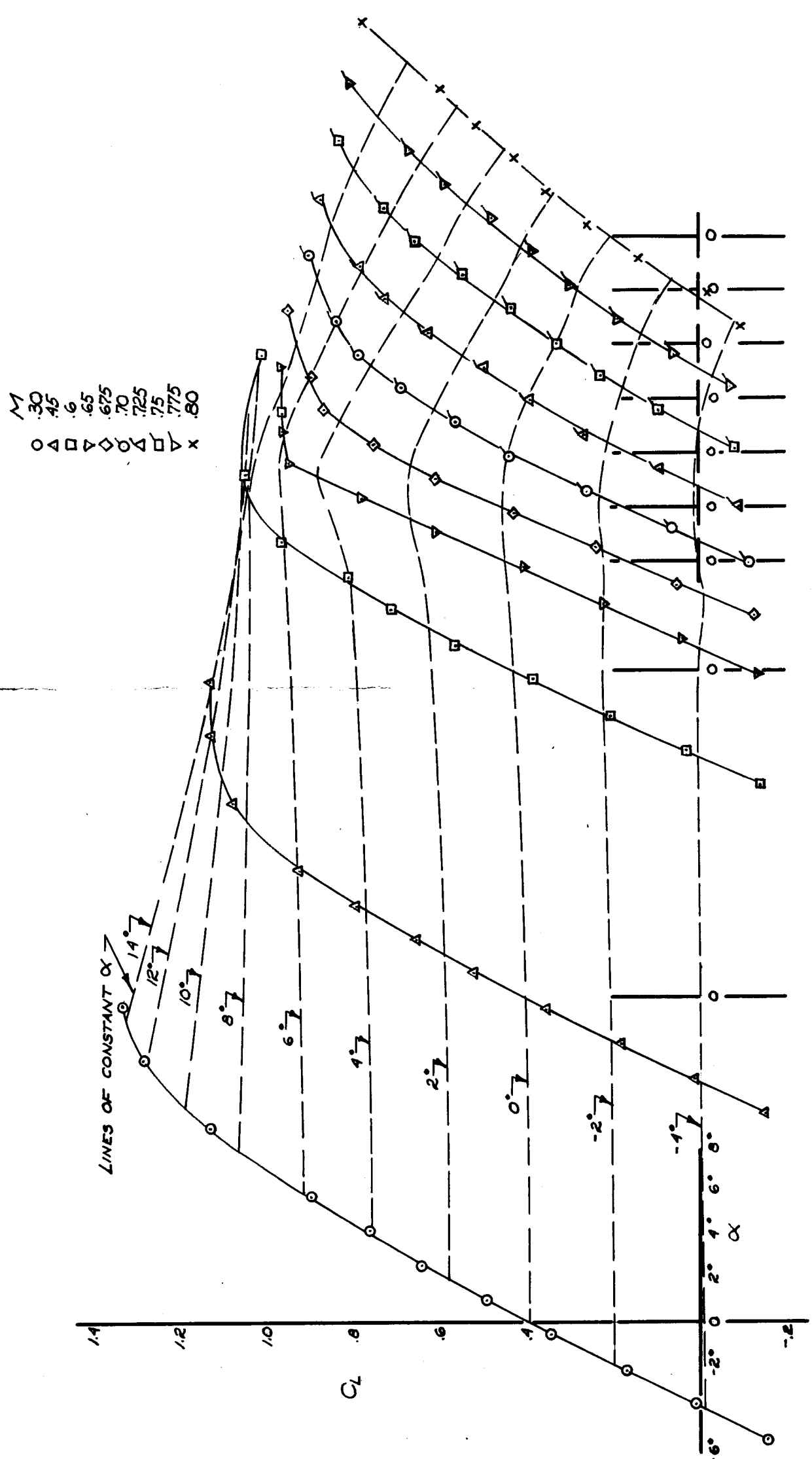
FIGURE 30.-THE LIFT COEFFICIENT FOR THE MODEL.
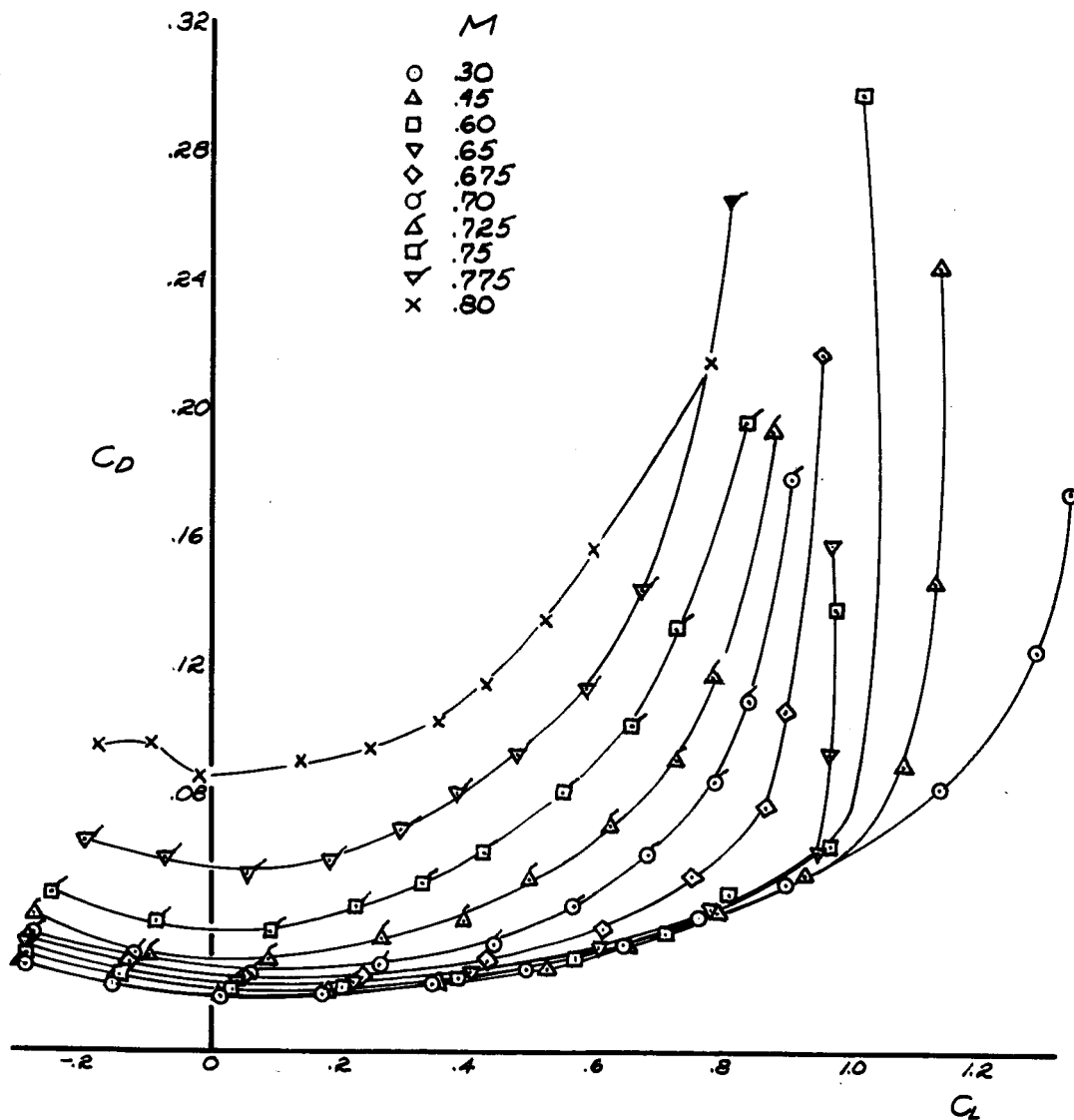
FIGURE 31.—THE DRAG COEFFICIENT AS A
FUNCTION OF LIFT COEFFICIENT FOR THE
MODEL.
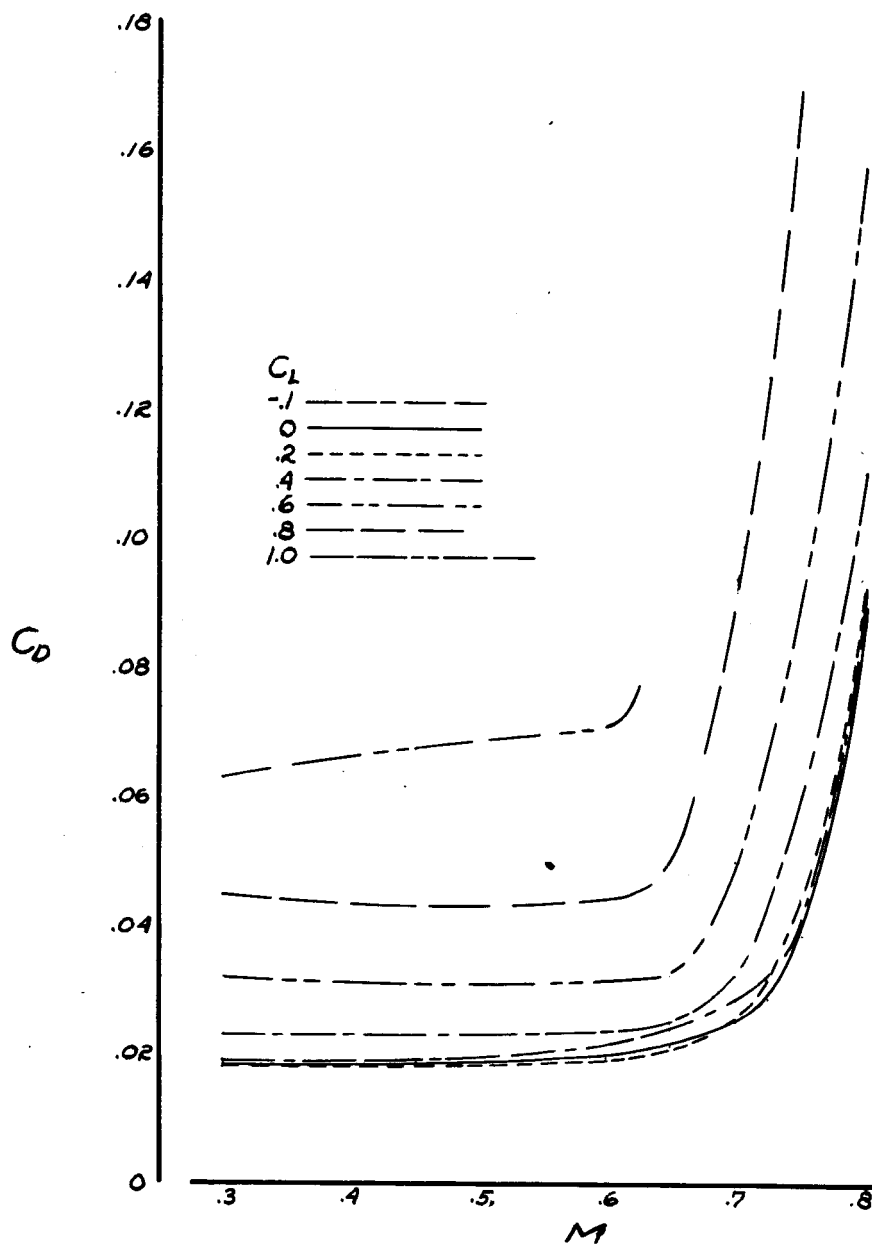
FIGURE 32.- THE DRAG COEFFICIENT IN RE-
LATION TO MACH NUMBER FOR THE COMPLETE
MODEL.
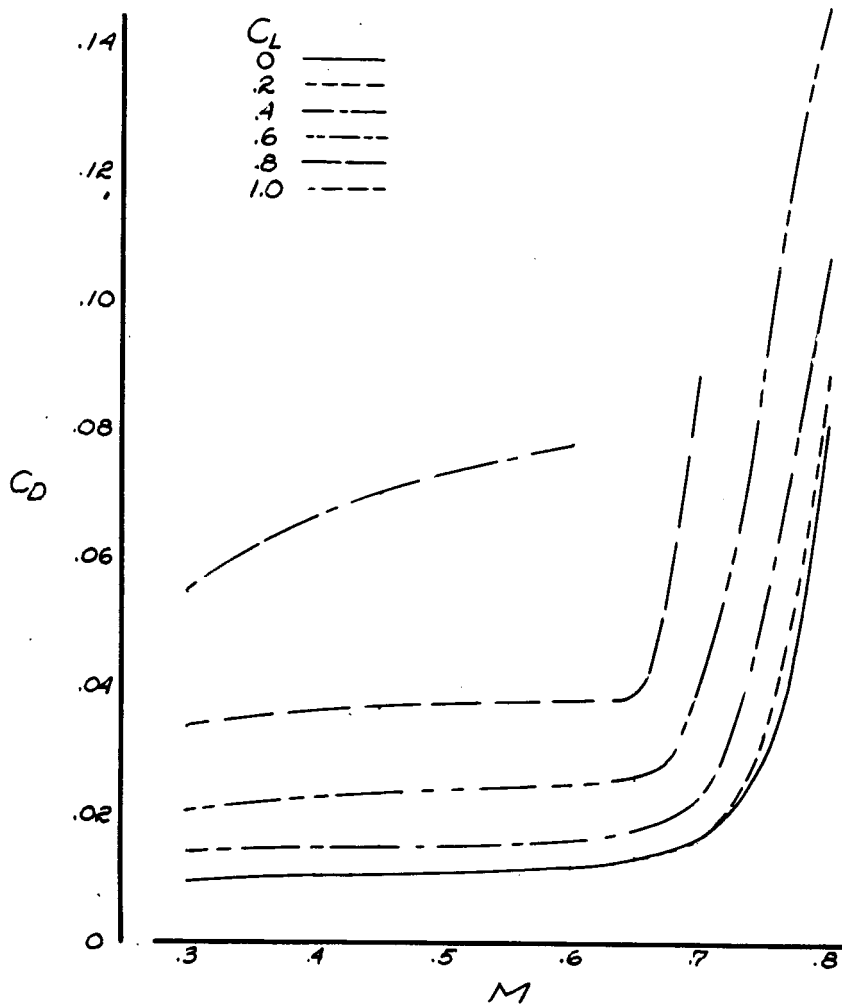
FIGURE 33.— THE DRAG COEFFICIENT IN RE-
LATION TO MACH NUMBER FOR THE WING OF
THE MODEL.

C_L
0 ——
2 – – –
4 – ·–
6 – ··–

FUSELAGE

EMPENNAGE

EMPENNAGE FOR WING-BUMP CONFIGURATION

WING BUMP
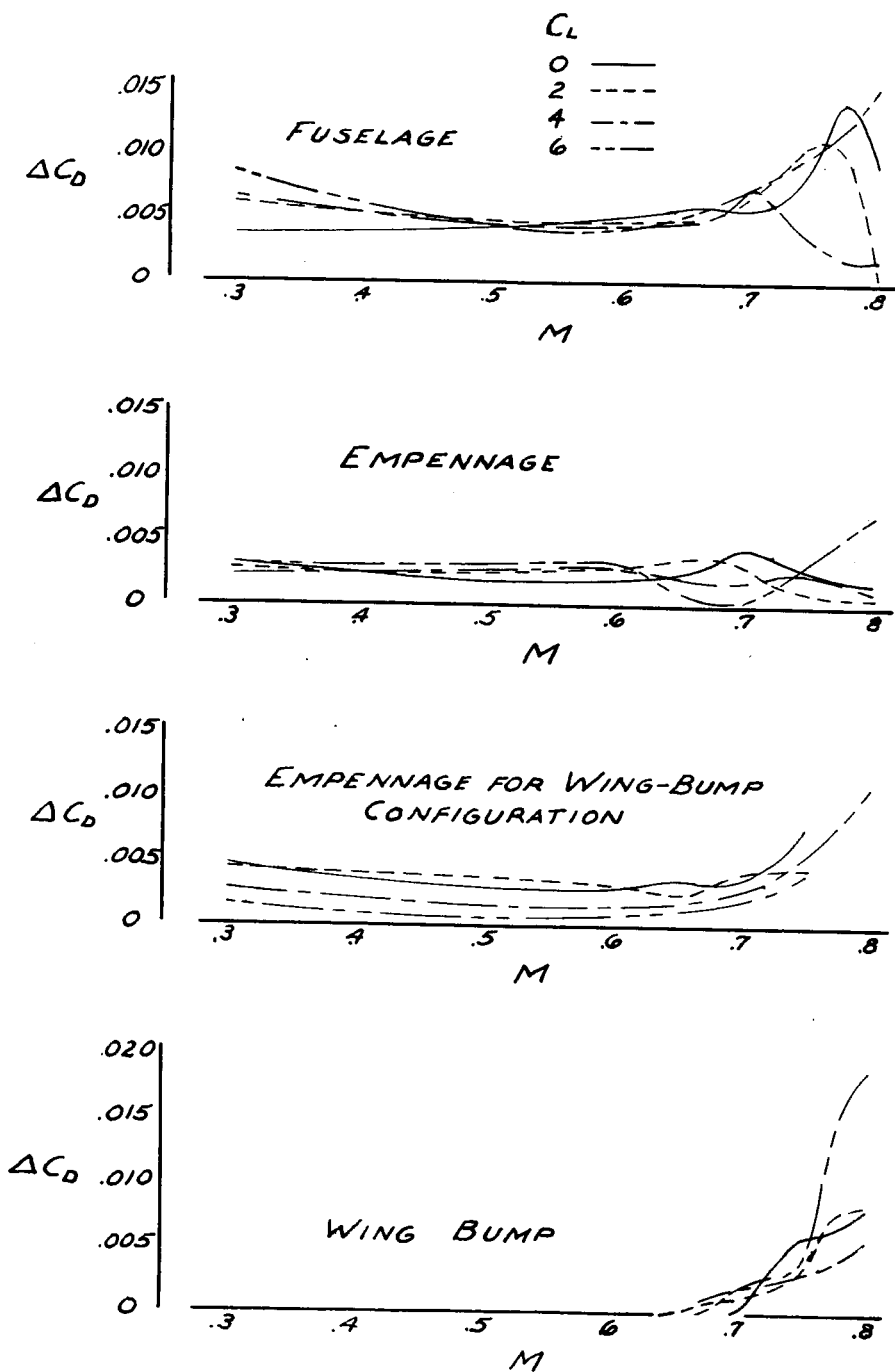
FIGURE 34.— THE INCREMENT OF DRAG COEFFICIENT DUE TO COMPONENT PARTS OF THE MODEL.
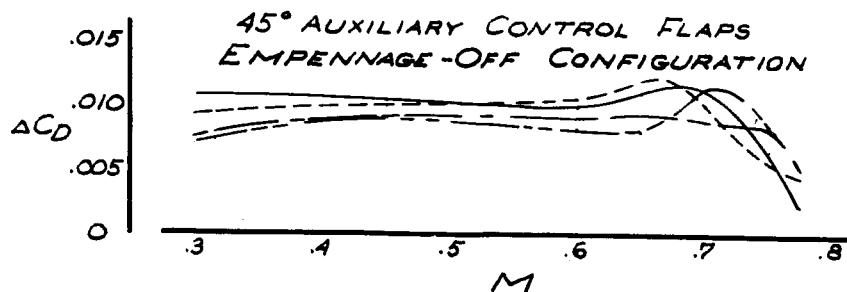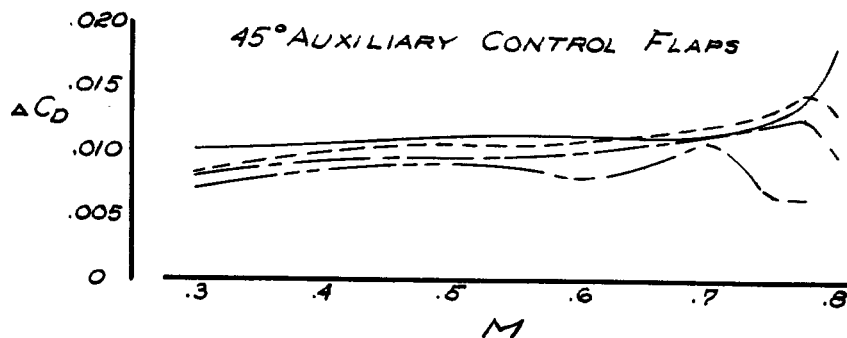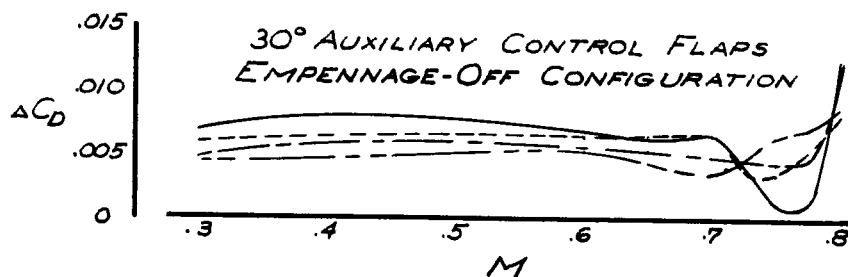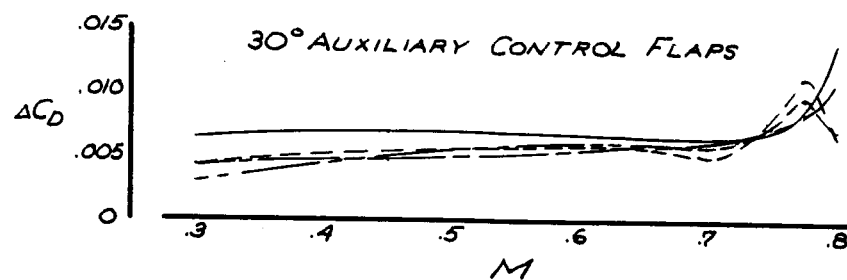
FIGURE 35.- THE INCREMENT OF DRAG
COEFFICIENT DUE TO AUXILIARY CONTROL FLAPS
ON THE MODEL.
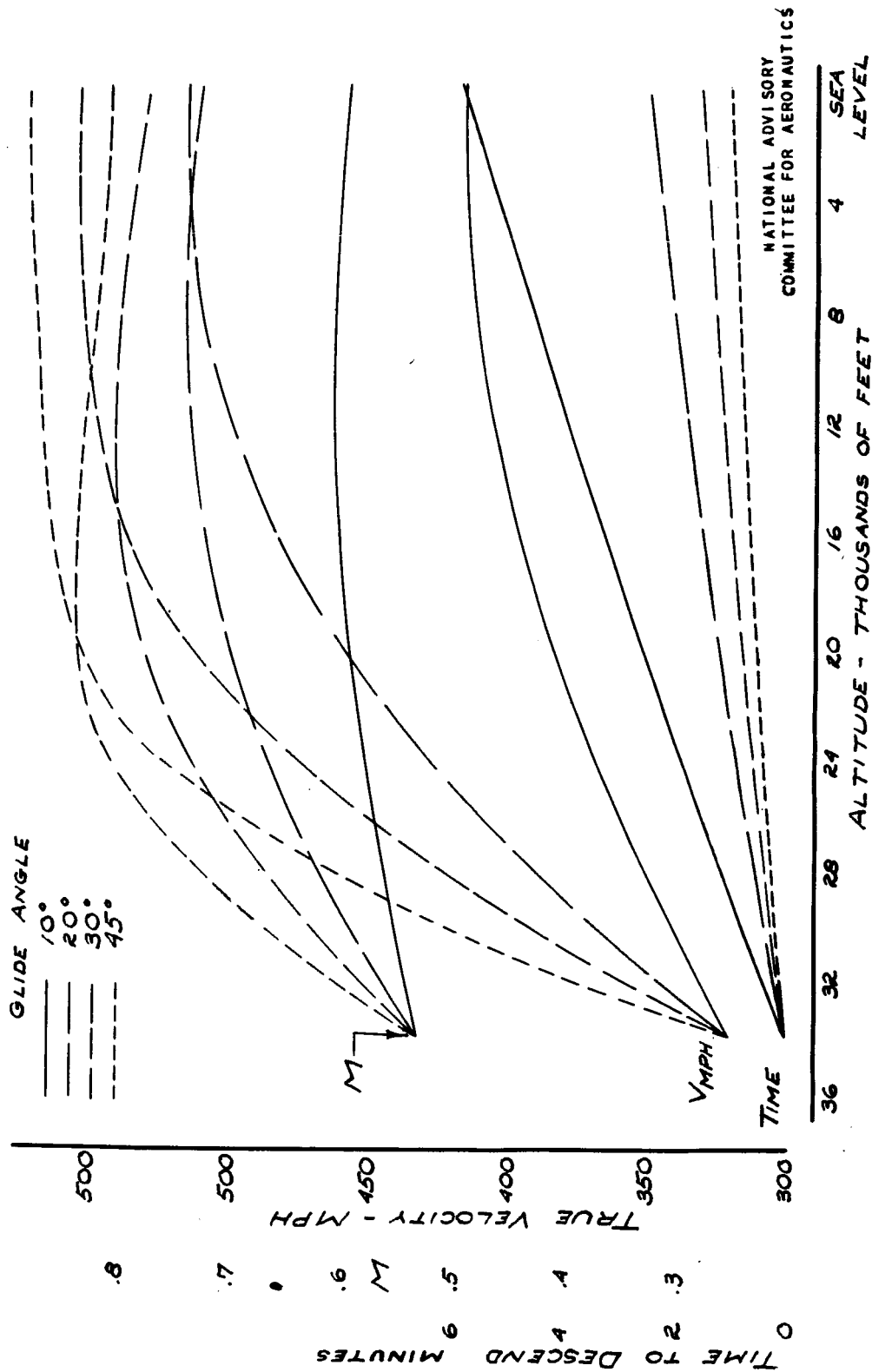
FIGURE 36.— THE VELOCITY, MACH NUMBER, AND TIME TO DESCEND FOR THE AIRPLANE GLIDING. ZERO PROPELLER THRUST.
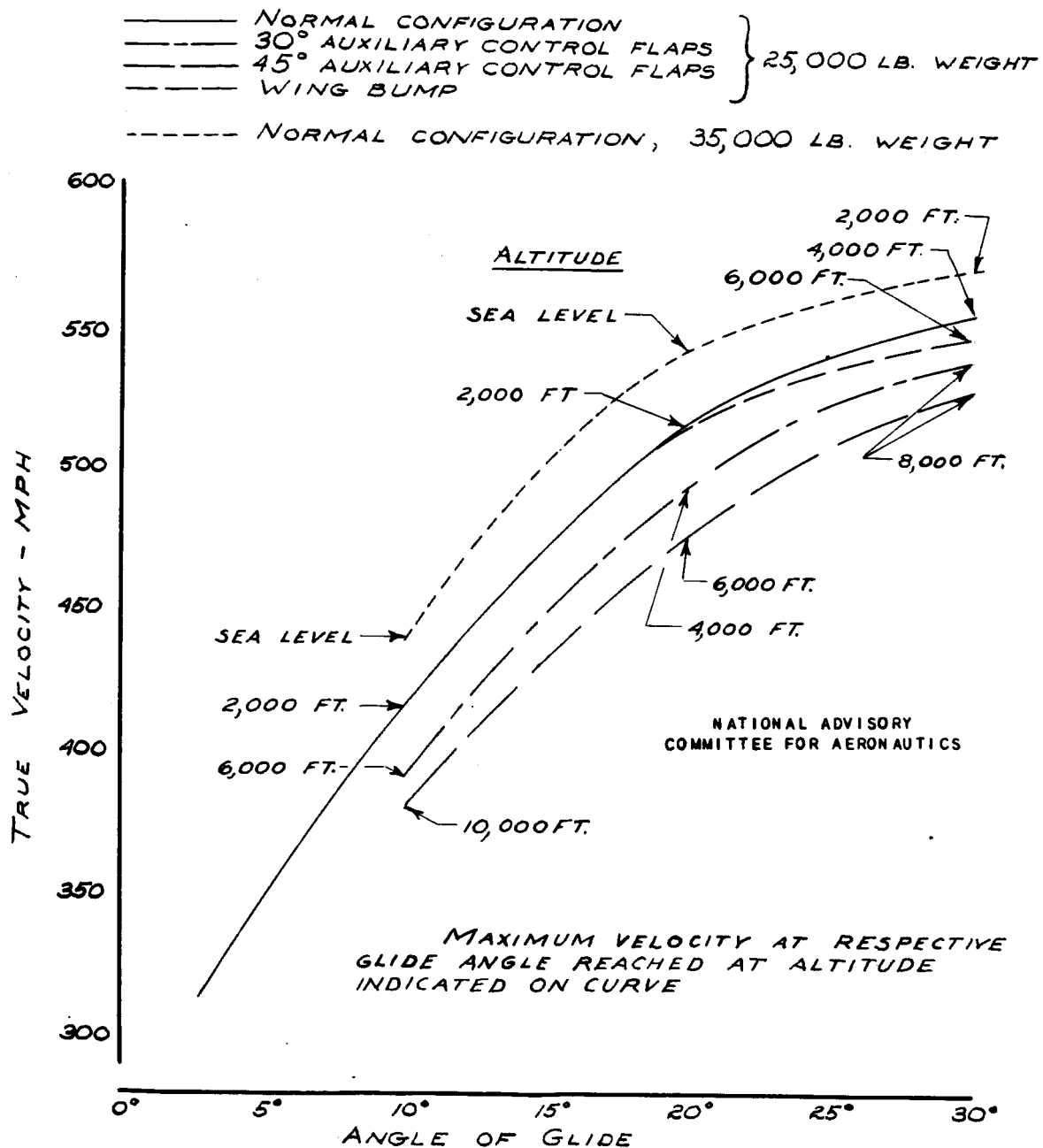
FIGURE 37.—THE MAXIMUM VELOCITY OBTAINED BY THE AIRPLANE IN RELATION TO THE ANGLE OF GLIDE. ZERO PROPELLER THRUST.
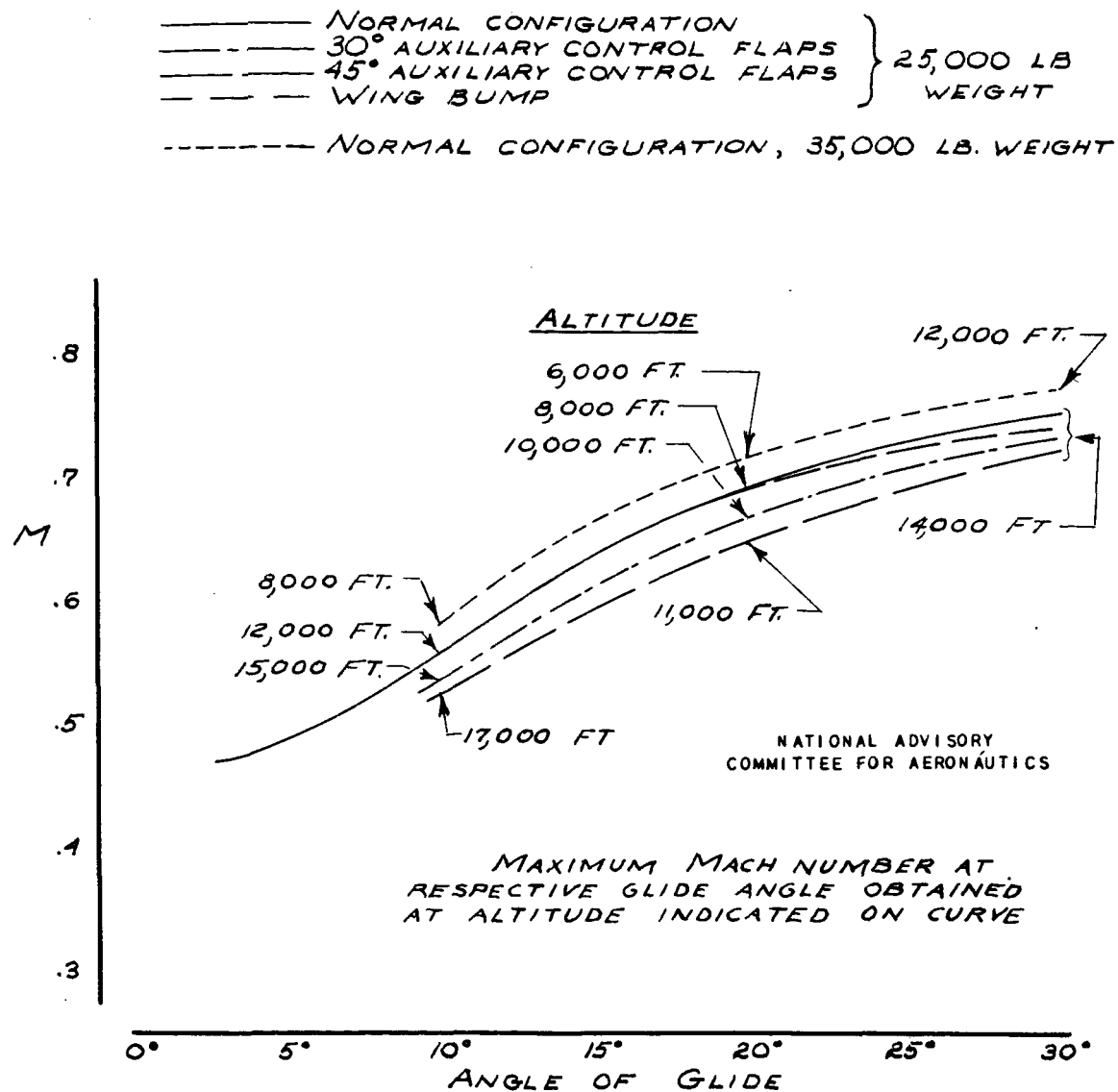
NORMAL CONFIGURATION
30° AUXILIARY CONTROL FLAPS
45° AUXILIARY CONTROL FLAPS   } 25,000 LB
WING BUMP   WEIGHT

NORMAL CONFIGURATION, 35,000 LB. WEIGHT

.8

.7

M

.6

.5

.4

.3

ALTITUDE

12,000 FT.
6,000 FT.
8,000 FT.
10,000 FT.

14,000 FT

8,000 FT.
12,000 FT.
15,000 FT.

11,000 FT.

17,000 FT

NATIONAL ADVISORY
COMMITTEE FOR AERONAUTICS

MAXIMUM MACH NUMBER AT
RESPECTIVE GLIDE ANGLE OBTAINED
AT ALTITUDE INDICATED ON CURVE

0°   5°   10°   15°   20°   25°   30°

ANGLE OF GLIDE

FIGURE 38.-THE MAXIMUM MACH NUMBER
OBTAINED BY THE AIRPLANE IN RELATION TO
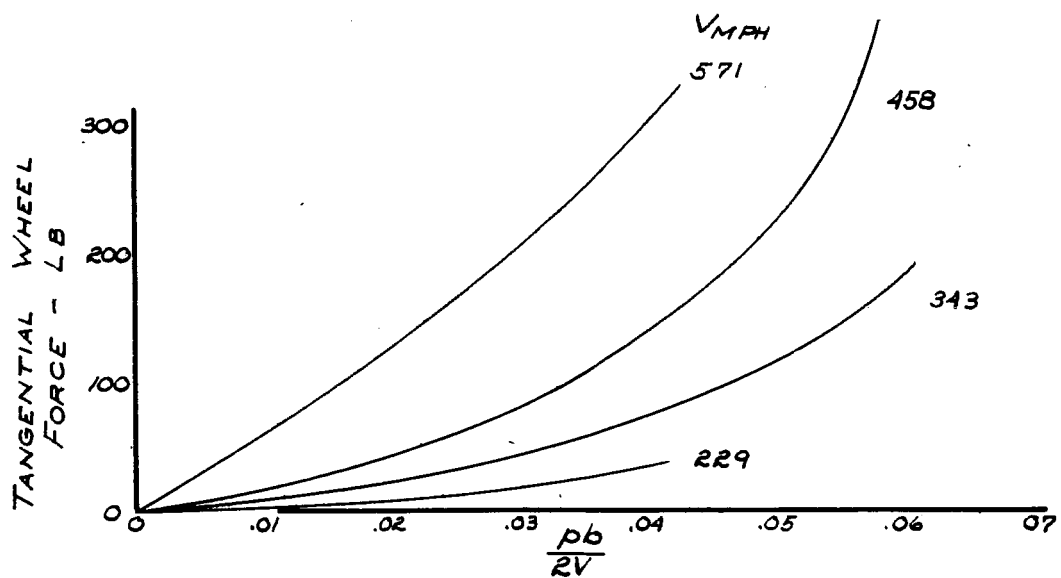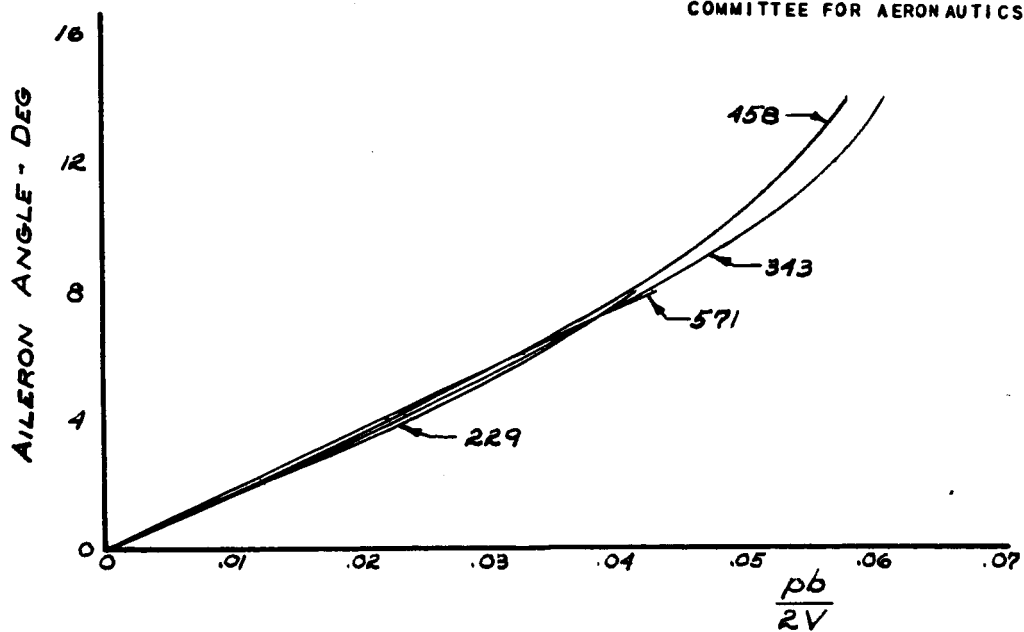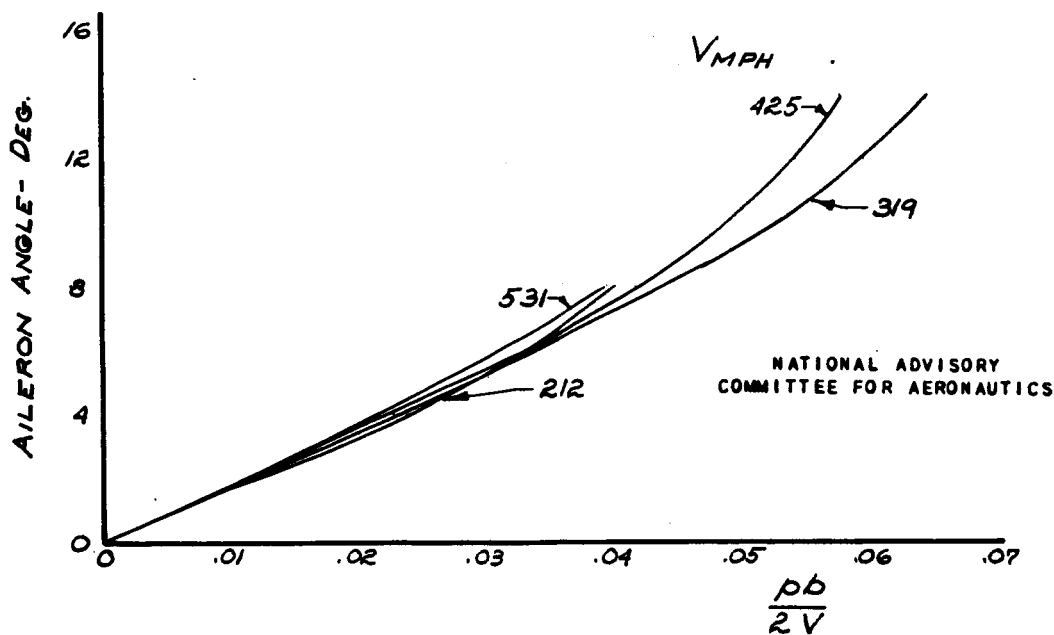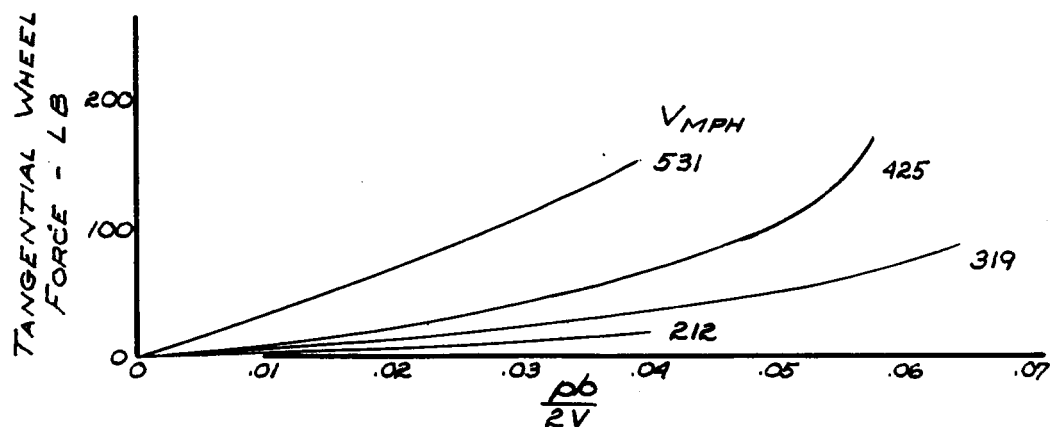THE ANGLE OF GLIDE. ZERO PROPELLER THRUST.
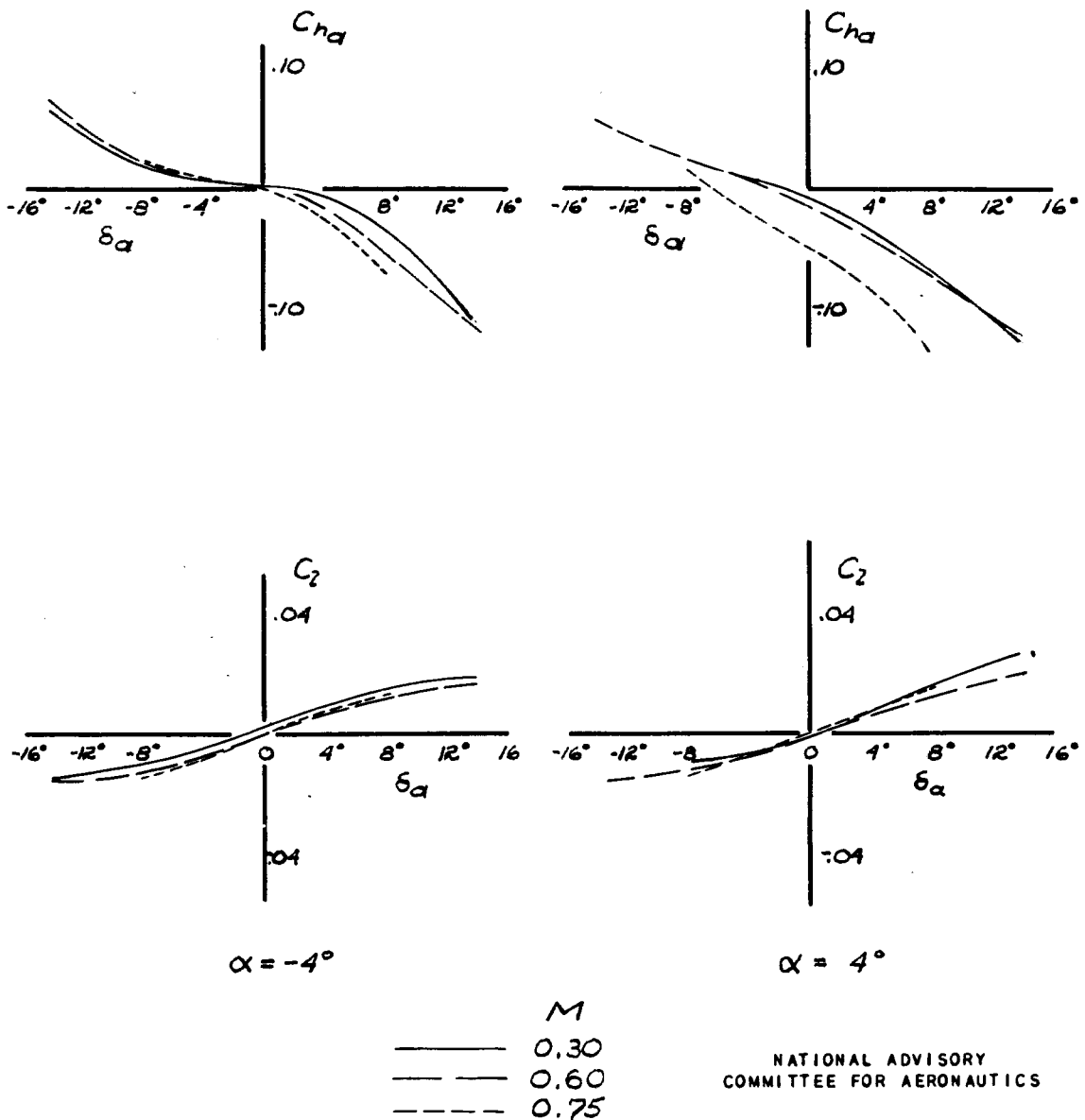
FIGURE 39.—THE EFFECT OF MACH NUMBER ON THE AILERON HINGE-MOMENT AND ROLLING-MOMENT COEFFICIENTS FOR THE MODEL. LEFT AILERON ONLY.

(a) SEA LEVEL
FIGURE 40.- THE AILERON CONTROL CHARACTER-
ISTICS OF THE AIRPLANE.

(b) 20,000-FT. ALTITUDE

FIGURE 40.- (CONCLUDED) THE AILERON CON-
TROL CHARACTERISTICS OF THE AIRPLANE.